1-1-2020

Evaluation Of Gas Hydrate In Gas Pipeline Transportation

Paschal Ogadi Mokwenye

Evaluation of Gas Hydrate in Gas Pipeline Transportation

Prepared by:

Paschal Ogadi Mokwenye

Bachelor of Engineering, Teesside University, 2016

A Thesis

Submitted to the Graduate Faculty

of the

University of North Dakota

In partial fulfillment of the requirements

for the degree of

Master of Science

Grand Forks, North Dakota

December

2020

Name: Paschal Ogadi Mokwenye

Degree: Master of Science

This document, submitted in partial fulfillment of the requirements for the degree from the University of North Dakota, has been read by the Faculty Advisory Committee under whom the work has been done and is hereby approved.

DocuSigned by: Kegang Ling
AE10F7CCAFC7487...
Kegang Ling

DocuSigned by: Vamegh Rasouli
0EB956E8C9C9456...
Vamegh Rasouli

DocuSigned by: Hui Pu
C83B8AB854E4448...
Hui Pu

DocuSigned by: Bailey Bubach
528DF1FF1C4F448...
Bailey Bubach

This document is being submitted by the appointed advisory committee as having met all the requirements of the School of Graduate Studies at the University of North Dakota and is hereby approved.

Chris Nelson
Dean of the School of Graduate Studies

Date

PERMISSION

Title	Evaluation of Gas Hydrate in Gas Pipeline Transportation
Department	Petroleum Engineering
Degree	Master of Science

In presenting this thesis in partial fulfillment of the requirements for a graduate degree from the University of North Dakota, I agree that the library of this University shall make it freely available for inspection. I further agree that permission for extensive copying for scholarly purposes may be granted by the professor who supervised my thesis work or, in his absence, by the Chairperson of the department or the dean of the School of Graduate Studies. It is understood that any copying or publication or other use of this thesis or part thereof for financial gain shall not be allowed without my written permission. It is also understood that due recognition shall be given to me and to the University of North Dakota in any scholarly use which may be made of any material in my thesis.

Paschal Ogadi Mokwenye

December 1, 2020

TABLE OF CONTENTS

LIST OF FIGURES

LIST OF TABLES

ACKNOWLEDGEMENTS

First, I give thanks to Almighty God for the grace, wisdom, and strength given to me throughout this study, without which I would not have completed it.

I would like to thank my graduate committee Dr. Kegang Ling, Prof. Vamegh Rasouli, Dr. Hui Pu, Mrs. Bailey Bubach, and Mrs. Minou Rabiei. Their thought-provoking discussions and editorial comments were greatly appreciated in the development of this thesis. I would especially like to thank my advisor, Dr. Kegang Ling for invaluable discussion, unwavering support, and guidance throughout this work.

I would like to thank my loving parents Mr. Lawrence and Mrs. Nelly Mokwenye for their guidance, support, motivation, and priceless effort to help me succeed in this thesis and overall my career in petroleum engineering, I will forever be grateful to God for giving me you two. I also thank my siblings Grace, Anthony, and Jennifer for their support and encouragement throughout my studies. May God bless you all.

Finally, I would like to thank my graduate colleagues and friends, Olusegun Tomomewo and Mousa Abusurra for their assistance and encouragement throughout this work.

Thank you all and Gog bless.

To my mom Nelly Mokwenye and my dad Lawrence Mokwenye.

The world’s greatest parents and my biggest motivators.

ABSTRACT

Gas hydrate formation and deposition is an inherent problem in the gas production and transmission industry. It causes plugging in pipelines and damages to equipment such as pumps and separators. The continuous constriction of pipelines by hydrates can cause a pressure difference between the upstream region behind the hydrate which has high pressure and the downstream region ahead of the hydrate which has low pressure, this pressure difference can cause pipelines to rupture, putting personnel and equipment in danger. The safest and cost-effective way of preventing hydrate formation is by predicting the temperature or pressure in which they form. In the past years, many correlations have been developed to predict the conditions of hydrate formation, but the models require a complex computation, or their accuracy is limited to certain gas mixtures. This study reviews the conditions of hydrate formation and numerus mathematical models developed to predict their formation temperature for natural gas. The study also involves the development of a new model to calculate the hydrate formation temperature of natural gas, the equation was developed by carrying out nonlinear regression of 460 experimental data points in MATLAB software. Hydrate formation temperatures calculated by the model were compared to experimental values as well as other reputable models. The proposed model showed superior accuracy in calculating the reference experimental hydrate formation temperature over models developed by Hammerschmidt (1934), Motiee (1991), Towler and Mokhatab (2005), Safamirzaei M. (2015), and Chavoshi S. (2018). Also, the model produced the lowest Average Relative Deviation and Average Absolute Deviation from experimental values. Despite having three adjustable parameters the model produced an accuracy ranking of 1 to 3 across a range of specific gas gravity from 0.55 – 1 compared to other models. The model was also applied to gas compositions obtained from The Bakken and it showed a reliable prediction of the hydrate formation temperature when compared to the Katz gas gravity chart. The model offers a simple and good mathematical model for the prediction of hydrate formation temperature of the Bakken Formation.

CHAPTER 1 INTRODUCTION

A major problem in the gas industry is the effect of water vapor during the transportation and measurement of natural gas. Water liquefies, freezes, and accumulates within the system causing interruptions in pipeline transmission of gas. The solid crystals that form resemble snow and the flow of gas causes it to compress and accumulate at the lower spots of the pipeline, these snow-like crystals are called gas hydrates and they are known to cause plugging in gas pipelines. Figure 1.1 shows a typical example of a gas hydrate from a pipeline (Hammerschmidt, 1934).

Figure 1.1 Gas hydrate showing its snow-like appearance

Gas hydrates are clathrate structures in which guest molecules are enclosed in cages of a host lattice. They are crystalline forms of water in which the stabilization of the solid is facilitated by the presence of gas molecules inside the crystal matrix (cage) at temperatures significantly above the normal freezing point of water. It is composed of gas molecules (methane predominantly) surrounded by a cavity of water molecules (Saleh, 2002). Gas hydrates usually form when 90% of the cage is occupied which gives the gas a solid volume ratio of about 160% (Riedel, et al 2010). The molecular arrangement of gas hydrates is shown in Figure 1.2.

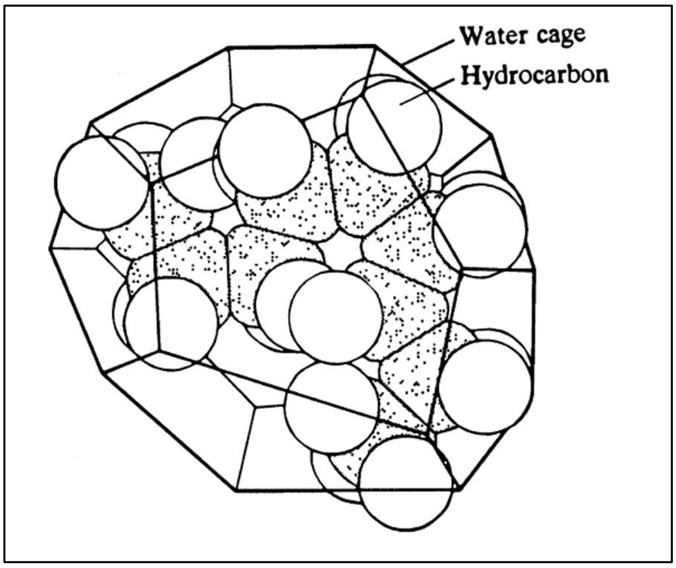

Figure 1.2 Molecular configuration of gas hydrates (Saleh, 2002)

Gas hydrate cages usually contain a single gas molecule and are composed of hydrogen-bonded water molecules. The structure of hydrates is called clathrates due to the entrapped (caged) nature of hydrogen molecules inside the crystal lattice of water molecules (Saleh, 2002), They form when water and gas combine at low temperature and high pressure in pipelines transporting natural gas, hydrates are lighter than water and as a result, they often reside at the point of interface between oil and water (Bellarby, 2009)**.** The crystals have a honeycombed structure with small channels that allow gases to pass through, but with further accumulation, the flow in the pipe is entirely blocked. Gas hydrates also exist in subsea and ocean floors where conditions are ideal for formation, they trap large amounts of energy near subsea seeps and around midline reservoirs (Saleh, 2002). Favorable conditions of natural gas hydrates exist in the sediment of Polar Regions and sediments covering 90% of the ocean floor. Most natural gas hydrates have more than 99% of their hydrocarbon as methane, low amounts of CO_2, and H_2S are present (Puall, et al 2001).

1.1 PROBLEM STATEMENT

Gas hydrates form inside the pipelines transporting natural gas at subsea levels and low-temperature regions. They form around the surfaces of the pipe and gradually accumulate until they constrict the flow or cause variations in flow pressure thereby causing damage to production equipment such as pumps, compressors, and separators at either end of the pipe. They can cause catastrophic rupture of the pipes and the failure of the gas transportation system. As a result, the safest and most cost-effective way of preventing gas hydrates is by predicting the temperature or pressure in which it will form for a natural gas mixture.

Many correlations have been developed to predict the conditions of hydrate formation, but the models require a complex computation, or their accuracy is limited to certain gas mixtures. Some of them can only be used in a limited range of temperature, pressure, or specific gravity and show a significant error at higher pressure. Also, some correlations are only useful when a comprehensive analysis of gas is accessible.

1.2 RESEARCH OBJECTIVES

The objective of this study is to develop a mathematical model for the prediction of gas hydrate formation temperature across a wide range of gas compositions, and pressure. Other objectives of this study, include:

- To determine the accuracy of the model by comparing the result of the model with experimental data as well as other reputable mathematical models.
- To estimate the hydrate formation temperature of natural gas compositions obtained from the Bakken Formation.

1.3 METHOD OVERVIEW

To fulfill the objectives of this study, the following steps were taken.

- The literature review presented previous research on hydrate formation and empirical correlations from reputable studies such as Hammerschmidt (1934), Motiee (1991), Towler and Mokhatab (2005), Chavoshi S. 2018, and Safamirzaei M. (2015). Also, their correlations were compiled in an Excel sheet.
- Gas composition data for The Bakken Formation were collected from various research and publications.
- A new model was developed by carrying Non-linear regression on 460 experimental data points using MATLAB.
- The new model was applied to the 460 data points in Excel and the calculated hydrate formation temperature was compared to experimental values as well as values calculated by other models.

- The model was evaluated by comparing its Average Relative Deviation and Average Absolute Deviation from reference experimental values, the deviation was compared to other models to assess its accuracy over other models.
- Gas composition data obtained from the Bakken Formation were applied to the model to calculate the hydrate formation temperature and compared with the Katz 1945 gravity chart.

1.4 THESIS OUTLINE

This thesis consists of six chapters. The outline of this thesis is as follows:

- Chapter 1 introduces gas hydrates and how they exist in the gas industry and nature. It also outlines the statement of the problem, research objectives, and methodology.
- Chapter 2 gives an in-depth overview of gas hydrates which includes how they form, mechanisms in play, causes and effects, the structures, methods of prevention, potential as an energy source in the future, and previous experiments and empirical correlations of hydrate formation temperature.
- Chapter 3 describes the methodology behind the development of the model, evaluation of the model, and data collection of gas compositions from the Bakken Formation.
- Chapter 4 presents the results of the calculated hydrate formation temperature of the proposed model and compares it to experimental data as well as values from other models. Also, the Average Relative Deviation and Average

Absolute Deviation of the model were compared to reference experimental values and that of other models.

- Chapter 5 discusses the result of the temperature-pressure curve of the new model as well as the Average Relative Deviation and Average Absolute Deviation from the reference experimental values.
- Chapter 6 presents the conclusions of the study including the recommendations for future work.

CHAPTER 2 LITERATURE REVIEW

2.1 DISCOVERY OF GAS HYDRATES

In 1810, Humphrey Davy discovered a crystalline compound formed by chlorine and water, this later became the first known gas hydrate. An acetylene hydrate was later reported by Cailletet in 1878, he discovered that a sudden decrease in pressure helped in the formation of crystalline compounds. The first carbon disulfide and double hydrate hydrogen sulfide were reported by Schutzenberger and in 1882 Bordet discovered the double hydrate of phosphine and carbon dioxide. Double hydrates are compounds having a definite melting point and are not mixtures of a single hydrate, this is because the decomposition temperature of the single hydrate may be overall different from the decomposition temperature of a double hydrate. In 1897, Sully Thomas and De Forcrand found that carbon tetrachloride and acetylene forms double hydrates, they also discovered double hydrates of sulfur dioxide and ethylene in the following compounds: ethylene bromide, methyl Iodide, methylene chloride, methyl bromide, methylene chloride, and methylene iodide (Hammerschmidt, 1934). The oil and gas industry began to take interest in gas hydrates in the 1930s when gas hydrate was found to cause blockages in pipelines. Hammerschmidt in 1934, discovered that natural gas hydrates were responsible for blocking gas pipelines.

2.2 GAS HYDRATE FORMATION

Gas hydrates are formed when water and gas (having lower molecular weight) combine at low temperature and generally high pressure (e.g. temperatures below 25 °C and pressures greater than 1.5MPa for natural gas hydrates) (Koh, et al 2001), precise conditions vary depending on the composition of the fluid. They exist onshore beneath the permafrost or offshore in shallow depths in the ocean (Sami, et al 2013). The gases that can form gas hydrates include methane (predominantly), propane, ethane, butane, chlorine, CO_2, nitrogen even oxygen can create hydrates. At high pressure, gas hydrates can exist at temperatures greater than the freezing point of water. The solid hydrate compounds form with the aforementioned gases at elevated pressures in the presence of water. At equilibrium conditions the hydrates cause a higher amount of water to be removed from the vapor phase than in the case of liquid water at the same pressure and temperature, this is due to the lower vapor pressure of the hydrates (Hammerschmidt, 1934).

2.2.1 Stages of Hydrate Formation

There are three main stages of hydrate formation: gas dissolution, hydrate nucleation, and lastly agglomeration as shown in Figure 2.1.

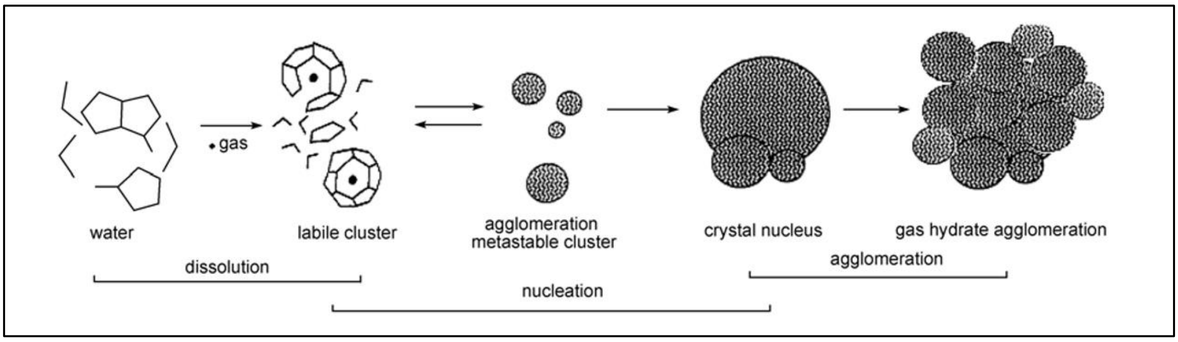

Figure 2.1 Stages of Hydrate Formation (Tang, et al 2010).

Tang, et al, 2010 found that under suitable conditions, water molecules form quasi-cavities from hydrogen bonds. Gas molecules are trapped inside these quasi-cavities when the gases dissolve, forming labile clusters. The clusters which are in quasi-equilibrium agglomerate and continue to attach until a critical radius is reached from which a stable hydrate nucleus is formed. It was found that during hydrate formation, ethane and methane occupy the smaller cavities while propane occupies large cavities. Also, when hydrates form there is a significant depletion of gas content, therefore gases in the fluid stream are consumed significantly (Tang, et al 2010).

2.2.1 Mechanisms of Hydrate Formation

The formation and deposition of hydrates in pipelines involve several processes from the formation of hydrate particles to the deposition and accumulation (growth) of the hydrate layer on the surface of the pipe. To forecast this dynamic deposition of hydrates in a pipeline, a model was developed by Zhang, et al 2019 in which the heat transfer and the hydrodynamic hydrate behavior in the pipeline were investigated. The model consisted mainly of two parts: Hydrate deposition and water condensation.

2.2.1.1 Heat Transfer

The temperature difference between the cold environment and the hot gas in the pipeline is large enough to cause heat transfer between gas pipelines in cold regions and the subseafloor (Gu, et al 2019), as a result, water condenses when the temperature of the fluid falls below the dew point temperature. In cold regions and subsea levels, low temperature and high flow pressure in pipelines causes the molecules of natural gas to diffuse around the surface of water to form hydrates which adhere to the inner surface of the pipe, this leads to variations in fluid velocity, effective inner diameter and the pressure in the pipeline relative to position and time (Rao, et al 2013). The heat exchange between the external environment and fluid leads to a decrease in fluid temperature and this takes place along the direction of fluid flow as shown in Figure 2.2 (Zhang, et al 2019).

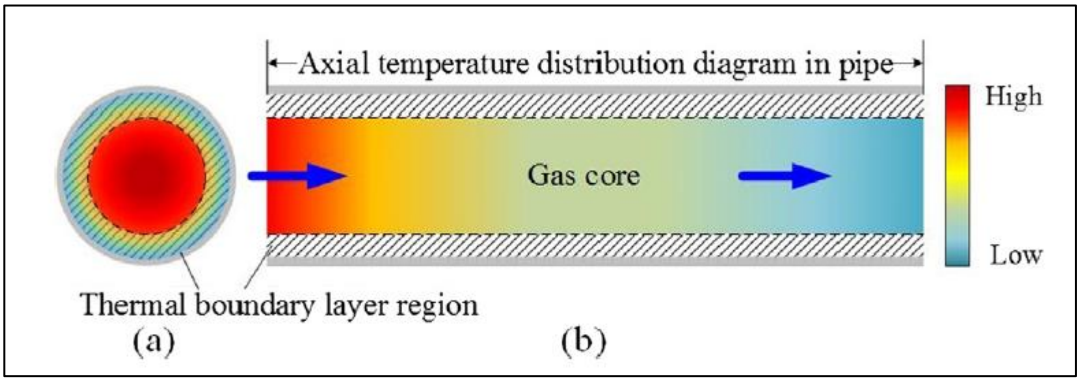

Figure 2.2 Fluid flow in a pipe showing its Thermal boundary layer region (Zhang, et al 2019)

2.2.1.2 Dissolved Water Condensate

There are two sources of liquid moisture in gas pipelines in cold regions and subsea levels: small droplets in the gas core and the liquid condensate film near the wall (Zhang, et al 2019). A heat boundary layer having a high variation in temperature forms on the surface of the pipe as shown in Figure 2.2. This is due to a significant difference in temperature between the fluid and the environment during long-distance gas transportation in cold regions and subsea levels (Dorstewitz, et al 1994). When the fluid temperature falls below the dew point, the free water condenses and precipitate around the heat boundary layer, a liquid film forms on the pipe wall and there is a significant drop in temperature along the axis of the pipeline, as a result, water condenses on the surface of insoluble particles and small droplets form on the gas core (Gorbunov, et al 1998). Gas molecules continue to diffuse around the liquid condensate in the fluid system which consists of a thin liquid film near the pipe wall and small droplets in the gas core. A hydrate shell forms rapidly on the surface of liquid droplets when the pressure and temperature satisfy equilibrium conditions for hydrate formation, the shell grows inside the droplet to form hydrates. Also, the liquid film on the surface of the pipe wall crystallizes with gas molecules to form hydrates. These two types of hydrates deposit and accumulate on the inner wall of the pipeline to form larger hydrate layers. These processes continue until the thickness of the hydrate increases as shown in Figure 2.3.

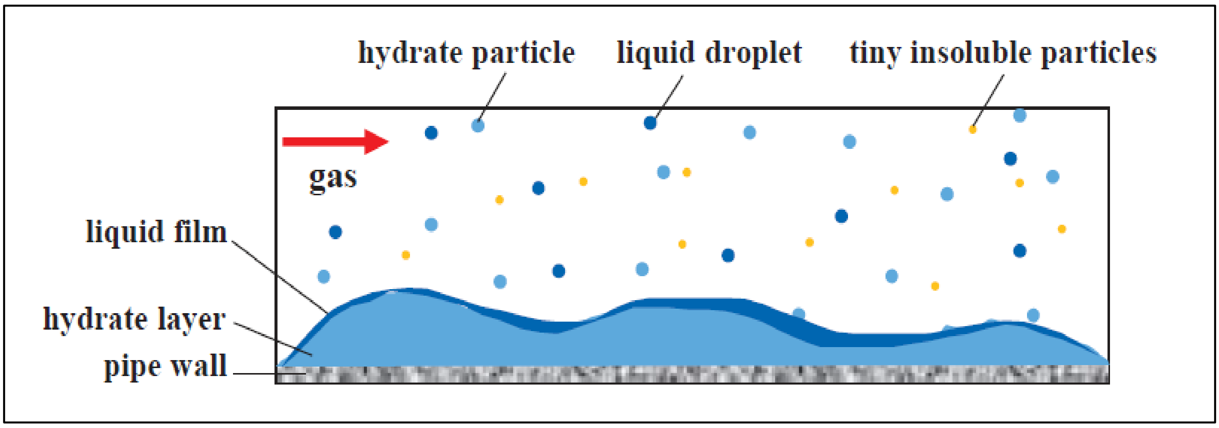

Figure 2.3 Schematic of hydrate formation and deposition mechanism in subsea and cold region long-distance gas transportation pipelines (Zhang, et al 2019).

The formed hydrate particles and the condensate droplets are transported downstream by the high-speed fluid due to their densities being in the same range.

2.2.1.3 Hydrate Layer Growth

The growth of hydrate layers is primarily due to the deposition process which combines the hydrates from scattered drops and thin condensate film (Zhang, et al 2019). The hydrate particles adhere to the pipeline wall due to strong adhesive forces between the wet pipe wall and the hydrates. New hydrate particles form from condensed water keeping the hydrate concentration in the pipe in constant dynamic equilibrium.

2.2.2 Causes of Hydrate Formation

The causes of gas hydrate are subdivided into primary and secondary causes.

2.2.2.1 Primary Causes of Hydrate Formation

The formation of gas hydrates in natural gas transportation pipelines depends primarily on the temperature, pressure, and composition of the gas-water vapor mixture (Hammerschmidt, 1934). After all primary conditions are in effect, hydrate formation is accelerated by pressure, high velocities of the gas stream, and pulsations. As shown by the melting point diagram in Figure 2.4, high pressure and low temperature are favorable to the formation of hydrates. On a practical basis, water vapor is the only component that can be controlled regarding the composition of the gas. Although removing moisture from the gas will eliminate the possibility of any hydrate forming, it is not necessary for the gas to be free of water vapor since hydrates only form when the gas reaches the dew point. Also, if the partial pressure of water vapor in the gas is less than the vapor pressure, the gas hydrate will lose water and dissociate. The driving force behind phase change from gas to solid hydrates is thermal sub-cooling. In this case, the phase change is caused by the temperature difference between the bulk temperature and the hydrate dissociation temperature (Hammerschmidt, 1934).

The conditions of temperature and pressure are represented in disassociation curves where hydrates separate into gas and water as shown in Figure 2.4. The point of hydrate formation lies within the curve, this means that hydrates are certain to form within the curve but will not form immediately if the temperature/pressure point lies outside the disassociation curve (Saleh, 2002). The risk of hydrate agglomeration increases further inside the curve although there is a time delay with an undefined duration. The curves are generated based on experimental values or numerical predictions using the Katz gas gravity chart (Zhang, et al 2019).

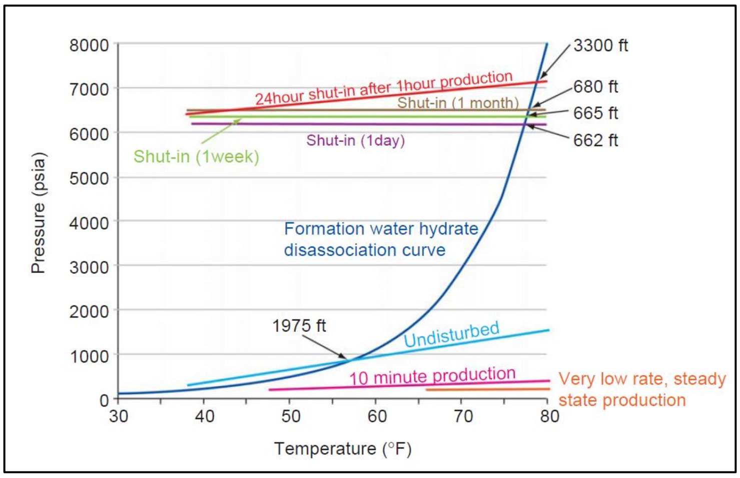

Figure 2.4 Disassociation curves showing the conditions of temperature and pressure (Zhang, et al 2019).

Figure 2.5 shows Katz's 1945 gas gravity chart.

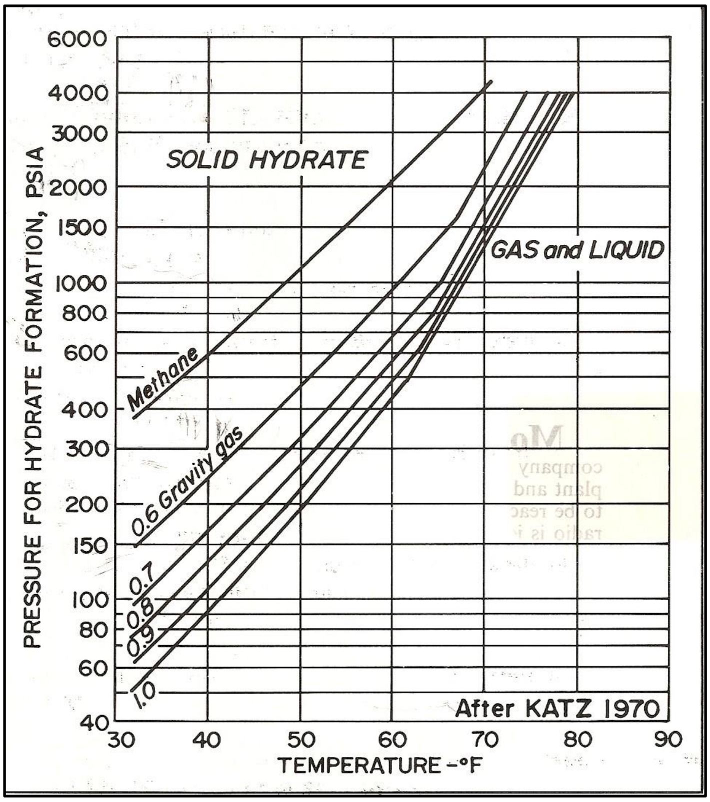

Figure 2.5 Katz gas gravity chat (Bahadori and Vuthaluru, 2009)

2.2.2.2 Secondary Causes of Hydrate Formation

As previously stated, a definite pressure, temperature, and gas-water composition are necessary for gas hydrates to form. However, it is not certain that hydrates will crystallize even after these conditions are met (Hammerschmidt, 1934). Certain secondary factors influence the formation of hydrates, these are:

1. Gas Stream velocity
2. Arrangement of the molecule of crystals
3. Water saturation (water vapor)
4. Porosity

2.2.2.2.1 Gas stream velocity

High gas velocity, pressure pulsation of the gas (due to compressors), or introducing small amounts of hydrate crystal can hasten the formation of hydrates. Under operating conditions, high gas stream velocity in the pipeline creates almost ideal conditions for the formation of hydrates provided the proper conditions of temperature, pressure, and water composition are established (Eucken. 1925).

2.2.2.2.2 Arrangement of crystal molecules

The general behavior of crystal formation described by Eucken (1925) explains the secondary causes of hydrate formation, it states that the formation of a crystal requires mostly a definite adjustment or generally a certain arrangement of molecules, this may not always be established at once and the lack of which is characterized by the liquid phase. Ideally, a certain amount of time elapses before the required number of molecules align into the correct position either by coincidence or accident. It is only after a nucleus or elementary crystal is formed that crystallization proceeds smoothly, this exerts a certain directional force on the neighboring liquid molecules and causes them to merge. As a result, hydrate formation is promoted by forces which tend to stir or mix, because the probability of the molecules aligning into the correct position is increased by those forces. Also, high-pressure pulsations and velocity impact a mixing action on the droplets of condensed moisture (Hammerschmidt, 1934).

2.2.2.2.3 Water Saturation (Water Vapor)

During the process of transporting natural gas, water is removed from the gas before transporting through pipelines, this is called separation and dehydration. However, these processes only remove the free water in the gas, therefore the pipeline system is a water-saturated gas transportation system. The phenomenon of hydrate deposition in pipelines was observed by (Lingelem, et al 1994), they suggested that for a water-saturated gas system the mechanism is similar in a continuous gas system, having small proportions of free water.

Gorbunov, et al 1998 verified that condensation of water vapor takes place on the surface of small-size insoluble particles, it also determined that vapor heterogeneous-phase nucleation forms alone on the surface of suspended particles with soluble sites. Gas molecules constantly diffuse in the gas core around the surface of the condensate liquid drops.

2.2.2.2.4 Porosity

Natural gas produced from the reservoir stratum generally contains small-sized insoluble particles, as a result, in an environment where small-sized insoluble particles are suspended, supersaturated vapor molecules collide constantly and undergo initial heterogeneous phase nucleation on particle surfaces. Nicholas, et al. 2008 found in a study that porosity influenced the thickness of hydrate deposition in the pipelines significantly. Free water is the main constraint of hydrate formation/deposition when conditions of pressure and temperature reach hydrate phase equilibrium in a water-saturated gas system. The study proposed that the condensate of free vapor on the cold walls of the pipe formed the free water in a water-saturated system.

2.2.2.3 Other Factors Affecting Hydrate Formation

Other factors that influence hydrate formation include (Zhang, et al 2019)

1. Adhesion between hydrate particles and the pipe wall,
2. Spatial distribution characteristic of the gas-liquid phase, and

3. Fluid flow rate.

Particle surface energy, the thickness of the dielectric layer, and Hamaker number affect the nature of deposition of the particles (Chein, et al 2005). A parametric analysis was carried out by (Chaudhari, et al 2018) to investigate the effect of mixture velocity, liquid loading, and interfacial tension on hydrate formation with the use of hydrate risk correlation which uses the steady-state and transient dynamic multiphase flow simulation on a long subsea tieback. The study deduced that the flow assurance risk increases with an increase in mixture velocity and liquid loading, however it decreases with a decrease in the interfacial tension.

2.2.3 Gas Hydrates Structures

Gas hydrates form pentagonal cubic structures in their crystal lattice. The hydrocarbon molecules (in this case methane) are lodged in the center of the cubes and bounded (caged) by water molecules. There are three main structures of gas hydrates that have been found Structure I (SI), Structure II (SII), and Structure H (SH) having a cubic (isometric) lattice (Sloan, et al 2008). All the structures contain large and small cavities but only molecules with the appropriate size and geometry enter the cavities (Dorstewitz, et al 1994). Figure 2.6 shows the physical geometry and lattice structure of methane hydrates, it shows that the gas molecule is located at the center of the water cavity.

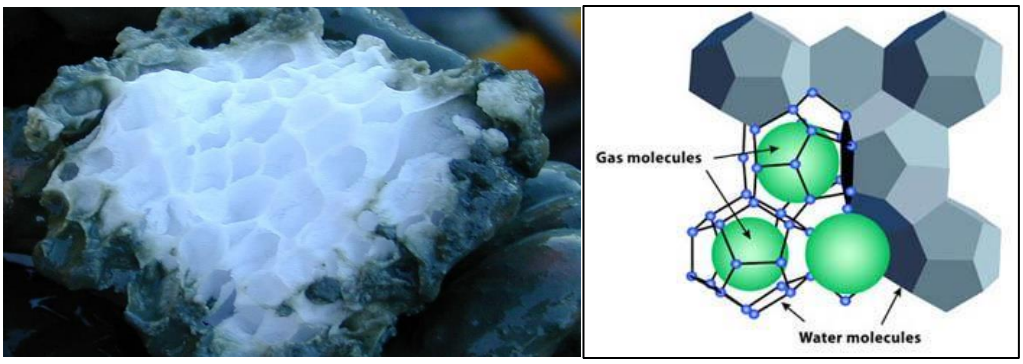

Figure 2.6 Physical geometry and Lattice structure of Gas hydrates (Studentenergy.org)

Methane and natural gas typically form hydrate Structure (I) but forms Structure II or H if higher hydrocarbons are present in the gas mixture as is the case with thermo-genic gas components (Riedel, et al 2010). Figure 2.7 shows the lattice structure of the gas hydrate.

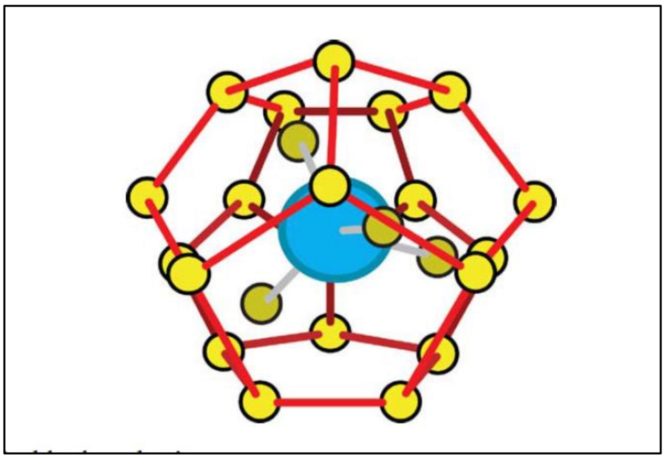

Figure 2.7 Lattice structure of gas hydrates (Bellarby, 2009)

2.2.3.1 The Structure I (SI)

Structure (I) has two main structures of cavities: a small pentagonal dodecahedral cavity which consists of 12 pentagonal rings of water (20 molecules of water) and a large tetrakaidekahedral cavity consisting of 2 hexagonal and 12 pentagonal rings of water (24 molecules of water) (Koh, et al 2002). The arrangement of the cubic cavities is an in-body-centered packing and the cavities are large enough to contain methane, ethane, and gases having a similar range of molecular diameter such as hydrogen sulfide and carbon dioxide hydrates (Sami, et al 2013).

2.2.3.2 Structure II (SII)

Structure (II) also has two main structures: a pentagonal dodecahedral cavity and a large hexakaidecahedral cavity which consists of 12 pentagonal and 4 hexagonal rings of water (28 molecules of water). They are packed like diamonds in an octagonal shape, this leads to some cavities being large enough to contain not only ethane and methane but also larger gas molecules such as isobutane and propane.

2.2.3.3 Structure H

This structure requires both small molecules such as methane and larger molecules of typical gas condensates or oil fractions. Figure 2.8 shows the cell units and structures of hydrates (Sami, et al 2013).

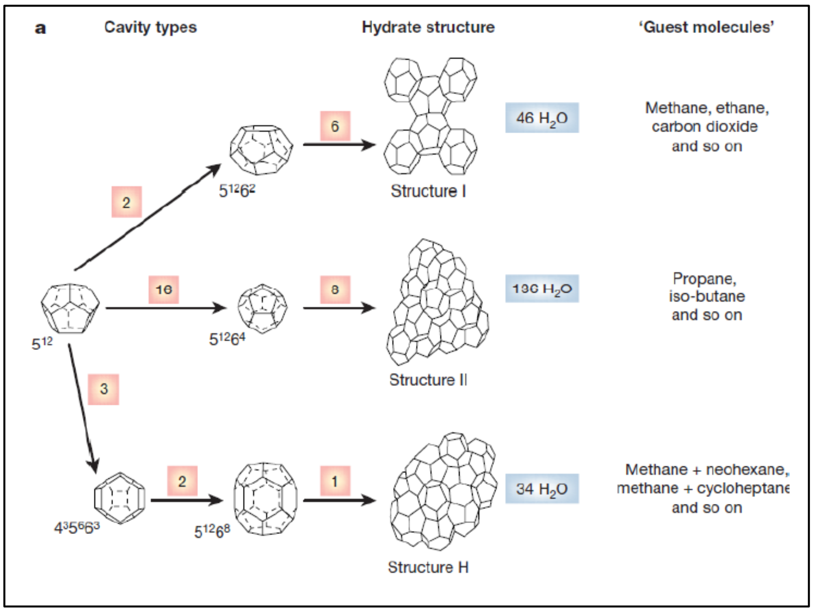

Figure 2.8 Cell unit structures of gas hydrate structure I, II, and H (Sami, et al 2013).

2.3 EFFECTS OF GAS HYDRATES

Gas hydrates have a wide range of effects on the oil and gas industry from upstream drilling and production to the midstream transportation, compression, and separation systems of natural gas. Gas hydrates are responsible for plugging in natural gas pipelines, they deposit on walls of the pipeline thereby reducing the effective flow diameter of the pipe. This causes fluctuations in the pressure of the fluid stream by causing an increase in pressure in areas where there are hydrate deposits and a decrease where there are no deposits (Sami, et al 2013).

2.3.1 Gas Hydrate Occurrence During Drilling in Offshore Regions

The complexity and challenges of offshore drilling increases with increase in water depth. One main challenge is the formation of gas hydrates, during deepwater drilling it is likely to encounter shallow sediments containing natural gas, if encountered, the gas could enter the drilling fluid causing gas hydrate formation under high pressure and low temperature (Poberezhny, et al 2019). Also, gas hydrates could easily form when drilling mud circulation is stopped and gas enter into the fluid, in cases where the drilling mud is not treated with hydrate inhibitors, this can lead to unexpected gas kick during drilling which can block the annular clearance, pipe or other equipment such as the blowout preventer (BOP) which may result in catastrophic failure of the system in some situations. (Xiaolan, et al 2011).

Solid hydrates can plug well kill-lines and chokes causing problems in well control. Hydrates can stop the circulation of drilling fluid and prevent the drill string from moving if it forms in the annulus between the drilling string and casing, this can seriously affect drilling operations. Hydrates can also form in the riser, plugging the flow of drilling fluid. Figure 2.9 shows a summary of the major problems caused by gas hydrates while drilling through gas hydrate formations (Sami, et al 2013).

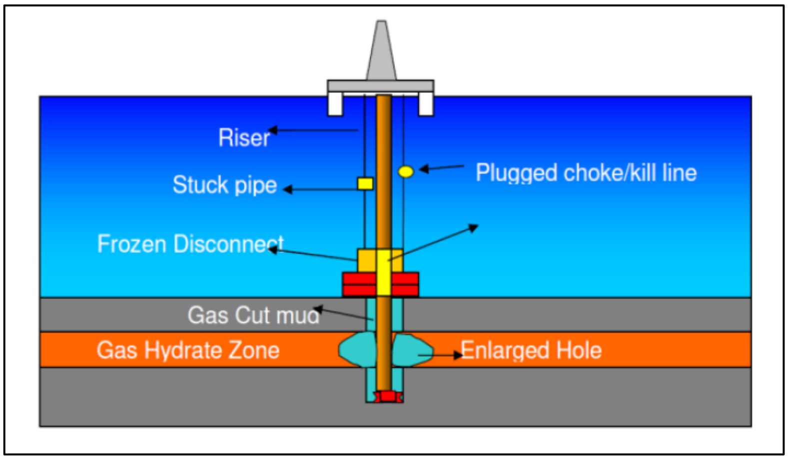

Figure 2.9 Pictorial summary of the major problems encountered during drilling operations through a hydrate formation (Sami, et al 2013).

2.3.2 Problems with Flow Assurance

Pipeline transportation is a common means of transporting oil and gas from the wellhead to production sites. Gas hydrate particles form when the pressure and temperature of the fluid in the pipeline falls within the hydrate zone in the phase diagram, these hydrate particles could eventually plug the pipeline. When gas hydrates plug transmission pipelines, operations become uneconomical, production stops for weeks or sometimes months in large extended pipelines. The propagation of hydrates tends to develop a plug that gradually separates the pipe into two pressure zones: a high-pressure zone between the high-pressure gas source and the plug, and a low-pressure zone between the plug and the gas recovery section. Figure 2.10 shows a typical hydrate plug in a gas transportation pipeline (Sami, et al 2013).

Figure 2.10 Gas hydrate plugging of gas transportation pipeline (Polartrec.com)

A pipe leak and explosion can occur due to the growth in pressure. The higher pressure can destroy the pipe when there is a large difference in pressure between the upstream and downstream sections. Both failures can put personnel in danger and damage equipment.

2.3.3 Corrosion in Gas Pipelines

Gas hydrates cause pitting corrosion of pipelines that are in acidic or neutral environments. Acidic gases such as CO_2 and H_2S, when dissolved in water accelerate the internal corrosion of pipelines as the gas components of hydrate formation (Poberezhny, et al. 2017). Specimen with gas hydrates formed on the inner surface show an increased rate of localized and general corrosion on their surfaces as shown in Figure 2.11.

Figure 2.11 General view of corrosion damage of the specimen after exposure to gas hydrates (Poberezhny, et al 2019).

(Poberezhny, et al 2019) investigated the influence of gas hydrates on the fatigue test of a St 20 steel pipe where tests were performed at pure bending in air. Specimens were tested after exposure to gas hydrate and without any pretreatment. The curve in Figure 2.12. shows a three-stage kinetics growth of fatigue crack, also a slight higher-level cyclic deformation on the fatigue growth curve was observed in the pipe after exposure to gas hydrates, it may be attributed to corrosion damage of the pipe surface.

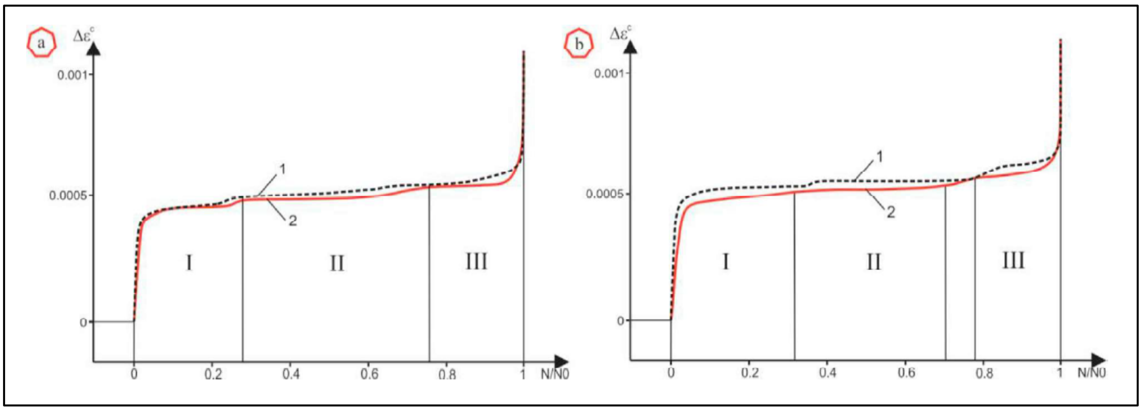

Figure 2.12 Fatigue crack growth curves for steel specimen (a) without exposure, (b) after exposure to hydrates (Poberezhny, et al 2019)

The rate of growth of fatigue crack was higher by 5-7% for the pipe specimen after exposure to hydrates compared to the specimen without pretreatment, it was attributed to the increase in surface damage due to the formation of hydrates. The fatigue test shows that the duration of the low-frequency fatigue stage was influenced by hydrates causing a shortening of the stage (III) shown in Figure 2.12, this corresponds to the serviceability of the pipeline. It also shows an increase in the deformation for steel specimen exposed to hydrates. Similar behaviors were noted for materials of sea pipelines and drill pipes (Poberezhny, et al 2019).

2.4 CURRENT HYDRATE PREVENTION METHODS

The most effective strategy for managing hydrates in an oil production system is staying outside the temperature-pressure envelope where hydrates are stable. Examples of this are insulating the flow path or adding a heat source which can keep the temperature of the fluid sufficiently above the predicted hydrate formation temperature during steady-state operation, this will also allow for adequate time to reduce or depressurize the flow. The purpose of reducing the pressure is to lower the temperature of hydrate formation to below the ambient temperature to allow for an extended shut-in time (Saleh, 2002). There are four main methods of combating gas hydrate plugs to ensure a continuous flow.

1. Hydraulic method
2. Thermal method
3. Mechanical method
4. Chemical method

2.4.1 Hydraulic Method

The hydraulic removal method involves depressurizing the fluid stream thereby dissociating the hydrate plug, due to the porous structure of the plugs in the gas pipelines, this method appears promising. However, it is only suitable for gaseous hydrocarbon as depressurization in liquid causes vaporization. Lowering the flow pressure does not dissolve a hydrate plug immediately, this is because the disassociation of hydrates is highly endothermic (absorbs heat from the surroundings) which delays the break-up of the plug (Saleh, 2002).

2.4.2 Thermal Method

The thermal method involves an in-situ delivery of high temperature (heat) flow towards the hydrate plug area through the pipeline wall to raise the temperature of the system above the hydrate formation temperature. This method can be achieved for external pipelines but not suitable for subsea pipelines.

2.4.3 Mechanical Method

The mechanical method involves pigging to clean the pipeline of hydrate deposits. This method involves moving a large spherical or cylindrical disc made of a flexible material, having an outside diameter almost equal to the inside diameter of the pipeline. An example of these flexible materials includes neoprene rubber. The disadvantage of this method is that shutting down production to pig the pipeline is expensive and causes downtime (Sorheim, 2005). Figure 2.13 shows an example of a pipeline pigging operation.

Figure 2.13 Pipeline pigging (Picchemicals, 2019).

2.4.4 Chemical Method

The technology adopted by the oil and gas industry for the prevention of gas hydrates in pipeline transportation involves the introduction of a thermodynamic inhibitor such as methanol into the natural gas fluid flow. However, as oil and gas exploration moves into extreme environments (such as deep-sea, offshore exploration, and production) the temperature and pressure conditions become more severe in the field, as such the concentration of inhibitors required for the prevention of hydrate formation increases significantly, most times to excess levels. Hence other technologies have been developed in the form of low-dosage chemicals such as kinetic or anti-agglomerate inhibitors. These compounds function by retarding the hydrate formation time to longer periods than the resident time of the gas inside the hydrate-prone area of the pipeline. Compared to thermodynamic inhibitors these low dosage inhibitors offer significant environmental and economic advantages. The main aim of low dosage inhibitors is to interfere with the mechanism of hydrate formation (Koh, et al 2002).

The chemical process involves the use of two types of additives thermodynamic inhibitors (THI) and Low dosage hydrate inhibitors (LDHI), they are further subdivided into the following (Sami, et al 2013)

1. Thermodynamic Inhibitors (THI)
   i. Alcohols (e.g. Methanol)
   ii. Glycols
2. Low-dosage hydrate inhibitors (LDHI)

i. Surfactants

ii. Kinetic Inhibitors

iii. Anti-agglomerates

2.4.4.1 Thermodynamic Inhibitors (THI)

Thermodynamic inhibitors reduce the water movement and reaction by shifting the hydrate phase boundary to a higher pressure and lower temperature, this can prevent hydrate formation effectively (Sami, et al 2013). Considering that hydrates are similar to ice, chemical deicers that remove or prevent ice from accumulating can also work for gas hydrates.

2.4.4.2 Alcohols (Methanol)

Alcohols have proven effective in combating ice formation and gas hydrate control. They contain the hydroxyl (OH) group which ensures solubility in water. The simplest form of alcohol is methanol (CH3OH) and it is the most available/widely used in the gas industry. The addition of sufficient amounts of these compounds creates a condition whereby the temperature and/or pressure required for hydrate formation needs to be lower for it to form (Koh, et al 2002). Methanol has a relatively low molecular weight, this allows it to penetrate the hydrate cavities and layers to effectively dissolve the hydrates.

However, due to this low molecular weight, methanol is lighter than water and as a result, may prove ineffective injecting it from the wellhead downhole into the hydrate plug submerged with oil. It is effective when dealing with very light oil. Thermodynamic inhibitors such as methanol are used to prevent hydrate formation after a shut-down where the range of time is much longer.

Plots showing the effectiveness of alcohols in hydrate inhibition are used to formulate the required dosage rates for hydrate inhibition of completion and intervention fluids, keeping in mind that less methanol or glycol should be used when brine is used in drilling fluid due to its inherent inhibition characteristics. Figure 2.14 is a curve showing the effectiveness of various alcohols in hydrate inhibition (Bellarby, 2009).

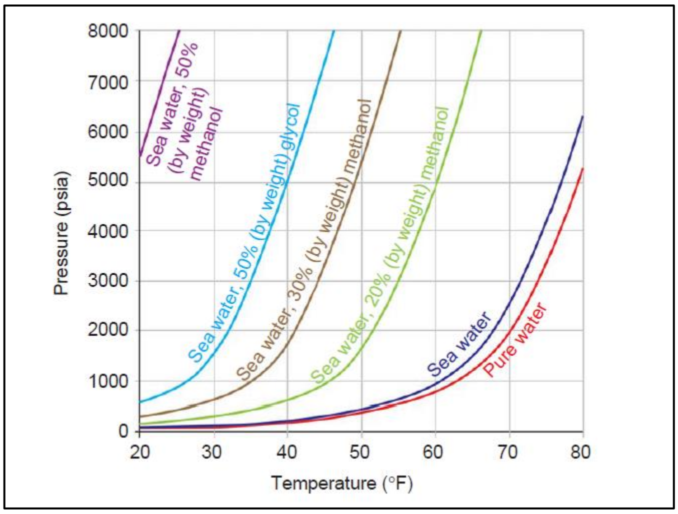

Figure 2.14 Hydrate inhibition with methanol and glycol (Bellarby, 2009)

In some fields, it is common for higher concentrations of methanol (up to 60 mass %) to be used and may also require the addition of glycol. These large volumes of methanol and glycol raise concerns about the environment, higher cost, and logistics. Low dosage hydrate inhibitors in contrast are new categories of chemical additives that can be effective at low volumes (mass %) for the same application. (Sami, et al 2013).

2.4.4.3 Glycols

Glycols are other types of hydrate inhibitors used in the industry. Two frequently used glycols are Triethylene glycol (TEG) (HO–C2H4–O–C2H4–O–C2H4–OH) and Monoethylene glycol (MEG) (HO–C2H4–OH) also diethylene glycol (DEG) is used occasionally (Elhady, 2005). MEG is denser and more viscous than water, it is flammable (but its flash point is higher than methanol). TEG is slightly denser and more viscous than methanol, this is due to the higher molecular weight of TEG. The greater viscosity and density of the inhibitors compared to methanol provide a useful means of removing hydrates when the glycol is injected above the hydrate plug if the glycol can migrate down the tubing and stay atop the plug before it circulates into water. Compared to methanol, glycols are easier to extract in the production system, for this reason, they are frequently used in wet gas pipelines (Brustad, et al 2005).

2.4.4.4 Low-Dosage Hydrate Inhibitors (LDHI)

LDHI can prevent the formation of gas hydrates during the nucleation and agglomeration stages. Examples of commercial low-dosage hydrate inhibitors are Inhibex 100, Inhibex 501, PVP, and GHI1 (Bellarby, 2009). Ping et al 2010 found that neither GHI1 nor PVP was able to inhibit gas hydrate nucleation, but GHI1 has a greater ability to inhibit hydrates than PVP. This higher inhibition ability is caused by diethylene glycol monobutyl-ether. The categories of low-dosage hydrate inhibitors are:

1. Surfactants
2. Kinetic Inhibitors
3. Anti-agglomerates

2.4.4.4.1 Surfactants

These chemicals disperse hydrate crystals as they form, preventing the accumulation of the hydrates in a particular location in the pipeline. A typical example of such a chemical is Lecithin which is environmentally friendly and is used as a food antioxidant. Lecithin is sometimes used as a drilling fluid additive to stop blowout preventers from freezing when gas influx occurs in deep-water. Pakulski, (2007) reported an increase in hydrate formation when natural or introduced surfactant (such as anti-agglomerates) are present.

2.4.4.4.2 Kinetic Inhibitors

Kinetic inhibitors are polymers of various types such as polyvinyl caprolactam, they work by preventing or reducing the nucleation and subsequent crystal growth of the hydrates, thereby delaying the hydrate formation (Sami, et al 2013). A one mass % concentration is sufficient to control the formation process of gas hydrates until the gas is transported to its destination where the thermodynamic conditions for hydrate formation do not exist. A major disadvantage to these inhibitors is that once nucleation occurs, these inhibitors are unable to prevent further crystallization of hydrates (Bellarby, 2009).

2.4.4.4.3 Anti-agglomerates

These inhibitors work by making the surface of the hydrate hydrophobic (avoid or repel when it makes contact with water) enabling it to be dispersed in the oil phase. Anti-agglomerates do not prevent hydrates from forming but hinders already formed gas hydrates from agglomerating into lumps that cause plugging, an example of an anti-agglomerate is quaternary ammonium salt (QUATS) which is the main active component used in corrosion inhibitors (Sami, et al 2013).

2.5 GAS HYDRATES AS A POSSIBLE SOURCE OF ENERGY

Gas hydrate is commonly known as the new clean energy (Zhang, et al 2019). Methane gas hydrate occurs in large deposits in the form of sedimentary rocks and solid sediments within 2000m of the earth's crust in deep-water and permafrost regions (Giavarini, et al 2011). The volume of methane hydrates under the same standard temperature and pressure condition contains 164 times more methane than one volume of gaseous methane. Potential deposits of gas in hydrates that are distributed on land and offshore are more than 1.5x1016m^3.

Methane gas can be extracted from the gas hydrates which can then be used as natural gas. Gas extraction is typically done by depressurization, thermal, and/or use of chemical inhibitors. During thermal stimulation, gas is released from the gas hydrate deposits by warming the formation through the direct heating of the formation or injection of heated fluid. Depressurization involves lowering the flow pressure of the gas hydrates, it is more preferred and economical than thermal stimulation, it does not require expending large energy and can be used to dissociate larger volumes of gas hydrates rapidly. Its main disadvantage is that it requires hydrate deposits with high porosity, also during the transportation phase the recovered gas and water may recrystallize into gas hydrates in the transportation pipelines leading to pipe plugging.

Hydrates occur in most arctic sedimentary regions and deep waters, this makes gas hydrate a widespread potential resource, they are naturally stable under cold temperature (deep-water or arctic) or high pressure (deep-water). The amount of gas (mostly methane) entrapped in natural hydrates is about 50 times greater than natural gas from conventional resources (Milkov and Sassen, 2002). A region of hydrate stability exists which is determined by overlapping the geothermal temperature gradient and hydrostatic pressure with the hydrate disassociation curve for seawater, Figure 2.15 shows a typical hydrate stability zone for three varying water depths. The curve indicates that the hydrate stability zone varies with the geothermal gradient and seabed temperature. The lower portion of the stability zone indicates the point where natural gas caged in hydrates (solid) transition to natural gas (vapor). This is often identified as a bottom simulating reflector (BSR) on seismic charts though it is not a reflection of multiple seabeds.

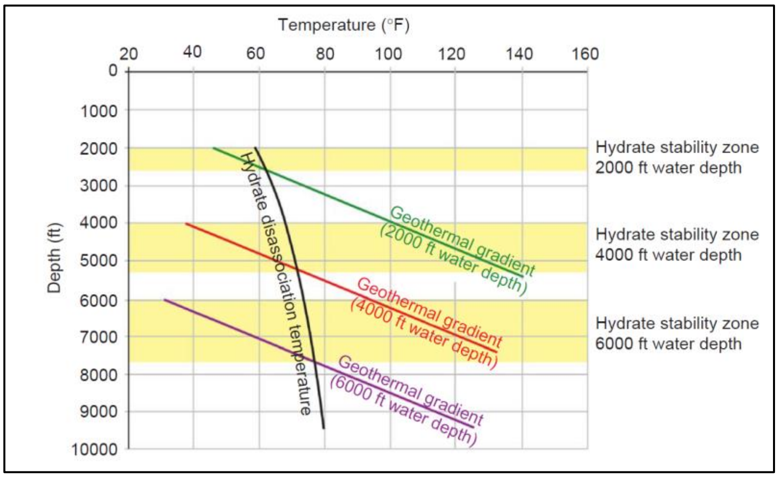

Figure 2.15 Natural hydrates stability (Bellarby, 2009).

In some circumstances, hydrates can form the cap for gas reservoirs. In a situation where the cap is penetrated by production wells due to the cap being thin, the melting of hydrates around the wellbore could breach the cap during the production of the warmer underlying gas (Bellarby, 2009).

2.6 RESEARCH AND EXPERIMENTS ON GAS HYDRATES

The Following studies are notable research and experiments on the formation and effects of gas hydrate.

2.6.1 Prediction of Hydrate Deposition in Pipelines to Improve Gas Transportation Efficiency and Safety By (Zhang, Et Al 2019)

The study simulated a 48 km long subsea pipeline transporting natural gas to predict the hydrate phase equilibrium region in the gas pipeline. The result shown in Figure 2.16 indicates that the region of hydrate phase equilibrium in the pipeline is around 220-48000m away from the pipe inlet. This suggests that hydrate deposition takes place at a distance of 220m away from the inlet.

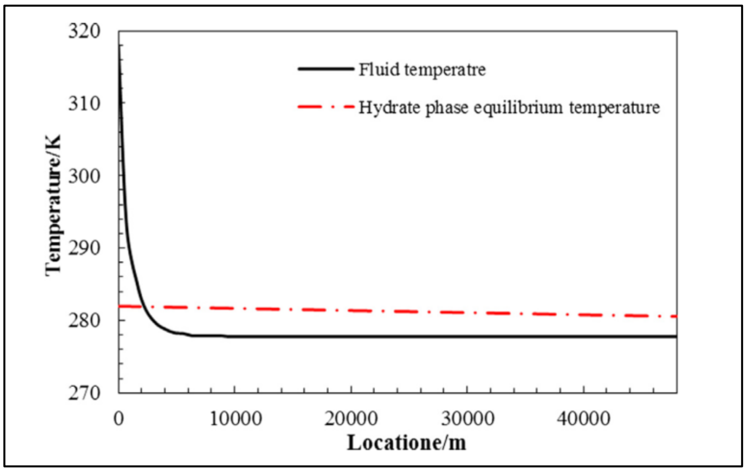

Figure 2.16 Prediction of hydrate phase equilibrium region in the subsea gas pipeline (Zhang, et al 2019).

Hence the safety and efficiency of the gas transportation system are significantly reduced by the formation and deposition of hydrates. It can be seen from the curve that the outlet pressure of the pipeline decreased significantly under the effect of hydrate deposition which decreased the effective inner diameter of the pipe and increased the flow velocity, this leads to an increase in pressure in the pipeline. Figure 2.17 shows a comparison between the effective radius of the pipeline and the proposed radius obtained from a test model, the results show that with an increase in hydrate deposition the effective radius of the pipe reduces. Also, there is a region of high-risk of hydrate deposition in the pipeline in which the two models showed similar results within the range of (5-20m) from the pipe inlet. Fluctuations in the outlet pressure of the pipeline due to hydrate deposition can damage pipeline joints and pumps, inducing severe accidents in production (Zhang, et al 2019).

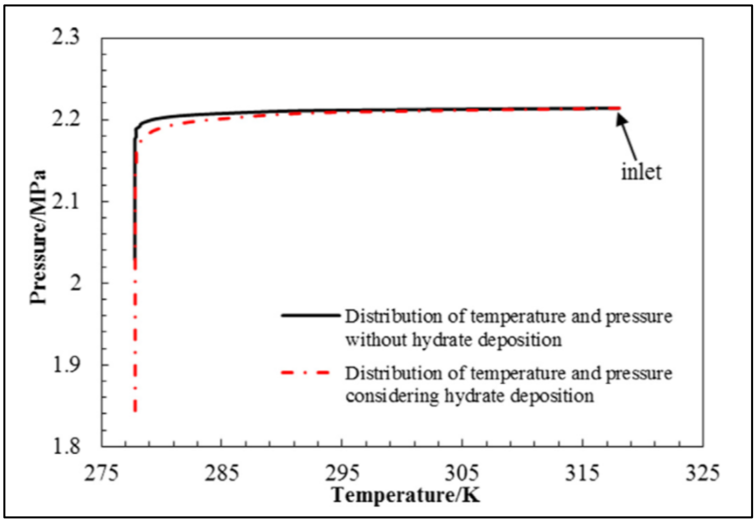

Figure 2.17 Comparison between temperature and pressure distribution in the pipeline (Zhang, et al 2019)

2.6.2 Hydrate Formation in Pipelines By (Dorstewitz And Mewes, 1995)

Hydrate formation was investigated experimentally in a horizontal pipe flow of gas and water by Dorstewitz, 1995. The pressure, temperature, and volumetric flow rate of each fluid were measured. The tubing made of glass had an inner diameter of 15mm. The formation of plugs starts on the pipe wall because the heat transfer is directed radially outwards. The onset of hydrate formation on the pipe wall is located at the interface between water and gas. Flow regime changed from the stratified flow of water and gas to intermittent flow pattern. Water was conveyed into the upper part of the pipe. The whole perimeter of the wall was covered by hydrates and a closed hydrate layer was achieved. The hydrate layer grew radially towards the center of the pipe. In certain volumetric flow rates and heat fluxes the hydrate, layer growth lead to plugging of the pipeline as shown in Figure 2.18.

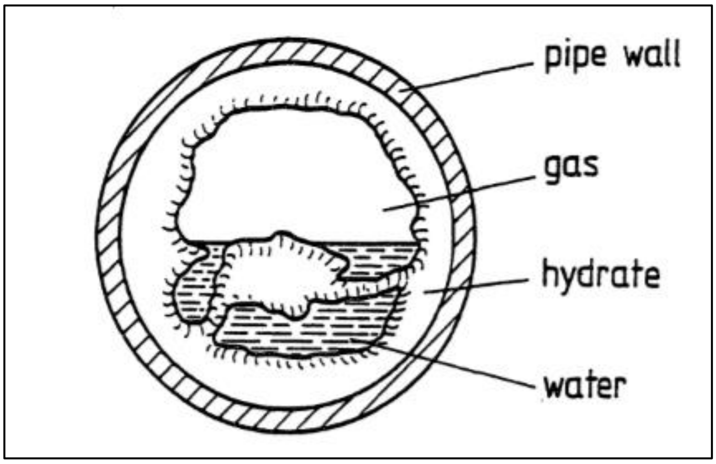

Figure 2.18 Hydrate formation pattern in a 15mm test pipe (Dorstewitz and Mewes, 1995).

Due to the void distribution, the value of the related pressure loss is low. The onset of hydrate formation occurred after 50 minutes. Only small hydrate particles were observed on the pipe wall. The particles were dragged along with the flow and the hydrates decompose in the bulk flow. Due to further deposition of hydrates, the whole perimeter of the pipe was covered by hydrates after 59 minutes and a solid hydrate layer developed.

2.6.3 Empirical Correlations

Other methods have been developed to predict the hydrate formation conditions of gas mixtures without the need for expensive experiments. The methods of predicting hydrate formation include empirical correlations, graphical calculations, software packages, and thermodynamic models. In this study, empirical correlations have been reviewed. The empirical correlations evaluated included: Hammerschmidt (1934), Motiee (1991), Towler and Mokhatab (2005), Safamirzaei M. (2015), and Chavoshi S. 2018. All the equations calculate the hydrate formation temperature (T-explicit) for gas mixtures. Most correlations used to estimate the hydrate formation conditions calculate for T-explicit because the pressure is usually known from the process and/or flow transfer requirements, and hydrate formation temperature is the parameter required.

In 1934, Hammerschmidt proposed a correlation for gas hydrate formation, shown in Equation 1 (Hammerschmidt, 1934).

$$T = 8.9P^{0.285} \ldots\ldots\ldots\ldots\ldots\ldots\ldots (1)$$

Where temperature T is in (°F) and pressure P is in (Psi). This equation, although simple does not consider the effect of gas specific gravity on hydrate formation.

Motiee (1991) developed Equation (2). Where temperature T is in (°F) and pressure P is in (Psi).

$$T = -238.24469 + 78.99667\ log\ P - 5.352544(log\ P)2 + 349.473877\gamma - 150.854675\gamma 2 - 27.604065\gamma log\ P \ldots\ldots\ldots\ldots (2)$$

The equation is widely used in the gas industry due to its accuracy in predicting the hydrate formation temperature for various natural gas mixtures but has 6 adjustable parameters which are relatively high and can lead to errors when carrying out quick hand calculations.

In 2005, Towler and Mokhatab proposed a relatively simple equation for estimating hydrate temperatures as a function of the pressure and the gas gravity shown in Equation 3.

$$T = 13.47 lnP + 34.27 ln\gamma - 1.675 ln\gamma lnP - 20.35 \ldots\ldots\ldots\ldots\ldots (3)$$

Where temperature T is in (°F) and pressure P is in (Psi). (Towler & Mokhatab, 2005)

In 2015, Safamirzaei proposed a T-explicit correlation for specific gravity $0.55 \leq \gamma \leq 1$ shown in Equation 4. (Safamirzaei M.,2015).

$$T = A\gamma^{B}(ln\, P)^{C} \ldots\ldots\ldots\ldots\ldots\ldots\ldots\ldots (4)$$

Where:

$A = 194.681789$

$B = 0.044232$

$C = 0.189829$

Where P is in (kPa) and T is in (K). The study and its subsequent equation are not peer-reviewed, also the method in which the model was derived was not stated in the study.

Chavoshi S. 2018 developed a hydrate formation equation shown in Equation 5 by fitting a polynomial function to 100 experimental data points using the curve fitting tool in MATLAB software.

$$T = 242 \times \gamma^{0.02} \times P^{0.021} \ldots\ldots\ldots\ldots\ldots\ldots (5)$$

where P is the pressure in (kPa), γ is specific gravity, and T is the temperature in (K).

Additionally, there are other equations such as Kobayashi (Kobayashi, Song, Sloan, & Bradley, 1987) and Ameripour and Barrufet (Ameripour & Barrufet, 2009). The main advantage of these correlations is their simplicity and portability. In most cases the required input data are accessible and can be calculated with a simple calculator, also the results agree with the experimental data and sometimes better than results obtained from commercial software. Despite the advantages, these correlations have limitations, most of them can only be used in a limited range of temperature, pressure, and specific gravity and they show a significant error at higher pressure. Some correlations are only accurate for certain gas mixtures such as sweet gas or with pure formers, also some correlations are only useful when a comprehensive analysis of gas is accessible. Some models use the artificial neural network (ANN) such as (Elgibaly & Elkamel, 1998), (Zahedi, Karami, & Yaghoobi, 2009), and (Khamehchi, Shamohammadi, & Yousefi, 2013). These models are often complicated and are not suitable for hand calculations (Safamirzaei M., 2015).

CHAPTER 3 METHODOLOGY

3.1 DATA COLLECTION

In this study, 460 experimental data points were collected from 15 different studies on hydrate formation, the studies are listed in Appendix A. The units of temperature for the data points were converted to Kelvin (K) and the pressure converted to Kilopascals (kPa). Gas compositions of natural gas from the Bakken Formation were collected from various wellheads of oil and gas producing wells by the Energy and Environmental Research Center (EERC) and presented in the study by (Wocken et al, 2012) and also (Eenews, 2013) as shown in Table 3.1.

Table 3.1 Gas Composition Data from Wellheads in the Bakken Formation in North Dakota (Provided to the EERC by several North Dakota operators)

Component	**Gas Composition (Mol%)**							
	A	B	C	D	E	F	G	H
H2O (Water)	0.02	0.29	0	0	0	0	0	0
N2 (Nitrogen)	5.21	7.10	1.72	0.86	1.435	1.715	9.9	2.09
CO2 (Carbon dioxide)	0.57	0.51	1.72	0.86	1.435	1.715	9.9	2.09
H2S (Hydrogen sulfide)	0.01	2.00	0.19	0.18	0.08	0.05	1.00	0.12

C1 (Methane)	57.67	59.30	70.23	48.07	73.93	68.05	52.9	66.17
C2 (Ethane)	19.94	17.73	13.94	18.78	13.25	14.2	11.32	13.15
C3 (Propane)	11.33	9.42	6.7	14.87	5.55	8.05	8.52	7.01
I-C4 (Isobutane)	0.97	0.70	5.5	16.38	4.32	6.22	6.46	9.37
N-C4 (N-butane)	2.83	2.03	0	0	0	0	0	0
I-C5 (Isopentane)	0.38	0.27	0	0	0	0	0	0
N-C5 (N-pentane)	0.55	0.38	0	0	0	0	0	0
C6 (Hexane)	0.22	0.16	0	0	0	0	0	0
C7	0.09	0.07	0	0	0	0	0	0
C8	0.04	0.03	0	0	0	0	0	0
C9	0.01	0.01	0	0	0	0	0	0
Specific gravity	0.87	0.84	0.79	1.04	0.76	0.82	0.93	0.85

The experimental data points and gas composition data were transferred to excel to calculate the hydrate formation temperature for all the empirical models reviewed in this study.

3.2 MODEL DEVELOPMENT

The model was developed by carrying out nonlinear regression on the 460 experimental data points in MATLAB 2020 using the curve fitting tool. Using the Custom Equation tool on MATLAB, a custom equation was obtained which achieved a 0.9742 R-square value indicating a 97.42% accuracy fitting the curve of all 460 experimental data points. The following steps were taken to carry out the regression analysis.

1. All 460 experimental data points of pressure, specific gravity, and temperature were imported into MATLAB as x, y, and z respectively with x and y being the input (independent variables) and z the output (dependent variable)
2. The curve fitting tool was selected, and the Nonlinear Least Square method was selected as shown in Figure 3.1

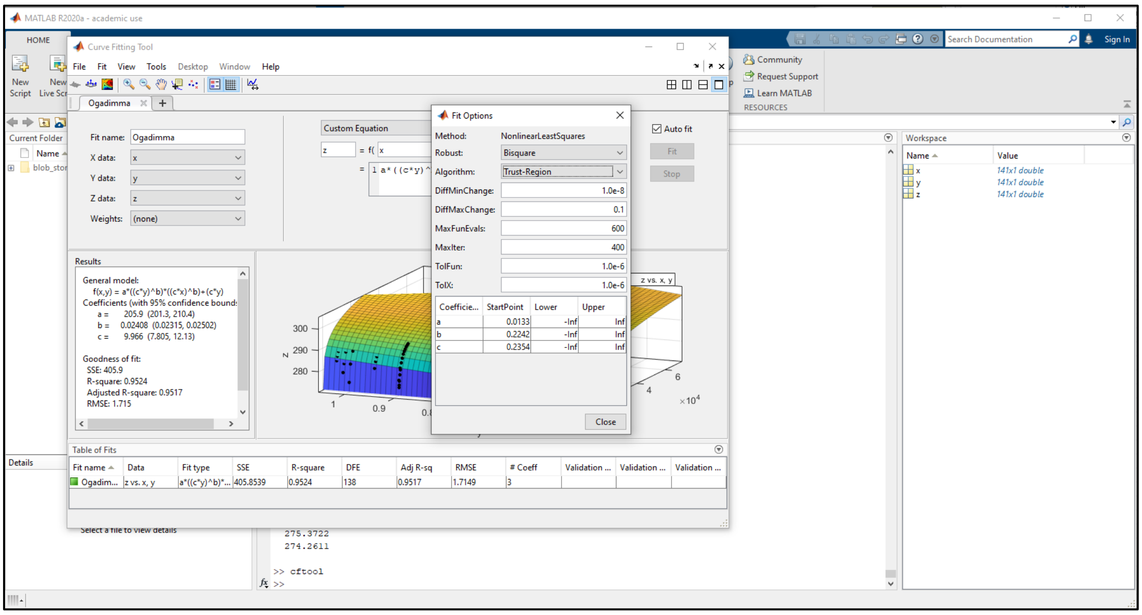

Figure 3.1 The Nonlinear Least Square method

3. By continuous trial, various equations were written inside the custom equation toolbox until an equation that fit the curve of all 460 data points more accurately was written. It produced an R-square value of 0.9742, this indicates a 97.42% coverage of the experimental data points as shown in Figure 3.2

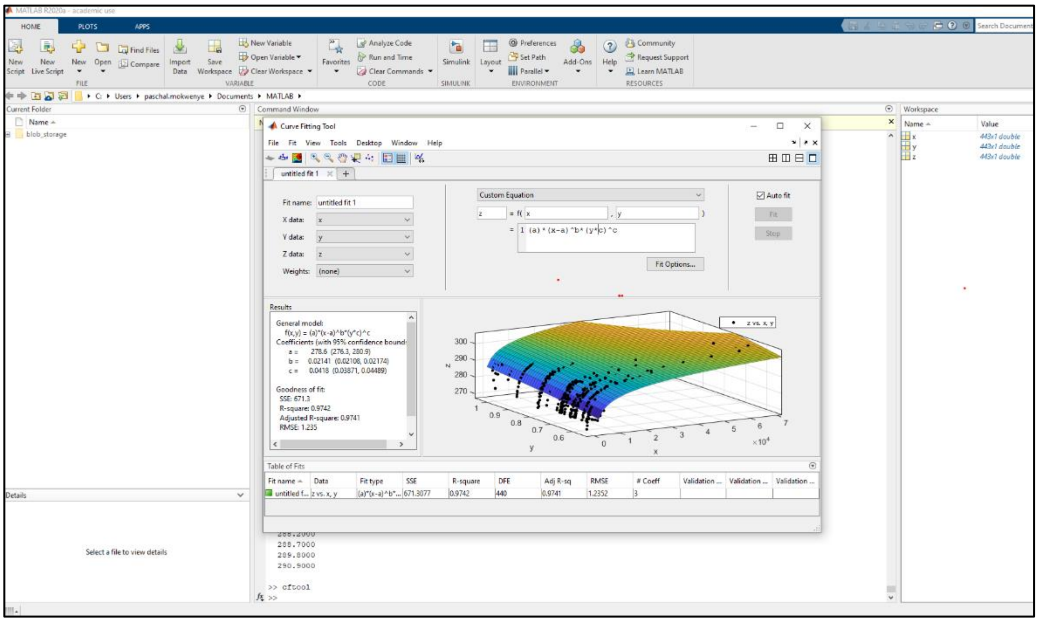

Figure 3.2 Custom equation giving 97.42% accuracy

4. The final equation called New Correlation was obtained, and the coefficients of A, B, and C were defined from the regression shown in Figure 3.3

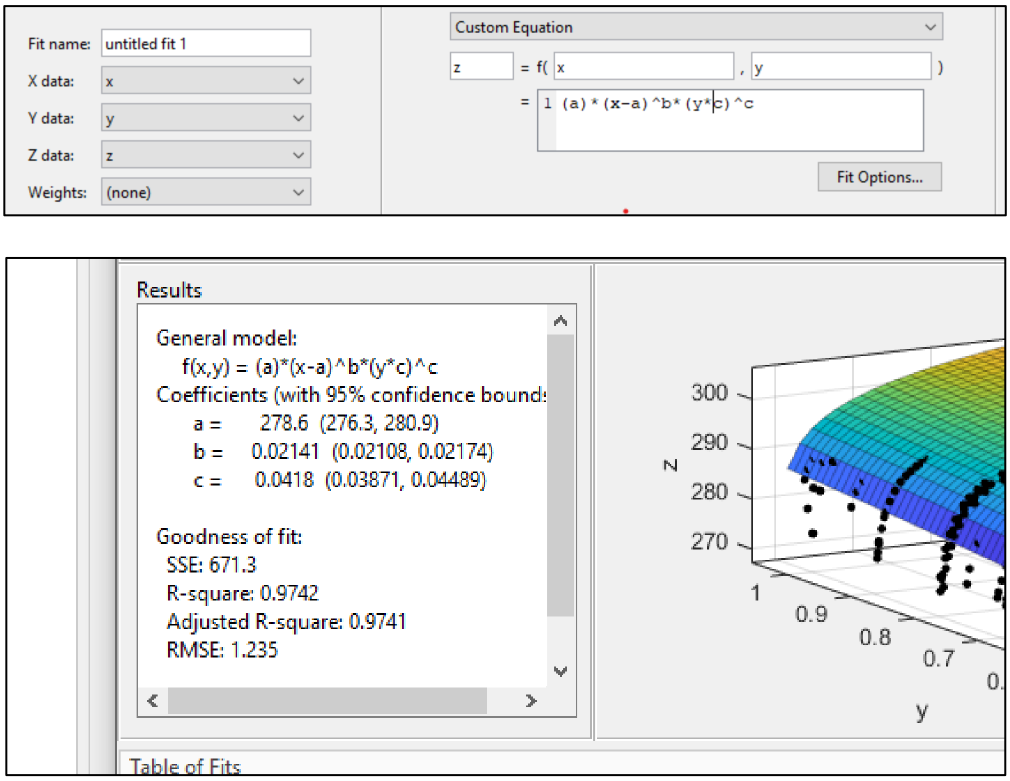

Figure 3.3 Custom equation and coefficients of A, B, and C

The equation for New Correlation is given in Equation 6, with the derived coefficients of A, B, and C given below. These coefficients were tuned optimally by MATLAB to cover the temperature range of 260 to 305 K.

$$T = A \times (P - A)^{B} \times (\gamma \times C)^{C} \dots\dots\dots\dots\dots\dots\dots.. (6)$$

$\mathrm{A} = 278.6$

$\mathrm{B} = 0.02141$

$C = 0.0418$

Where

$T = Hydrate\ formation\ temperature\ (in\ Kelvin)$

$\gamma = Specific\ gravity$

$P = Pressure\ (in\ Kilopascals)$

The molecular weight and specific gravity of the gas can be calculated from the gas composition of the gas mixture as shown in Equations 6 and 7.

$$Molecular\ Weight\ (MW^{NG}) = \sum \left[\frac{mol\ \%}{100} \times Molecular\ \ weight\ of\ gas\right] \dots\dots\dots. (7)$$

$$Specific\ gravity\ (\gamma) = \frac{MW^{NG}}{MW^{air}} \dots\dots\dots\dots\dots\dots\dots\dots\dots\dots.. (8)$$

$MW^{NG} = \ Molecular\ weight\ of\ Natural\ gas$

$MW^{air} = Molecular\ weight\ of\ Air$

The correlation was carried out in Excel with the values of pressure and specific gravity used to calculate the hydrate formation temperature.

The gas composition data of the Bakken formation obtained from EERC were designated as Gas Composition A to H.

3.3 MODEL EVALUATION

The proposed model New Correlation was evaluated based on its accuracy in calculating the reference experimental hydrate formation temperature from the 460 data points, it was also compared to models developed by Hammerschmidt (1934), Motiee (1991), Towler and Mokhatab (2005), Safamirzaei M. (2015), and Chavoshi S. 2018.

The accuracy of the models was evaluated based on their deviation from reference experimental values. The Average Relative Deviation (ARD) and Average Absolute Deviation (AAD) was used to assess the deviation of the models, it shows the suitability of a correlation to calculate the hydrate formation temperature by highlighting its deviation from the reference experimental value (Safamirzaei M. 2015). The equation for Average Relative Deviation (ARD) and Average Absolute Deviation (AAD) are shown in Equations 9 and 10.

$$ARD\ (\%) = \frac{100}{n} \sum_{i=1}^{n} \left| \frac{T_{(K)}^{exp} - T_{(K)}^{cal}}{T_{(K)}^{exp}} \right| \ldots\ldots\ldots\ldots\ldots\ldots\ldots\ldots\ldots\ldots\ldots\ldots (9)$$

$$AAD = \frac{1}{n} \left| T_{(K)}^{exp} - T_{(K)}^{cal} \right| \ldots\ldots\ldots\ldots\ldots\ldots\ldots\ldots\ldots\ldots\ldots\ldots\ldots (10)$$

where:

$n = number\ of\ data\ points$

$T_{(K)}^{exp} = Experimental\ hydrate\ formation\ temperature$

$T_{(K)}^{cal} = Calculated\ hydrate\ formation\ temperature$

The models will also be evaluated based on their number of adjustable parameters, the higher the parameters the more the models will require complex calculations to calculate the hydrate formation temperature, this will lead to errors when carrying simple hand calculations.

Using the New correlation, the hydrate formation temperature was calculated and compared to experimental values as well as other correlations. The gas compositions of natural gas from The Bakken were applied to the New Correlation and the hydrate formation temperature was calculated and also compared to values of Katz 1945 gas-gravity chart.

CHAPTER 4 RESULTS

The result of the hydrate formation temperature calculated for all the models including the New Correlation are given in Appendix B. Calculations were made using the pressure and specific gravity of 460 experimental data points obtained from the studies 15 listed in Appendix A. The specific gravity of the gas mixtures ranges from 0.55 – 1.

4.1 AVERAGE RELATIVE DEVIATION (ARD) AND AVERAGE ABSOLUTE DEVIATION (AAD)

Table 4.1 shows the Average Relative Deviation (ARD) and Average Absolute Deviation (AAD) of the models from the reference 460 experimental values of hydrate formation temperature. Table 4.1 also shows the number of adjustable parameters of each model. The models include the New Correlation (NC), Hammerschmidt (1934), Motiee (1991), Towler and Mokhatab (2005), Chavoshi S. 2018, and Safamirzaei M. (2015). A lower value of ARD indicates a lower deviation from experimental values and therefore a higher accuracy.

Table 4.1 ARD and AAD of all empirical models compared to experimental hydrate formation temperature.

Correlations	Average Relative Deviation (ARD)	Average Absolute Deviation (AAD)	Number of Adjustable Parameters
New Correlation	0.393	1.115	3
Towler and Mokhatab (2005)	0.485	1.395	4
Motiee (1991)	0.592	1.675	6
Hammerschmidt (1934)	0.998	2.892	2
Chavoshi S. (2018)	0.529	1.497	3
Safamirzaei M. (2015)	0.406	1.157	3

The model by Motiee (1991) has the highest number of adjustable parameters with 6, this is followed by Towler and Mokhatab (2005) with 4 parameters. Models with a high number of parameters require a long and complex calculation to obtain results, this is prone to errors when doing quick hand calculations. The New correlation, Safamirzaei M. (2015) and Chavoshi S. (2018) have 3 adjustable parameters while Hammerschmidt (1934) has 2 parameters.

Table 4.2 shows the ARD and AAD of the models compared to experimental values obtained from the study by Wilcox W. et al (1941) with specific gravity ranging from 0.597 to 0.668.

Table 4.2 ARD and AAD of models compared to experimental values from Wilcox W. et al (1941).

Models	Average Relative Deviation ARD	Average Absolute Deviation AAD
New Correlation	0.241	0.700
Towler and Mokhatab (2005)	0.437	1.282
Motiee (1991)	0.618	1.779
Hammerschmidt (1934)	1.275	3.747
Chavoshi S. (2018)	0.314	0.909
Safamirzaei M. (2015)	0.360	1.048

Table 4.3 shows the ARD and AAD of the models compared to experimental values obtained from Sloan D. (1990) with specific gravity ranging from 0.57 to 0.8.

Table 4.3 ARD and AAD of the models compared to experimental values obtained from Sloan D. (1990)

Models	Average Relative Deviation ARD	Average Absolute Deviation AAD
New Correlation	0.353	1.006
Mokhatab 2005)	0.441	1.268
Motiee (1991)	0.670	1.901
Hammerschmidt (1934)	0.955	2.778
Chavoshi S. 2018	0.496	1.407
Safamirzaei M. (2015)	0.436	1.250

Table 4.4 shows the ARD and AAD of all 6 models compared to experimental values obtained from the study carried out by Bahadori and Vuthaluru (2009).

Table 4.4 ARD and AAD of all 6 models compared to experimental valves obtained from (Bahadori and Vuthaluru, 2009)

Models	Average Relative Deviation ARD	Average Absolute Deviation AAD
New Correlation	0.550	1.543
Towler and Mokhatab (2005)	0.646	1.841
Motiee (1991)	0.451	1.277
Hammerschmidt (1934)	1.393	3.973
Chavoshi S. (2018)	0.662	1.853
Safamirzaei M. (2015)	0.465	1.305

Table 4.5 shows the ARD and AAD of all 6 models compared to experimental values obtained from the study carried out by Davarnejada R. (2014) on the Lavan gas field which has a specific gravity of 0.65.

Table 4.5 ARD and AAD all 6 models compared to experimental valves obtained from (Davarnejada R. 2014)

Models	Average Relative Deviation ARD	Average Absolute Deviation AAD
New Correlation	0.480	1.380
Towler and Mokhatab (2005)	0.951	2.787
Motiee (1991)	0.336	0.962
Hammerschmidt (1934)	2.080	6.163
Chavoshi S. (2018)	0.463	1.310
Safamirzaei M. (2015)	0.320	0.918

CHAPTER 5 DISCUSSION

The most accurate way of determining the hydrate formation conditions of natural gas transported in pipelines is by measuring the formation pressure and temperature directly, this process is expensive, time-consuming, and not feasible for long and subsea pipelines. As a result, correlations, and thermodynamic models have been developed to estimate the hydrate formation conditions without carrying out experiments. When using thermodynamic models, it is possible to improve the model's accuracy by adjusting parameters, if the predicted results significantly deviate from experimental values. The ARD and AAD of the New Correlation was compared to that by Hammerschmidt (1934), Motiee (1991), Towler and Mokhatab (2005), Chavoshi S. 2018, and Safamirzaei M. (2015) to assess its accuracy. The result of the pressure-temperature curve of all the models will be discussed in this chapter.

5.1 Analysis of Pressure -Temperature Curves, Average Relative Deviation (ARD) and Average Absolute Deviation (AAD) of the Models

Figure 5.1 shows the pressure-temperature curve of 460 experimental data points compared to the values calculated by the 6 models. Specific gravity range from 0.55-1. The New correlation (colored yellow) showed the highest accuracy in following the experimental curve compared to other models. It tracked the experimental curve more closely across the range of pressure and specific gravity. There is a slight deviation at higher pressure, but overall, the New Correlation followed the experimental points very closely.

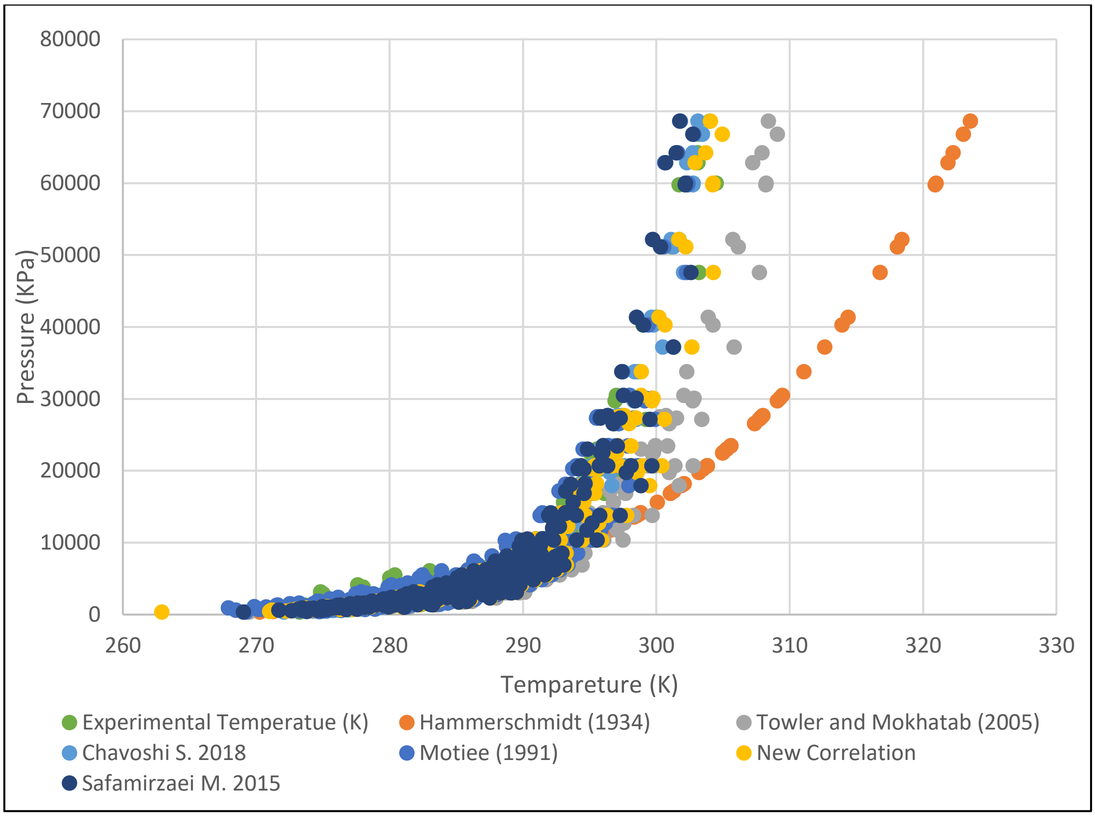

Figure 5.1 Pressure – temperature curve of experimental values from 460 data points compared to all 6 models

Figure 5.2 shows the bar chart of ARD and AAD for all 6 models, the New correlation has the lowest ARD of 0.3932 and AAD of 1.1149 compared to other models. This shows that the New correlation has superior accuracy in calculating the HTF across the range of specific gravity, due to its lower deviation from experimental values compared to the other models. Safamirzaei M. (2015) model shows the second-highest accuracy followed by the Towler and Mokhatab (2005)

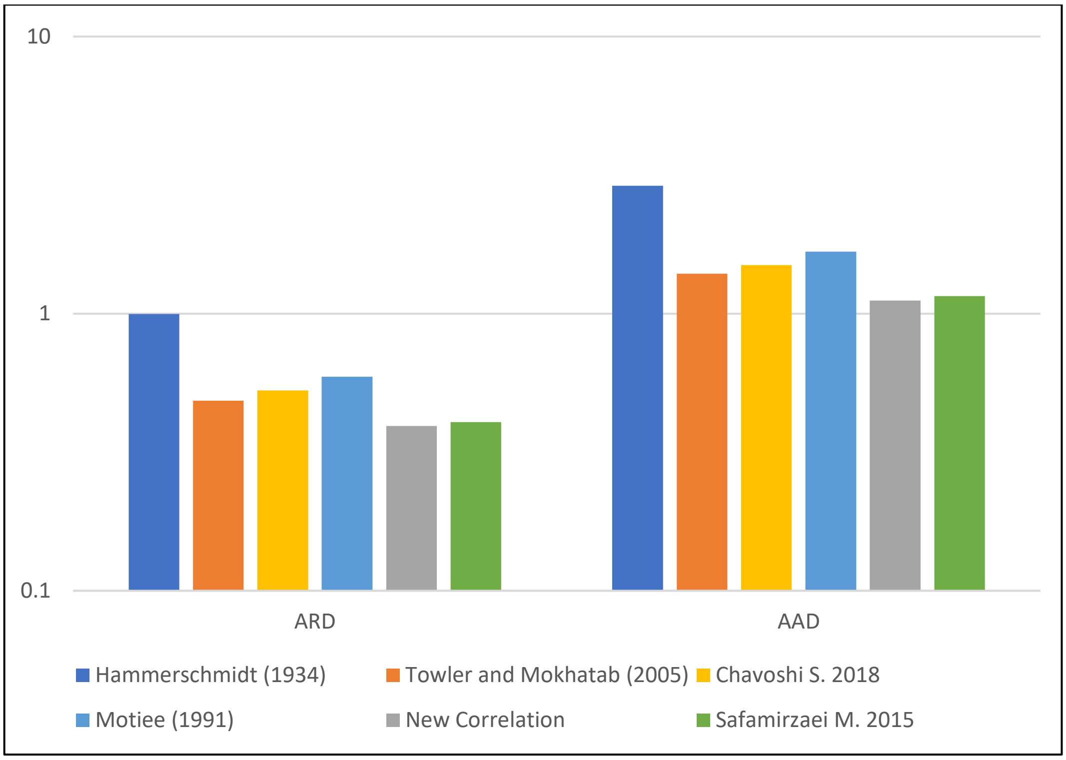

Figure 5.2 ARD and AAD of the models from 460 experimental values.

Figure 5.3 shows the pressure-temperature curve of experimental values obtained from Wilcox W. et al (1941) compared to all 6 models. The study has 32 data points with the specific gravity ranging from 0.59-0.67. The New Correlation shows excellent accuracy, tracking the experimental points more accurately than all the other models. This is confirmed by the values of ARD and AAD in Figure 5.4 which shows that New Correlation has the lowest ARD of 0.2413 and AAD of 0.4644. It is followed by Chavoshi S. 2018 which has the second-lowest ARD and AAD.

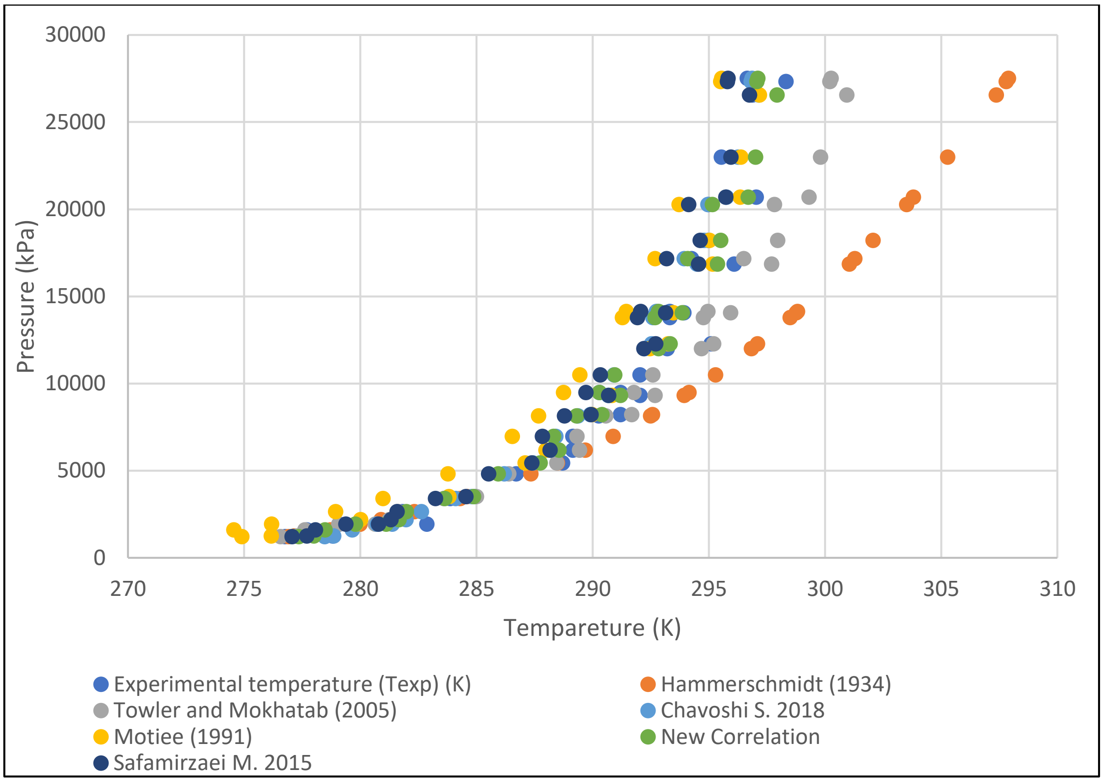

Figure 5.3 Pressure - temperature curve of experimental data obtained from Wilcox W. et al (1941) and all 6 models.

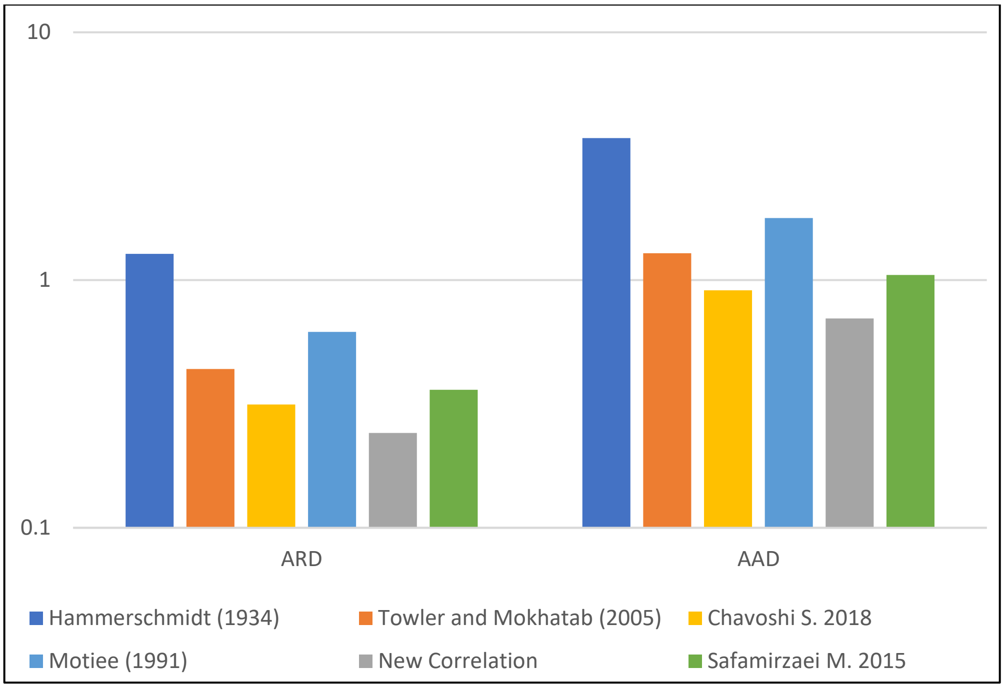

Figure 5.4 ARD and AAD of all 6 models from the experimental values of Wilcox W. et al (1941).

Figure 5.5 shows the pressure-temperature curve of experimental values obtained from Sloan D. (1990) compared to the 6 models. The study has 123 data points with the specific gravity ranging from 0.58-0.80. The New Correlation produced the highest accuracy following the experimental points more accurately than the other models. This is followed by Safamirzaei M. 2015 which produced the second-highest accuracy. The chart of ARD and AAD, showed in Figure 5.6, shows that the New Correlation has the lowest deviation from experimental values with ARD of 0.3524 and AAD of 1.0057. Safamirzaei M. 2015 has the second-lowest deviation with ARD of 0.4360 and AAD of 1.2498.

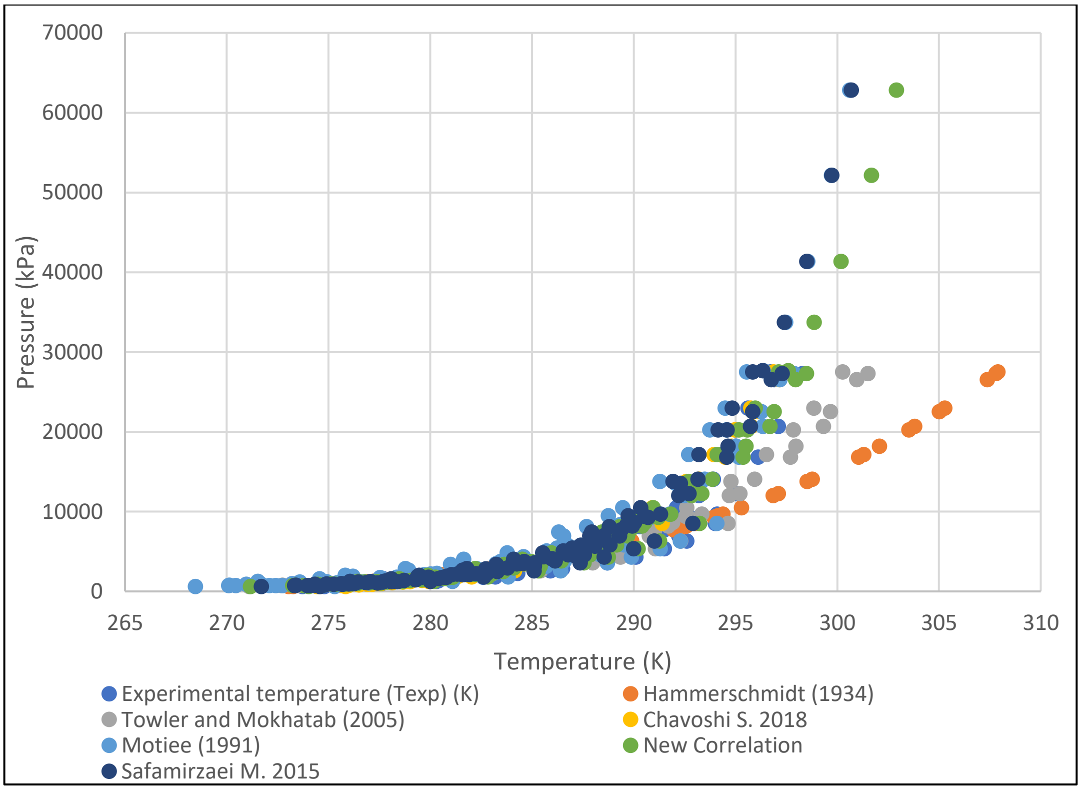

Figure 5.5 Pressure – temperature curve of experimental values obtained from Sloan D. (1990) compared to the 6 models.

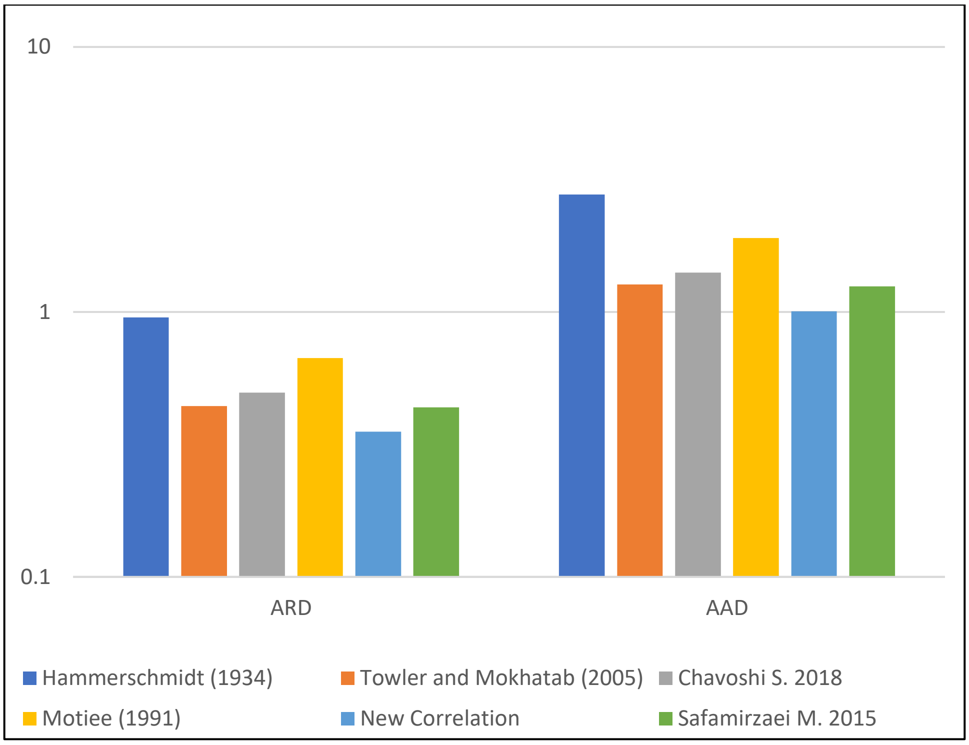

Figure 5.6 ARD and AAD of all 6 models for experimental values obtained from Sloan D. (1990)

Figure 5.7 shows the pressure-temperature curve of experimental data collected from (Bahadori and Vuthaluru, 2009) compared to values from all 6 models. The study has 22 data points with the specific gravity ranging from 0.55-1. The model by Motiee (1991) produced the highest accuracy, tracking the experimental point, this is followed by the Safamirzaei M. (2015) model. The New Correlation produced the third-highest accuracy compared to the other models, it followed the experimental curve closely except for slight deviations at high pressure. The chart of ARD and AAD in Figure 5.8 shows that the model by Motiee (1991) with the ARD of 0.4514 and AAD of 1.2765. Safamirzaei M. (2015) showed the second-lowest ARD and AAD, followed by the New Correlation produced the third-lowest ARD of 0.5503 and AAD of 1.5427.

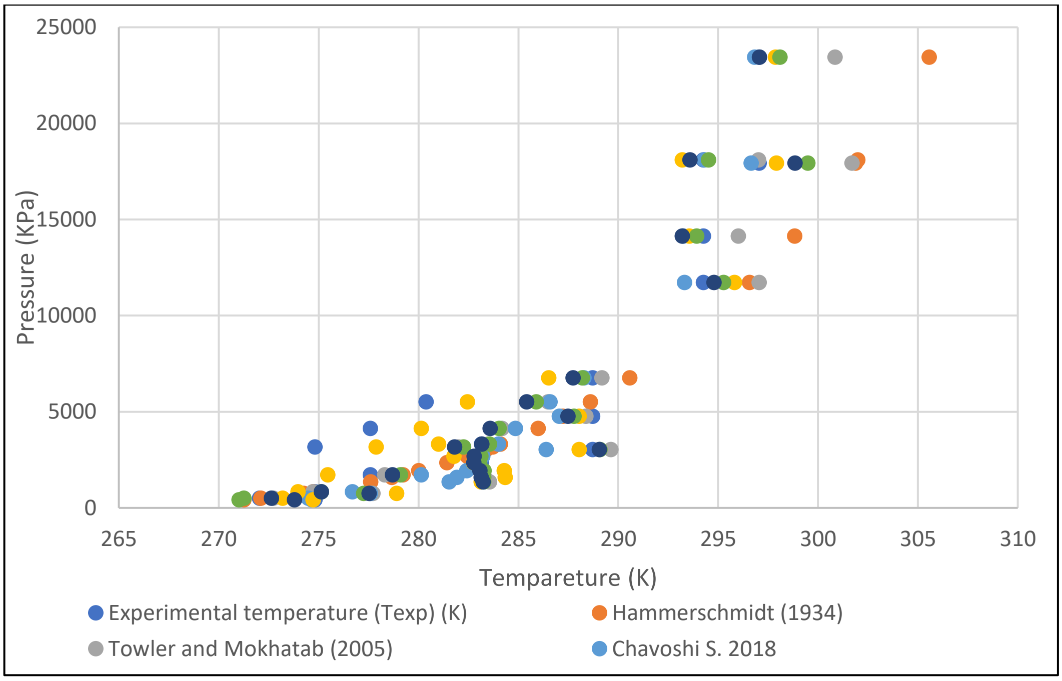

Figure 5.7 Pressure – temperature curve of experimental data from (Bahadori and Vuthaluru, 2009) compared to the 6 models

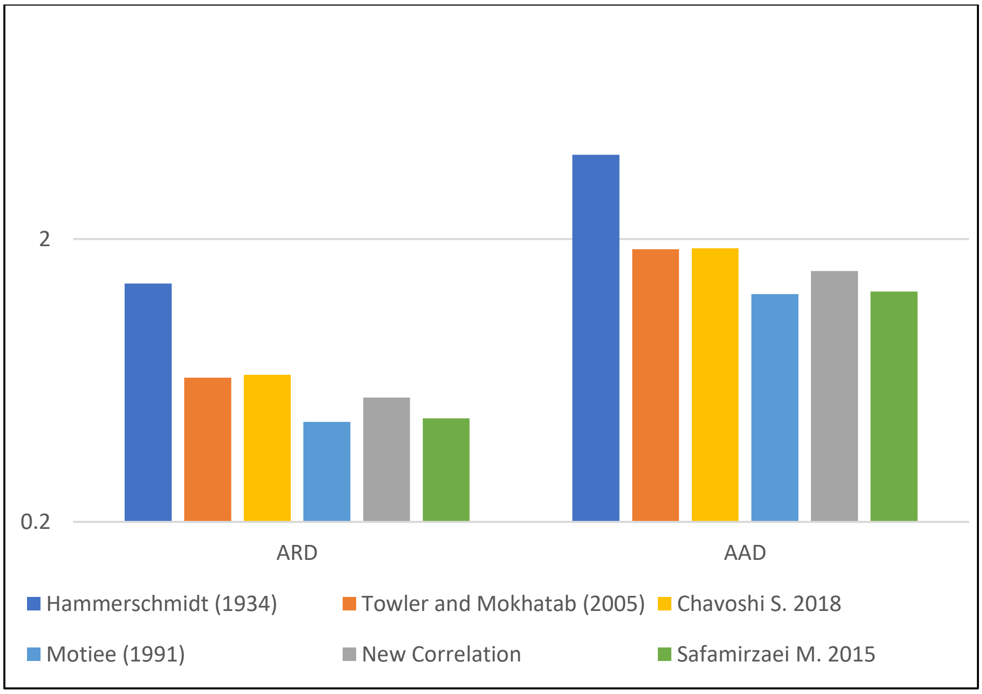

Figure 5.8 ARD and AAD of the models compared to experimental data from (Bahadori and Vuthaluru, 2009)

Figure 5.9 shows the pressure-temperature curve of experimental data collected by Davarnejad, R. (2014) from the Lavan gas field with a specific gravity of 0.65. The curve is compared to that of all 6 models. The curve shows that Safamirzaei M. (2015) produced the highest accuracy, tracking the experimental point closely, this is followed by the model by Motiee (1991). The New Correlation produced the third-highest accuracy following the experimental curve closely up to the pressure of 10000 kPa where it starts to deviate. The chart of ARD and AAD in Figure 5.10 shows that Safamirzaei M. (2015) has the lowest ARD (0.3203) and AAD (0.9184) followed by Motiee (1991). The New Correlation produced the third-lowest ARD and AAD with values of 0.4796 and 1.3803, respectively.

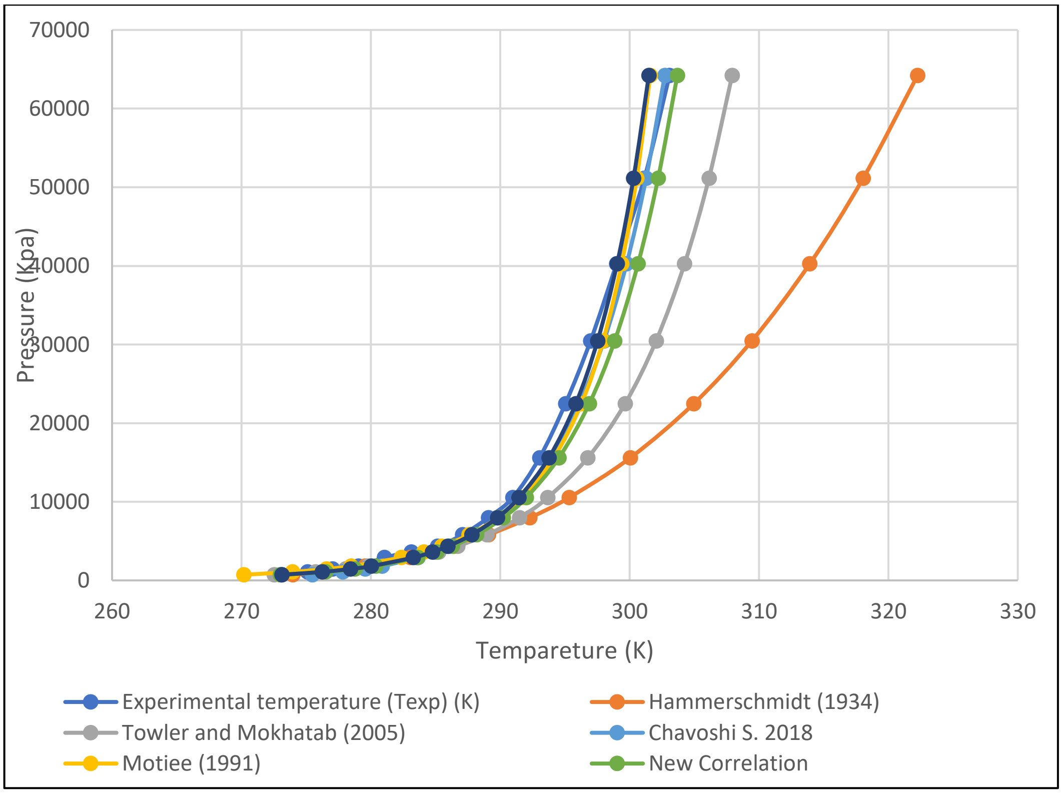

Figure 5.9 Pressure – temperature curve of experimental data collected by Davarnejad, R. (2014) compared to the 6 models.

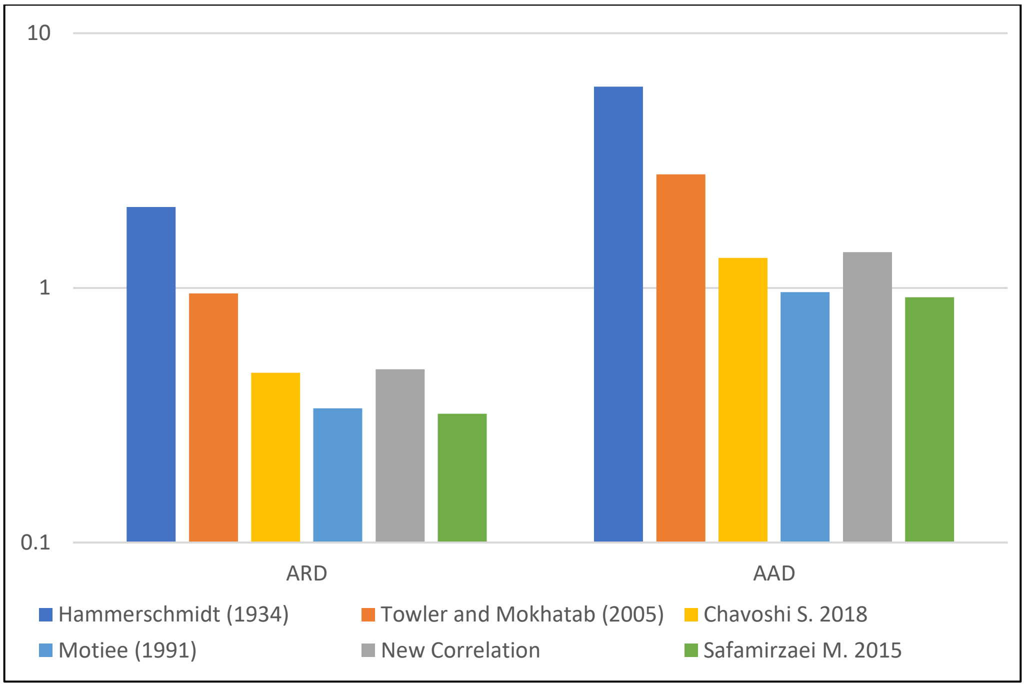

Figure 5.10 ARD and AAD of the models compared to experimental data from Davarnejad, R. (2014)

The New Correlation produced consistently high accuracy and overall superior accuracy in predicting the hydrate formation temperature of natural gas mixtures compared to other models. The experimental values of pressure and specific gravity range from 330 to 68600 kPa and 0.55 to 1.0 respectively. The New correlation having only three adjustable parameters, requires less complex calculations than those proposed by Motiee (1991), Towler and Mokhatab (2005), and Safamirzaei M. (2015) which have logarithmic functions and as such require more complex calculations. The New Correlation offers a simple mathematical equation that can accurately predict the hydrate formation temperature of various gas mixtures.

Figure 5.11 shows the scatterplot of Experimental HTF from all 460 data points T(exp) versus Calculated HTF from New Correlation T(cal). The plot shows that the points of New Correlation align accurately with experimental hydrate formation temperature indicating a strong agreement with the experimental data, except for some slight deviations at high temperature.

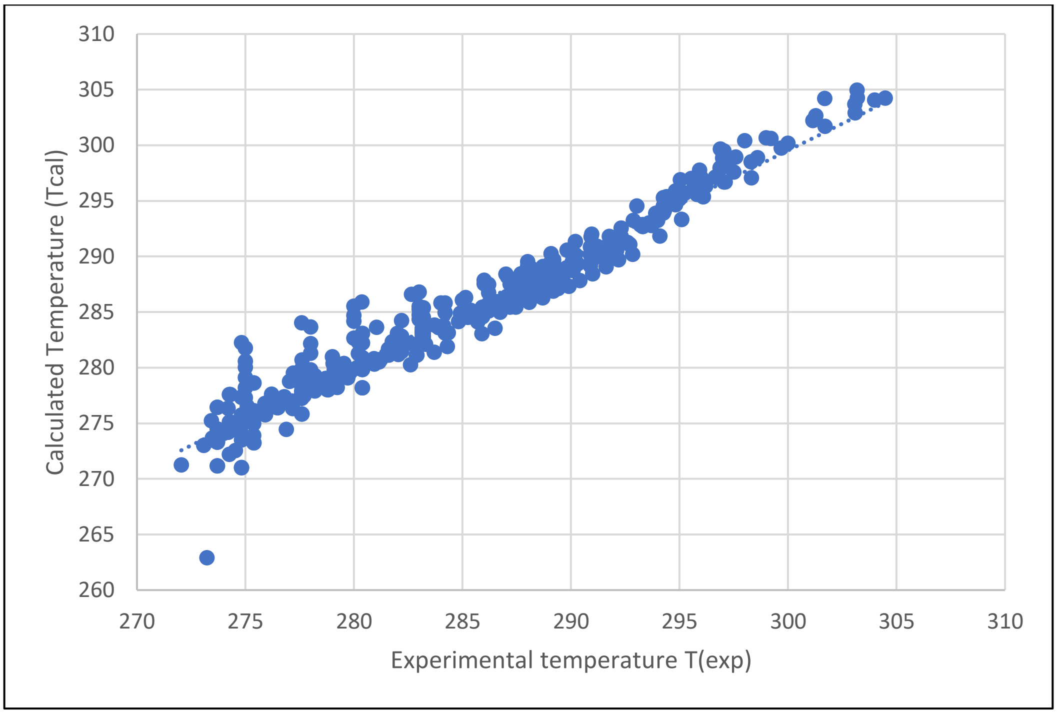

Figure 5.11 Scatterplot of Experimental temperature T(exp) (K) versus Calculated Temperature Tcal (K) from New Correlation

5.2 Analysis of the Hydrate Formation Temperature (HTF) for The Bakken Gas Compositions

Figure 5.12 shows the pressure-temperature curve of The Bakken gas composition A with a specific gravity of 0.87. The values of HFT were calculated using the New Correlation and compared to Katz's 1945 gravity chart having a specific gravity of

0.9. The curve of New Correlation shows very good accuracy tracking the Katz's 1945 gravity chart, with a slight deviation at higher pressures from 10000 kPa and above.

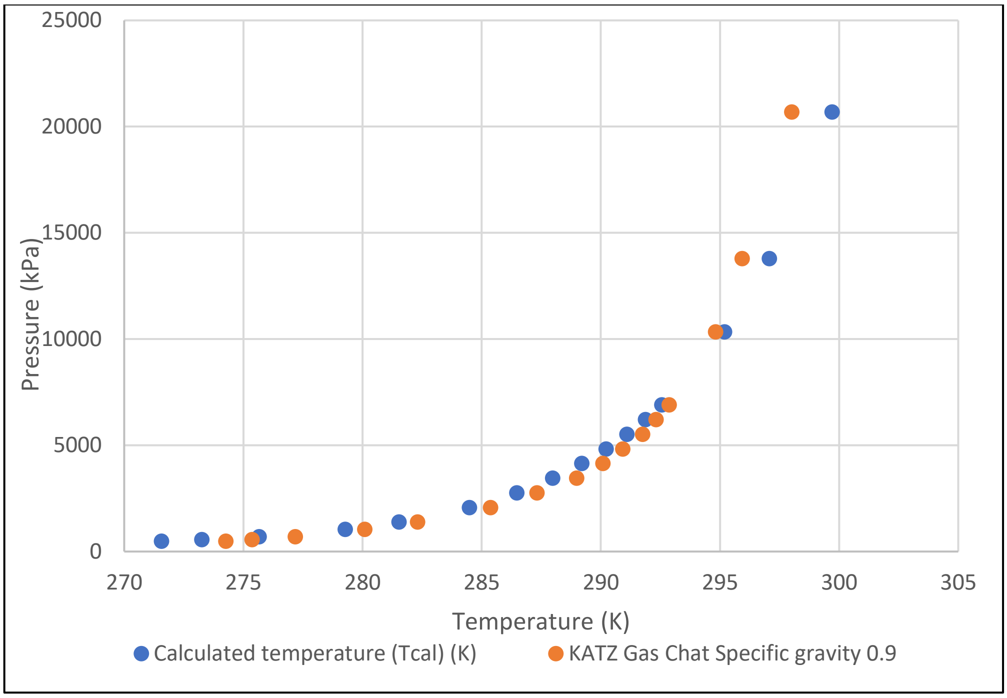

Figure 5.12 Pressure – temperature curve for The Bakken Gas Composition A

The curve also indicates that the hydrate formation temperature increases rapidly at lower pressures than at higher pressures. For example, within the pressure range of 482.63 to 6205.28, there is an increase in hydrate formation temperature of 20.31 K, this is a large increase in temperature for a small increase in pressure. However, moving to a higher pressure range of 6894.75 to 20684.27 kPa there is an increase in hydrate formation temperature of 7.14 K, this represents a small increase in temperature for a large increase in pressure.

The same increase in HFT relative to pressure can be seen in the curve of Gas Composition B shown in Figure 5.13.

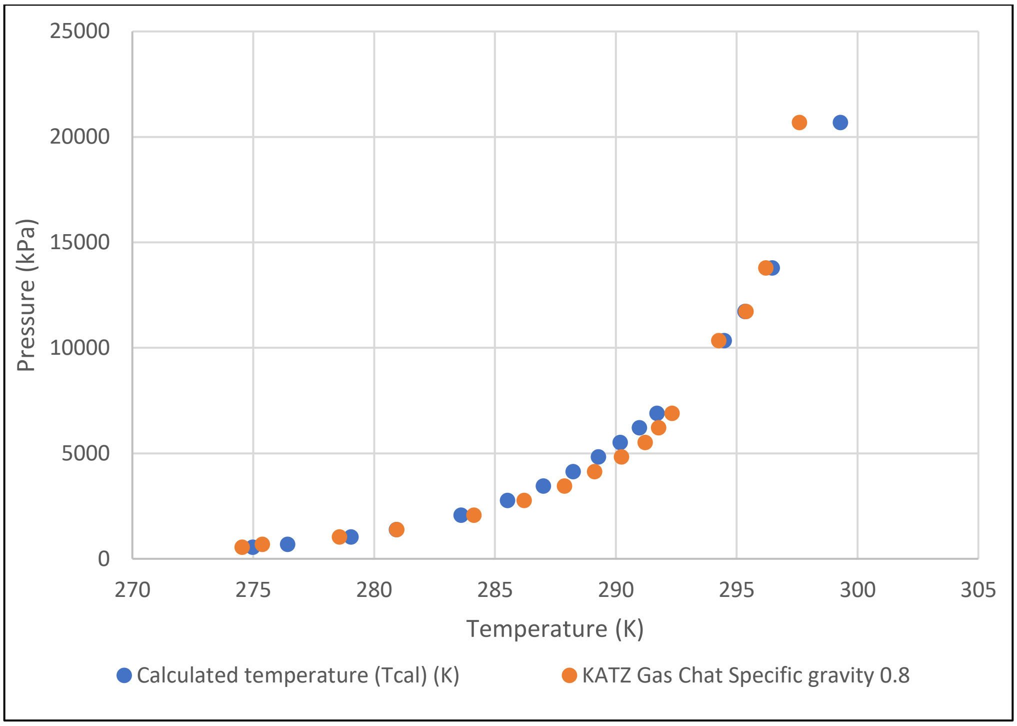

Figure 5.13 Pressure – temperature curve for The Bakken Gas Composition B

Figure 5.13 shows the pressure-temperature curve of The Bakken gas composition B with a specific gravity of 0.84 compared to Katz's 1945 gravity chart having a specific gravity of 0.8. The curve of New Correlation shows very good tracking of Katz's 1945 gravity chart with slight deviations at higher pressures of 14000 kPa and above. Figures 5.14 shows the pressure-temperature curves for hydrate formation temperature calculated for The Bakken gas compositions C, D, E, F, G, and H. The curves indicate that an increase in the specific gravity causes an increase in the hydrate formation temperature at high pressures. For example, the gas composition E which has a specific gravity of 0.76 produced a HTF of 298.20 K at the pressure of 20684.27 kPa. However, gas composition D having a specific gravity of 1.04 produced a higher HTF of 302.22 (K) at the same pressure. This shows a 4.02 K increase in HFT moving from the specific gravity of 0.76 to 1.04 suggesting that gases with higher specific gravity produce higher hydrate formation temperature.

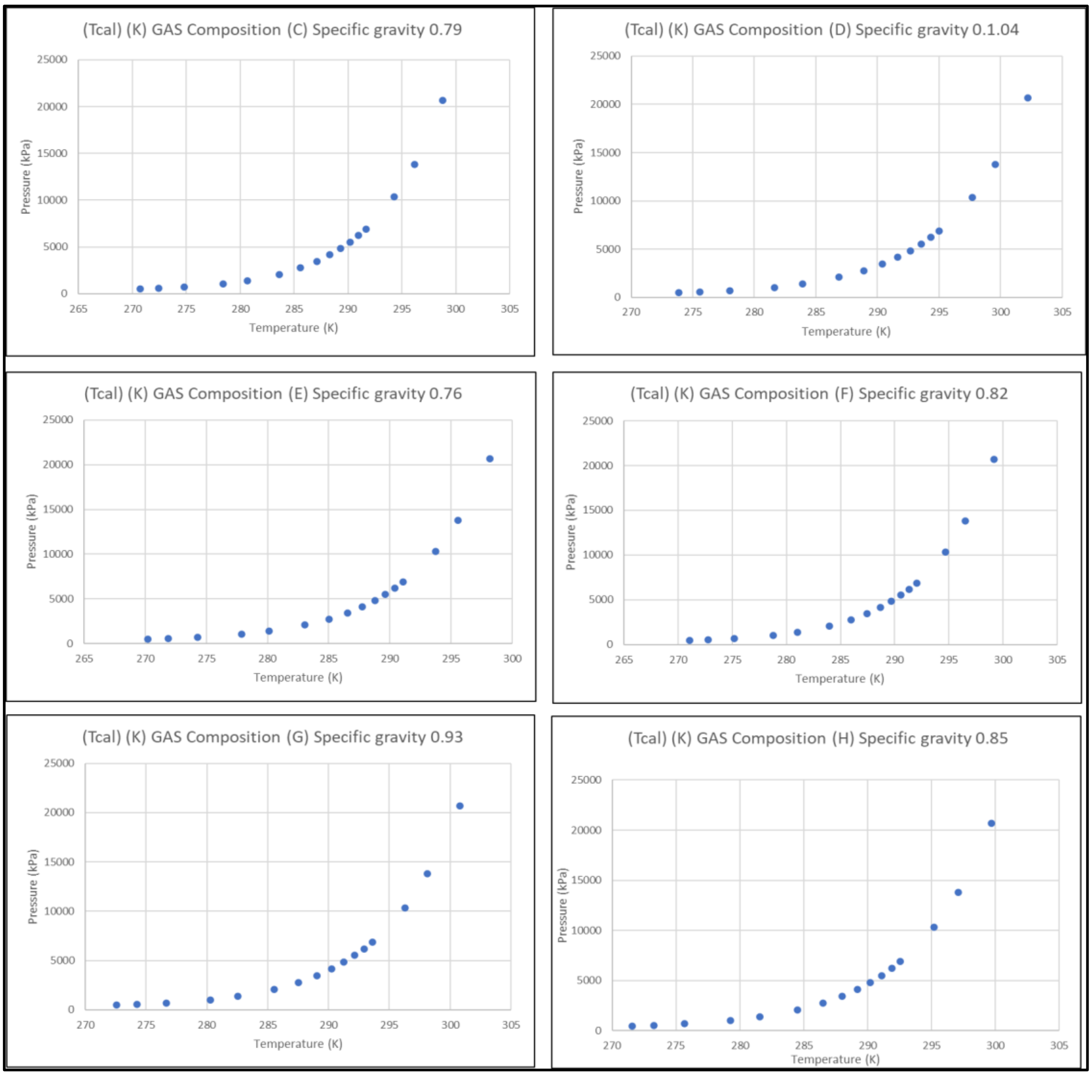

Figure 5.14 Pressure - temperature curve for hydrate formation temperature calculated for The Bakken gas compositions C-H.

Overall, the result of the calculated HTF for The Bakken gas composition A and B compared to Katz's 1945 gravity chart show that the New Correlation calculated the HTF with reliable accuracy and the pressure-temperature curve followed the Katz gravity chart sufficiently.

CHAPTER 6 CONCLUSION AND RECOMMENDATIONS

6.1 CONCLUSION

The model (New Correlation) proposed in this study shows a high potential for estimating the hydrate formation temperature for natural gas with a wide range of gas compositions.

The model's equation, which was developed by nonlinear regression of 460 experimental data points in MATLAB was compared to models by Hammerschmidt (1934), Motiee (1991), Towler and Mokhatab (2005), Chavoshi S. 2018, and Safamirzaei M. (2015). Overall, the New Correlation produced the highest accuracy in predicting the hydrate formation temperature compared to the other models when all data points were considered.

The following findings were made from the analysis of models.

1. The pressure-temperature curve of 460 experimental data points obtained from 15 studies shows that New Correlation produced the most accurate tracking of experimental points compared to the other models. The Average Relative Deviation (ARD) and Average Absolute Deviation (AAD) show that the New Correlation has the lowest deviation from experimental values.
2. The pressure-temperature curve of experimental values obtained from Wilcox

3. W. et al (1941) having 32 data points with the specific gravity ranging from 0.59-0.67 show that the New correlation produced the highest accuracy in following the experimental points across various specific gravities. The Average Relative Deviation (ARD) and Average Absolute Deviation (AAD) show that the New Correlation has the lowest deviation from experimental values.
4. The pressure-temperature curve of HFT obtained from Sloan D. (1990) having 123 experimental data points with the specific gravity ranging from 0.58-0.80 shows that the New correlation produced the most accurate tracking of HFT points than the other models. The Average Relative Deviation (ARD) and Average Absolute Deviation (AAD) show that the New Correlation has the lowest deviation from experimental values.
5. The pressure-temperature curve of HFT obtained from the study by (Bahadori and Vuthaluru, 2009) having 22 data points show that Motiee (1991) produced the most accurate results of HFT, this is followed closely by Safamirzaei M. (2015). The New correlation produced the third-highest accuracy compared to the other models. ARD and AAD also show that Motiee (1991) has the lowest deviation. The New Correlation has the third-lowest ARD and AAD.
6. The result of HTF for The Bakken Gas Composition with a specific gravity of 0.837 and 0.869 calculated with the New correlation shows that it produced reliable accuracy compared to Katz 1945 gravity chart. There were slight deviations at the higher pressure.

Compared to other reputable models the New Correlation provides consistently high accuracy in predicting the hydrate formation temperature of gas mixtures with a specific gravity ranging between 0.55 to 1. The model produced the highest accuracy at the range of 0.55-0.8 specific gravity. Also, the New correlation offers less complicated calculations having only three adjustable parameters and without the use of complex logarithmic functions as in the case of other models. It also offers a reliable accuracy in estimating the hydrate formation temperature of natural gas from the Bakken Formation.

6.2 RECOMMENDATIONS

The following recommendation is suggested for future research:

1. Further investigation of correlations of hydrate formation temperatures and pressure.
2. Further tuning of the adjustable parameters to obtain more accurate hydrate formation temperature at higher pressures.
3. Further development of the equation on MATLAB to cover the data points more accurately.
4. Further development of models to predict hydrate formation temperature and pressure.

NOMENCLATURE

ARD	Average Relative Deviation
AAD	Average Absolute Deviation
HFT	Hydrate Formation Temperature
K	Kelvins
kPa	Kilo Pascals
NC	New Correlation
P	Pressure
T(exp)	Experimental Temperature
T(cal)	Calculated Temperature
γ	Specific gravity
Mol %	Mol percentage
MW^{air}	The molecular weight of air
MW^{NG}	The molecular weight of Natural gas

APPENDIX A

- Bahadori, A., & Vuthaluru, Hari. B. (2009). A novel correlation for estimation of hydrate forming condition of natural gases. *Journal of Natural Gas Chemistry*, *18*(4), 453–457. https://doi.org/10.1016/S1003-9953(08)60143-7
- Chavoshi, S., Safamirzaei, M., & Pajoum Shariati, F. (2018). Evaluation of Empirical Correlations for Predicting Gas Hydrate Formation Temperature. *Gas Processing*, *6*(2). https://doi.org/10.22108/gpj.2018.112052.1036
- Chen, G.J. and Guo, T.M.: "Thermodynamic Modeling of Hydrate Formation Based on New Concepts," *Fluid Phase Equilibria* (1996) **122**, 43.
- Davarnejad, R. (2014). Prediction of Gas Hydrate Formation using HYSYS Software. *International Journal of Engineering*, **27** (9 (C)).
- Deaton, W. M., & Frost, E. M. (n.d.). *Gas Hydrates and Their Relation to the Operation of Natural-gas Pipe Lines*. 126.
- Elgibaly, A. A., & Elkamel, A. M. (1998). A new correlation for predicting hydrate formation conditions for various gas mixtures and inhibitors. *Fluid Phase Equilibria*, *152*(1), 23–42. https://doi.org/10.1016/S0378-3812(98)00368-9
- Hammerschmidt, E. G. (1934). Formation of Gas Hydrates in Natural Gas Transmission Lines. *Industrial & Engineering Chemistry*, *26*(8), 851–855. https://doi.org/10.1021/ie50296a010

- Jossang, A. and Stange, E.: "A New Predictive Activity Model for Aqueous Salt Solutions," *Fluid Phase Equilibria* (2001) **181**, 33.
- Nasrifar, K. and Moshfeghian, M A Model for Prediction of Gas Hydrate Formation Conditions in Aqueous Solutions Containing Electrolytes and/or Alcohol," J. Chem. Thermodynamics (2001) 33, 999"
- Salufu, S., & Nwakwo, P. (2013). *New Empirical Correlation for Predicting Hydrate Formation Conditions*. https://doi.org/10.2118/167571-MS
- Safamirzaei, M. (2015). Predict gas hydrate formation temperature with a simple correlation. *Gas, 51*. http://www.gasprocessingnews.com/features/201508/predict-gas-hydrate-formation-temperature-with-a-simple-correlation.aspx
- Sloan, E.D. Jr.: *Clathrate Hydrates of Natural Gases*, Marcel Dekker, New York (1990).
- Sun, C.-Y., Chen, G.-J., Lin, W., & Guo, T.-M. (2003). Hydrate Formation Conditions of Sour Natural Gases. *Journal of Chemical & Engineering Data*, *48*(3), 600–602. https://doi.org/10.1021/je020155h
- Towler, B., & Mokhatab, S. (2005). Quickly estimate hydrate formation conditions in natural gases. *Hydrocarbon Processing*, *84*, 61–62.
- Wilcox, W. I., Carson, D. B., & Katz, D. L. (1941). *Natural Gas Hydrates*. *33*(5), 4.

APPENDIX B

	Specific gravity	Pressure (MPa)	Experimental Temperatue (K)	Hammerschmidt (1934)	Towler and Mokhatab (2005)	Chavoshi S. 2018	Motiee (1991)	New Correlation	Safamirzaei M. 2015
Davarnejad, R. (2014).	0.650283952	720	273.08	273.9707836	272.5210923	275.4745036	270.1759873	272.9982404	273.1317095
	0.650283952	1080	275.09	276.249091	275.7176958	277.8301194	273.9416086	276.5065362	276.2500843
	0.650283952	1450	277.03	278.0776387	278.0402815	279.5542858	276.5619575	278.7628952	278.4250623
	0.650283952	1810	279.04	279.5589984	279.7886176	280.8592144	278.4702113	280.3668972	280.0157119
	0.650283952	2900	281.04	283.0367347	283.5049113	283.6532635	282.3431733	283.6121195	283.2741455
	0.650283952	3620	283.12	284.8416385	285.2532475	284.9773257	284.0790016	285.0895484	284.7533444
	0.650283952	4350	285.14	286.4256131	286.7015148	286.0788169	285.4751322	286.2981896	285.9543022
	0.650283952	5800	287.08	289.0789481	288.9695411	287.8123427	287.5854531	288.1716553	287.7928535
	0.650283952	7980	289.08	292.2878634	291.4851061	289.7473599	289.8175138	290.2321001	289.7751073
	0.650283952	10520	290.96	295.3127756	293.6637122	291.4336914	291.6583076	292.0086932	291.4462687
	0.650283952	15600	293.04	300.0591092	296.7698697	293.854972	294.1347004	294.5379281	293.7604101
	0.650283952	22480	295.04	304.9630707	299.6502543	296.118233	296.2754942	296.8861864	295.8389537
	0.650283952	30460	296.98	309.4479798	302.0452589	298.0133741	297.9415271	298.8444589	297.5209881
	0.650283952	40260	298.99	313.9224537	304.2443966	299.7642075	299.3801414	300.6490025	299.0305106
	0.650283952	51140	301.14	318.0532917	306.1302676	301.2738254	300.5443084	302.2022972	300.2995872
	0.650283952	64200	303.08	322.250807	307.9233282	302.7161995	301.5916572	303.6846736	301.4853421
Davarnejad, R. (2014).	0.794322761	330	273.22	270.2629548	269.4595679	272.0846861	269.2274629	262.9044129	269.0356737
	0.794322761	660	276.88	273.5152436	274.7951432	276.0741405	275.4946336	274.4312199	274.8641138
	0.794322761	1000	279.23	275.7961653	277.9936183	278.4936557	278.9931942	278.2016534	278.1201716
	0.794322761	1340	281.16	277.5728093	280.2464743	280.2105657	281.3411697	280.5112134	280.3195785
	0.794322761	1670	283.17	279.0103886	281.9411336	281.5090441	283.044059	282.1418196	281.9267798
	0.794322761	2340	285.24	281.3957465	284.5377469	283.5102984	285.5478104	284.5262695	284.3160059
	0.794322761	3010	287.32	283.3318279	286.4759211	285.0133498	287.3334757	286.2458276	286.0451032
	0.794322761	4350	289.18	286.4256131	289.3104557	287.2258878	289.8169161	288.7026496	288.4962212

	0.794322761	5690	291.32	288.8955086	291.3775283	288.8501941	291.5320502	290.466676	290.2292192
	0.794322761	8040	293.32	292.3667566	294.0387364	290.9549051	293.6210585	292.7182313	292.3972432
	0.794322761	12700	295.24	297.5150479	297.5578743	293.7617078	296.1776584	295.6802706	295.1628082
	0.794322761	19760	297.24	303.1734299	300.9606612	296.501457	298.4267817	298.543021	297.7356967
	0.794322761	27120	299.22	307.6873333	303.3978146	298.4794182	299.9029337	300.598545	299.5217806
	0.794322761	37180	301.28	312.6093413	305.8264062	300.4635563	301.2620467	302.6540869	301.2574887
	0.794322761	47560	303.19	316.7701223	307.7217197	302.0211695	302.2451498	304.264494	302.5830086
Bahadori, A., & Vuthaluru, Hari. B. (2009).	0.552401687	3157.8	274.82	283.7164225	282.0005391	283.2354068	277.8724706	282.2510391	281.8053215
	0.552401687	4136.85	277.59	285.9841357	284.1706253	284.8462663	280.1292691	284.025385	283.5743892
	0.552401687	5515.81	280.37	288.5997662	286.4823378	286.5723342	282.4433605	285.8896745	285.4085002
	0.600736835	1723.69	277.59	279.2245326	278.301746	280.1268216	275.4516788	279.0927999	278.6899038
	0.600736835	3309.48	283.15	284.0979555	283.4926401	283.9906268	280.9960843	283.5539291	283.1647267
	0.600736835	6756.86	288.71	290.5782392	289.1724733	288.2794565	286.515846	288.2030726	287.7383057
	0.600736835	18098.74	294.26	301.9919109	297.0129133	294.3063729	293.1964127	294.5149124	293.5822567
	0.650798238	2688.96	283.15	282.4473883	282.9199037	283.208031	281.7625015	283.1122834	282.7724447
	0.650798238	14134.25	294.26	298.8199762	296.0014173	293.2513509	293.5485175	293.9142014	293.1984033
	0.700859641	827.37	274.82	274.7223584	274.7092557	276.6939621	273.9674029	275.1338379	275.1278253
	0.700859641	2344.2	283.15	281.40905	282.8472274	282.8120272	282.7548276	283.0536753	282.7584869
	0.700859641	4757.38	288.71	287.228089	288.3776773	287.0468013	288.0322879	287.7829025	287.4826638
	0.700859641	23442	297.04	305.5588564	300.8398509	296.8232219	297.8647615	298.0877137	297.0558935
	0.800982446	496.42	272.04	272.1007081	272.7284615	274.4736519	273.1975569	271.2541523	272.6339521
	0.800982446	1930.53	283.15	280.0074969	283.1722431	282.4145278	284.2883866	283.2793538	283.0686631
	0.800982446	11721.09	294.26	296.5625712	297.0415994	293.3162703	295.8187237	295.2641005	294.7943891
	0.901105252	758.42	277.59	274.2483921	277.7147991	277.5805179	278.9028523	277.2412095	277.5156217
	0.901105252	1585.79	283.15	278.6643739	283.3059856	281.9136052	284.3404869	283.2544291	283.1277552
	0.901105252	17926.37	297.04	301.8649377	301.6894967	296.643076	297.9171063	299.4866906	298.8396097
	1.001228058	413.69	274.82	271.2537388	274.7247848	274.6478488	274.7238211	271.0099295	273.7845718
	1.001228058	1344.48	283.15	277.5939376	283.5436373	281.5306399	283.1367091	283.2642687	283.2295397
	1.001228058	3033.69	288.71	283.3943677	289.6324379	286.3831234	288.0358513	289.0825439	289.0427481

Elgibaly, A. A., & Elkamel, A. M. (1998).	1.03042	1810	284	279.5589984	286.1664316	283.4568141	284.6269859	285.813689	285.775422
	1.03042	2310	286	281.3002215	287.9849695	284.9124998	286.0446432	287.5478853	287.5166857
	1.03042	3080	288	283.5156211	290.1297682	286.6389581	287.6308659	289.5333391	289.5141426
	1.015404	990	279	275.7377478	281.4563459	279.8056517	280.9893904	280.9878512	281.0796713
	1.015404	1710	283	279.1703879	285.5385401	283.0355984	284.4976887	285.225683	285.1778977
	1.015404	2990	288	283.2787549	289.7121286	286.3764086	287.7381256	289.1535045	289.1231409
	0.952433	1420	282	277.9427529	283.2489986	281.5724177	283.7360597	283.0878987	283.0100369
	0.952433	2140	285	280.7414657	286.3368806	284.0081114	286.4062706	286.0677026	285.9785665
	0.952433	3000	287	283.3053231	288.8801189	286.0300098	288.4637971	288.403459	288.3283823
	0.764976	945	275	275.4695195	277.0138031	277.9536556	277.6273433	277.293012	277.224369
	0.764976	1290	278	277.3335027	279.4202976	279.7761607	280.2014213	279.7809622	279.5720321
	0.764976	2430	283	281.6771661	284.316984	283.5215366	285.103663	284.3389264	284.1045821
	0.646301	68600	304	323.5263187	308.3815967	303.1006509	301.7896964	304.0397149	301.7452188
	0.646301	23500	296	305.5942139	299.9296253	296.3578856	296.4005857	297.0955365	296.006752
	0.646301	7000	289	290.9347426	290.3747147	288.9156859	288.7579037	289.3132804	288.8896042
	0.600284	1520	275	278.3847865	277.2904586	279.3837978	274.3018657	278.1776564	277.7817221
	0.600284	2890	280	283.0095136	282.4039982	283.1792036	279.8592692	282.6421012	282.2502361
	0.600284	3970	283	285.627064	284.9308172	285.0736668	282.4344544	284.7443761	284.3513483
	0.578002	1840	275	279.6725802	278.2874136	280.2948557	274.7060219	279.1052885	278.6758665
	0.578002	2530	278	281.9812459	280.8329555	282.1756173	277.4972355	281.3007814	280.8793237
	0.578002	4770	283	287.25215	285.9018137	285.9583871	282.7164993	285.4909988	285.0592615
	0.56783	2160	275	280.8088134	279.3260183	281.140402	275.5168793	280.0136794	279.5749212
	0.56783	2960	278	283.1986674	281.8498066	283.0067921	278.2438029	282.1459554	281.7175112
	0.56783	4030	280	285.7566827	284.3214987	284.8466647	280.8065011	284.1816864	283.7505433
	0.564439	2370	275	281.4903998	279.9877088	281.6549716	276.1267478	280.5785266	280.1389068
	0.564439	4410	280	286.5470878	284.9652364	285.3519973	281.3440212	284.698064	284.2573325
	0.564439	6090	283	289.5509206	287.5524392	287.2927519	283.8849884	286.7854562	286.3012384
	0.559595	2860	275	282.927444	281.378332	282.7199981	277.461638	281.7443585	281.3053358
	0.559595	3810	278	285.2744269	283.6795497	284.4279473	279.8738315	283.6409622	283.2022403

	0.559595	5090	280	287.8475961	286.0035629	286.1632872	282.2162727	285.5254592	285.0644349
KATZ Gas Chat Specific gravity (γ) 0.6	0.6	20684.27188	294.4	303.8002808	298.0612715	295.125568	293.9883914	295.3553008	294.3212086
	0.6	13789.51459	293.7055556	298.5152927	294.8343024	292.6233107	291.4297973	292.7594775	292.0028783
	0.6	10342.13594	292.0388889	295.1191449	292.5447314	290.8608079	289.5026066	290.9188709	290.3090518
	0.6	6894.757293	289.1222222	290.7815353	289.3177624	288.3947098	286.6287551	288.3182768	287.8477017
	0.6	6205.281564	288.15	289.7340785	288.4792312	287.7573215	285.8517958	287.6397477	287.1931694
	0.6	5515.805835	287.3166667	288.599759	287.5418332	287.0464495	284.9684883	286.8791109	286.4538471
	0.6	4826.330105	286.3444444	287.3589963	286.4790989	286.242653	283.9482553	286.0134042	285.6057016
	0.6	4136.854376	285.65	285.9841449	285.2522622	285.3175367	282.7456105	285.008381	284.6130301
	0.6	3447.378647	283.7055556	284.4341188	283.8012224	284.227215	281.2887768	283.8096111	283.419546
	0.6	2757.902917	281.7611111	282.6434442	282.0252931	282.8984379	279.4550113	282.3225705	281.9290211
	0.6	2068.427188	279.5388889	280.4967009	279.7357221	281.1945091	277.0084548	280.3597659	279.9563649
	0.6	1378.951459	276.2055556	277.7548489	276.5087531	278.8103679	273.4025982	277.4547669	277.0711914
	0.6	1034.213594	273.4277778	275.9929273	274.2191821	277.131062	270.7323629	275.2310335	274.9435465
KATZ Gas Chat Specific gravity (γ) 0.7	0.7	20684.27188	296.7611111	303.8002808	299.8476496	296.0368482	297.1761776	297.2645668	296.3348634
	0.7	13789.51459	294.8166667	298.5152927	296.6788428	293.5268645	294.8876299	294.6519633	294.0006718
	0.7	10342.13594	293.2888889	295.1191449	294.4305386	291.7589194	293.1520401	292.7994584	292.2952566
	0.7	6894.757293	291.7611111	290.7815353	291.2617318	289.2852066	290.5482349	290.1820533	289.8170667
	0.7	6205.281564	290.9277778	289.7340785	290.4383141	288.6458502	289.8414475	289.499138	289.1580563
	0.7	5515.805835	289.8166667	288.599759	289.5178115	287.9327832	289.0365854	288.7335843	288.4136758
	0.7	4826.330105	288.9833333	287.3589963	288.4742318	287.1265048	288.1052865	287.8622813	287.5597276
	0.7	4136.854376	287.8722222	285.9841449	287.2695073	286.1985319	287.0053085	286.8507614	286.5602645
	0.7	3447.378647	286.4833333	284.4341188	285.8446208	285.1048436	285.6699039	285.6442422	285.358615
	0.7	2757.902917	284.8166667	282.6434442	284.1007005	283.7719635	283.9847557	284.1475889	283.8578924
	0.7	2068.427188	282.5944444	280.4967009	281.8523963	282.0627734	281.7298001	282.1720962	281.8717399
	0.7	1378.951459	279.2611111	277.7548489	278.6835895	279.6712705	278.3939899	279.2483184	278.9668269
	0.7	1034.213594	277.0388889	275.9929273	276.4352853	277.9867793	275.9153556	277.0102101	276.8246253

	0.7	689.4757293	273.5666667	273.7425752	273.2664785	275.6298352	272.264288	273.4204038	273.6797792
KATZ Gas Chat Specific gravity (γ) 0.8	0.8	20684.27188	297.5944444	303.8002808	301.3950807	296.8285091	298.687801	298.9284215	298.090303
	0.8	13789.51459	296.2055556	298.5152927	298.2766563	294.3118132	296.6692996	296.3011947	295.742284
	0.8	10342.13594	294.2611111	295.1191449	296.064099	292.5391403	295.1253108	294.438321	294.0267662
	0.8	6894.757293	292.3166667	290.7815353	292.9456746	290.0588123	292.791552	291.8062656	291.5338959
	0.8	6205.281564	291.7611111	289.7340785	292.1353489	289.4177461	292.1549363	291.1195279	290.8709817
	0.8	5515.805835	291.2055556	288.599759	291.2294819	288.7027722	291.4285197	290.3496892	290.1221915
	0.8	4826.330105	290.2333333	287.3589963	290.2024945	287.8943377	290.5861548	289.4735094	289.2631847
	0.8	4136.854376	289.1222222	285.9841449	289.0169246	286.9638832	289.5888437	288.4563278	288.2578009
	0.8	3447.378647	287.8722222	284.4341188	287.614693	285.8672701	288.3748683	287.2430555	287.049033
	0.8	2757.902917	286.2055556	282.6434442	285.8985002	284.5308257	286.8383373	285.7380251	285.5394204
	0.8	2068.427188	284.1222222	280.4967009	283.6859429	282.8170648	284.7749826	283.751475	283.5415023
	0.8	1378.951459	280.9277778	277.7548489	280.5675186	280.4191666	281.7092188	280.8113322	280.619381
	0.8	1034.213594	278.5666667	275.9929273	278.3549613	278.7301707	279.4221854	278.5606967	278.4644894
	0.8	689.4757293	275.3722222	273.7425752	275.2365369	276.3669237	276.0411642	274.9507975	275.3010138
	0.8	551.5805835	274.5388889	272.6106696	273.5203441	275.0748939	274.1017818	272.5542905	273.491602
KATZ Gas Chat Specific gravity (γ) 0.9	0.9	20684.27188	298.0111111	303.8002808	302.7600116	297.5285606	298.5232616	300.4037739	299.64734
	0.9	13789.51459	295.9277778	298.5152927	299.6860277	295.0059292	296.7748066	297.7635805	297.2870565
	0.9	10342.13594	294.8166667	295.1191449	297.5050014	293.2290756	295.4224187	295.8915126	295.5625779
	0.9	6894.757293	292.8722222	290.7815353	294.4310175	290.7428979	293.3587063	293.2464668	293.0566864
	0.9	6205.281564	292.3166667	289.7340785	293.6322397	290.1003198	292.7922624	292.5563397	292.3903095
	0.9	5515.805835	291.7611111	288.599759	292.7392821	289.3836596	292.1442912	291.7827015	291.6376082
	0.9	4826.330105	290.9277778	287.3589963	291.7269303	288.5733184	291.3908604	290.9021973	290.7741144
	0.9	4136.854376	290.0944444	285.9841449	290.5582558	287.6406696	290.4962162	289.8799954	289.7634792
	0.9	3447.378647	288.9833333	284.4341188	289.1760073	286.5414702	289.4036699	288.6607351	288.5483974
	0.9	2757.902917	287.3166667	282.6434442	287.4842719	285.2018739	288.0157562	287.1482766	287.0308995
	0.9	2068.427188	285.3722222	280.4967009	285.3032456	283.4840712	286.1440024	285.151922	285.0225455

	0.9	1378.951459	282.3166667	277.7548489	282.2292617	281.0805177	283.348285	282.1972682	282.0851609
	0.9	1034.213594	280.0944444	275.9929273	280.0482354	279.3875384	281.2528525	279.9355248	279.9190135
	0.9	689.4757293	277.1777778	273.7425752	276.9742515	277.0187178	278.1418777	276.307809	276.7390138
	0.9	551.5805835	275.3722222	272.6106696	275.2825161	275.7236408	276.3511125	273.8994742	274.9201508
	0.9	482.6330105	274.2611111	271.9669619	274.2701643	274.9515509	275.2527879	272.1976077	273.8066654
Wilcox, W. I., Carson, D. B., & Katz, D. L. (1941).	0.668408755	1254.845827	278.8166667	277.1612497	277.2909389	278.8602461	276.1760821	277.9966125	277.7044484
	0.668408755	1923.637285	282.8722222	279.9823971	280.6480074	281.3732426	279.8206202	281.1197542	280.7870148
	0.668408755	12265.77322	295.0944444	297.0992688	295.2060921	292.535652	293.2565023	293.3312737	292.7130921
	0.668408755	16843.89207	296.0944444	301.0469208	297.6985238	294.4906428	295.1708218	295.3698037	294.560043
	0.668408755	20684.27188	297.0388889	303.8002808	299.3124867	295.7635522	296.3502355	296.6912979	295.7301718
Gas C	0.596668956	27323.92315	298.3166667	307.7991444	300.2138086	296.822924	295.5094684	297.0728974	295.7961115
	0.596668956	1599.583692	277.7055556	278.7219369	277.612205	279.6495863	274.5520953	278.4776549	278.0736864
	0.596668956	3392.220588	283.8722222	284.3008315	283.598972	284.0993242	280.9829584	283.6369176	283.2431669
	0.596668956	6963.704866	289.15	290.8820931	289.3267983	288.4228622	286.5423026	288.3151778	287.8383004
	0.596668956	10500.71536	292.0388889	295.2918951	292.5978107	290.9213749	289.4567975	290.9485563	290.3282073
Gas C 2nd Series	0.596668956	14127.35769	293.3166667	298.813937	294.9604491	292.7394918	291.4442195	292.8461671	292.0715631
	0.596668956	1923.637285	279.0944444	279.9823971	279.0813344	280.7350395	276.1888963	279.7887586	279.3804405
	0.596668956	2647.586801	281.8166667	282.3280021	281.6252382	282.6245535	278.9328575	281.9819599	281.5833241
	0.596668956	4819.435348	286.7055556	287.3459665	286.3956588	286.202191	283.7698734	285.9375654	285.5262439
	0.596668956	8135.813606	290.2611111	292.4918723	290.56569	289.3666361	287.6684271	289.3141257	288.7921528
	0.596668956	9480.291278	291.2055556	294.145612	291.7836779	290.2974962	288.7490878	290.2941908	289.7169829
	0.596668956	13782.61983	293.3166667	298.5091437	294.7637032	292.5876577	291.2824877	292.6881589	291.9280741
	0.596668956	20263.69168	294.9833333	303.5175761	297.8331549	294.9654335	293.7277061	295.1549405	294.1331721
	0.596668956	17161.0509	294.2611111	301.2903949	296.5096531	293.9378115	292.6937989	294.0907281	293.1910368
	0.596668956	27503.18684	296.65	307.8969429	300.2658863	296.8636878	295.5473248	297.1149193	295.8320459
Gas D	0.649441297	22994.01557	295.5388889	305.2836295	299.8135921	296.2511707	296.3767586	297.0156098	295.9485691
	0.649441297	1206.582526	276.7611111	276.9190502	276.5730092	278.4702865	274.8959915	277.3610518	277.0609988
	0.649441297	2185.638062	281.5944444	280.8944977	281.2576129	281.966366	280.010038	281.6715233	281.3225158

	0.649441297	3516.32622	284.9277778	284.5986005	285.0070014	284.7960991	283.8178735	284.8817901	284.5450676
	0.649441297	5446.858262	288.7055556	288.4808531	288.457653	287.4254577	287.0981909	287.7485528	287.3791672
	0.649441297	8204.761179	291.2055556	292.5812554	291.6879458	289.9089005	289.9743421	290.3951677	289.9283222
Gas D 2nd Series	0.649441297	11996.87769	293.2055556	296.8364935	294.6837085	292.2312104	292.4734179	292.8362402	292.2098247
	0.649441297	6170.807777	289.15	289.6795638	289.4416284	288.1796744	287.9942309	288.5573239	288.1658933
	0.649441297	9307.922346	292.0388889	293.9433756	292.6826489	290.6779387	290.8220827	291.2064738	290.6943636
	0.649441297	14065.30488	293.9277778	298.7594697	295.9379338	293.2089996	293.4716113	293.8571738	293.1428537
	0.649441297	18202.15925	294.9833333	302.0676782	297.9709166	294.8008593	295.0293046	295.5127762	294.628808
	0.649441297	26544.81558	296.8722222	307.3686861	300.9458819	297.1458971	297.1743566	297.9406419	296.7472448
Sun, C.-Y., Chen, G.-J., Lin, W., & Guo, T.-M. (2003).	0.656106473	22545.85635	295.9277778	305.0044319	299.7759013	296.189224	296.4711798	297.0156625	295.9720199
	0.656106473	1044	274.2	276.0483512	275.5784939	277.681894	273.9321215	276.3375223	276.1038958
	0.656106473	1580	277.2	278.6401047	278.841828	280.1087344	277.5895595	279.4958364	279.1555645
	0.656106473	2352	280.2	281.4337113	281.975026	282.4587521	280.9199143	282.2968242	281.95733
	0.656106473	3126	282.2	283.6347791	284.2155127	284.1512827	283.1925121	284.2205983	283.8902997
	0.656106473	3964	284.2	285.6140253	286.085939	285.5720236	285.0202147	285.7947478	285.4620463
	0.656106473	5121	286.2	287.9038431	288.1028238	287.1119724	286.920133	287.4702827	287.116479
	0.656106473	6358	288.2	289.9730063	289.8067994	288.419476	288.4679555	288.8738738	288.4832001
	0.656106473	7212	289.2	291.2384309	290.7993678	289.1838415	289.3453616	289.6879742	289.2667551
82.45% CH4 + 10.77% CO2 + 6.78% H2S	0.700059936	8220	290.2	292.6009384	292.6367861	290.355715	291.7016614	291.3196163	290.9037843
	0.700059936	1114	276.2	276.4343319	277.0173062	278.4214298	276.5671193	277.6071795	277.385854
	0.700059936	1385	278.2	277.7827857	278.7190024	279.6974556	278.4334697	279.2820943	278.9999371
	0.700059936	1815	280.2	279.5780217	280.8321069	281.2901209	280.6770117	281.25224	280.9503399
	0.700059936	2265	282.2	281.1552568	282.563081	282.6015261	282.453732	282.8033445	282.5060507
	0.700059936	3110	284.2	283.5934759	285.0408615	284.4893668	284.9012324	284.9576229	284.6712317
	0.700059936	4065	286.2	285.8316576	287.133691	286.0937314	286.880647	286.7363563	286.4467962
	0.700059936	4570	287.2	286.8653437	288.048842	286.7981269	287.7209256	287.5059769	287.208676

	0.700059936	4890	288.2	287.4786965	288.5777649	287.2060318	288.1995612	287.9490123	287.645111
	0.700059936	6110	289.2	289.582873	290.3184703	288.5525628	289.7384896	289.3997352	289.0618221
	0.700059936	6862	290.2	290.7335077	291.2255929	289.2567721	290.5184048	290.1522567	289.7885142
	0.700059936	7650	290.9	291.8461976	292.0751531	289.9178535	291.2351252	290.8554313	290.4621116
82.91% CH4 + 7.16% CO2 + 9.93% H2S	0.684840337	8024	291.2	292.3457597	292.1740948	290.0810521	291.0727759	290.896398	290.4732394
	0.684840337	1192	278.2	276.8445103	277.2331122	278.6948568	276.4867396	277.8828004	277.62177
	0.684840337	1932	282.2	280.0128417	281.0171114	281.5355892	280.5665072	281.4358294	281.1194034
	0.684840337	2460	284.2	281.7693149	282.9102396	282.9676512	282.5094287	283.1106701	282.8018031
	0.684840337	3303	286.2	284.0819143	285.2191582	284.7241025	284.7904469	285.098151	284.7975434
	0.684840337	4212	288.2	286.1416043	287.1240463	286.1814028	286.5989915	286.7067383	286.4002557
Deaton, W. M., & Frost, E. M.	0.80260126	3103	282.65	283.575358	286.8486081	285.2546811	287.7069478	286.5752658	286.38238
(Sample A)	0.80260126	627.4229137	274.8166667	273.2553837	274.5593745	275.8380225	275.3058196	274.0258585	274.5819006
	0.80260126	1261.740585	280.3166667	277.1953031	279.9303882	279.9147179	281.0783389	280.1729961	280.0017208
	0.80260126	1806.426411	283.15	279.545379	282.6892768	282.0321307	283.8306257	282.8299511	282.6202916
	0.80260126	2571.74447	285.9277778	282.105642	285.404925	284.131999	286.3986989	285.2996314	285.1004782
	0.80260126	3592.16855	288.7055556	284.7768884	287.9740231	286.1329376	288.6993494	287.5569777	287.3649595
	0.80260126	4295.433794	290.0388889	286.3140949	289.3486032	287.2093078	289.8788578	288.7443716	288.5459527
	0.80260126	5364.121174	291.4833333	288.3367369	291.0567142	288.5524944	291.2945977	290.2064203	289.9853378
	0.80260126	6301.808166	292.5388889	289.8855763	292.2952757	289.5303741	292.2865267	291.2597609	291.0102887
(Sample B	0.650836699	599.8438845	273.7055556	273.0277412	271.0943005	274.42496	268.4507045	271.1569537	271.6866181
	0.650836699	737.7390304	275.3722222	274.1002428	272.7254572	275.620023	270.4370702	273.2383394	273.3334998
	0.650836699	992.8450502	277.5944444	275.7544106	275.0665869	277.3443466	273.2040817	275.8355775	275.625613
	0.650836699	1337.582915	280.3722222	277.561389	277.4160756	279.0856725	275.8815066	278.171277	277.8469188
(Sample C	0.693380674	723.9495158	273.7055556	273.9998028	273.5080409	275.8599636	272.4063859	273.7836992	273.9512778
	0.693380674	806.6866033	274.8166667	274.5832443	274.3547127	276.4875641	273.3976997	274.7843639	274.8002782
	0.693380674	903.2132054	275.9277778	275.2121378	275.2390168	277.1445843	274.4190503	275.7737559	275.6752227
	0.693380674	972.1607783	276.4833333	275.6324792	275.8145763	277.573052	275.0761098	276.3926684	276.2383862
	0.693380674	1172.10874	277.5944444	276.7417755	277.2779809	278.66545	276.719397	277.8957625	277.6486092

	0.693380674	1241.056313	278.15	277.0927396	277.725193	279.0001404	277.2137521	278.3383746	278.0735337
	0.693380674	1461.688546	279.8166667	278.1296526	279.0054428	279.9604948	278.6086975	279.5710506	279.2748922
(Sample D	0.679262806	2213.217091	283.15	280.9858702	281.9701303	282.2939866	281.4365067	282.2873791	281.9689268
	0.679262806	751.528545	273.7055556	274.1993493	273.4987181	275.9630764	272.074569	273.9005059	273.9964524
	0.679262806	882.5289335	274.8166667	275.0815741	274.7589858	276.8958397	273.5501757	275.3381366	275.2462842
	0.679262806	1089.371652	276.4833333	276.3005617	276.4104923	278.1229455	275.4400275	277.0798732	276.8482992
	0.679262806	1399.635731	278.7055556	277.8500258	278.3760898	279.5905176	277.624478	279.0087444	278.7048339
	0.679262806	1675.426022	280.3722222	279.0322521	279.7867363	280.6485179	279.1487653	280.3257283	280.0053901
(Sample E	0.652785123	2096.006217	282.0388889	280.5917223	280.9978899	281.7474635	279.8195176	281.4417643	281.0949103
	0.652785123	944.5817492	275.3722222	275.4669841	274.7169844	277.0708273	272.8482716	275.4571219	275.2830581
	0.652785123	1716.794566	280.3166667	279.1972994	279.4251961	280.5691109	278.140845	280.0351535	279.687486
	0.652785123	3454.273404	285.9277778	284.4506722	284.9346786	284.7188769	283.825695	284.8249188	284.4917976
(Sample F	0.638798761	5253.805057	289.2611111	288.1420884	287.960564	287.1128303	286.3889352	287.3156098	286.9401576
	0.638798761	765.3180595	273.7055556	274.2971639	272.7411495	275.7295604	270.1258525	273.3663846	273.39537
	0.638798761	1241.056313	277.5944444	277.0927396	276.5604021	278.5430127	274.5982557	277.3860948	277.0669076
	0.638798761	1730.584081	280.3722222	279.2516828	279.1872464	280.4947223	277.5221736	279.8389109	279.4766206
	0.638798761	1730.584081	280.3722222	279.2516828	279.1872464	280.4947223	277.5221736	279.8389109	279.4766206
	0.638798761	3461.168161	285.9277778	284.4672021	284.6633701	284.6074892	283.2188708	284.5803895	284.2325882
	0.638798761	4909.067193	288.7055556	287.5143261	287.4243762	286.7039166	285.8867239	286.8742225	286.5072379
	0.638798761	4895.277678	288.7055556	287.4885684	287.4021529	286.686981	285.8657974	286.855905	286.4892344
	0.638798761	8652.920403	292.0388889	293.1495264	291.9024118	290.1369653	289.9223836	290.5365994	290.0402671
(Sample G	0.639836517	9390.659433	292.7055556	294.0407802	292.5688134	290.6453401	290.5155576	291.0820039	290.5562268
	0.639836517	758.4233022	273.7055556	274.2484156	272.6934567	275.6861138	270.0974173	273.3014383	273.3442253
	0.639836517	1234.161555	277.5944444	277.0582802	276.5394576	278.5194691	274.6026319	277.3622195	277.0456535
	0.639836517	1723.689323	280.3722222	279.22453	279.1782721	280.4803142	277.5399183	279.8293806	279.4682749
	0.639836517	3468.062918	285.9277778	284.4837084	284.7006004	284.6286237	283.2817325	284.6128857	284.2661719
	0.639836517	5033.172824	288.7055556	287.7438484	287.6425675	286.8635873	286.1167795	287.0561945	286.6874023
	0.639836517	5033.172824	288.7055556	287.7438484	287.6425675	286.8635873	286.1167795	287.0561945	286.6874023
(Sample H	0.691360127	7729.022926	291.4833333	291.9531824	291.9990973	289.9079127	291.0344827	290.7698117	290.3647951
	0.691360127	758.4233022	274.2055556	274.2484156	273.8292208	276.1134723	272.7396034	274.1876397	274.2822228
	0.691360127	944.5817492	275.3722222	275.4669841	275.547207	277.3891585	274.7281846	276.1189734	275.9830236

	0.691360127	1254.845827	277.5944444	277.1612497	277.7702187	279.0486015	277.2211251	278.3892006	278.1194584
	0.691360127	1758.16311	280.3722222	279.359527	280.4098594	281.0319488	280.0637651	280.8784887	280.5685908
(Sample I	0.632186651	2130.480004	282.0388889	280.70925	280.6870584	281.6633233	278.9603464	281.1779149	280.8101003
	0.632186651	792.8970887	273.7055556	274.4890746	272.868684	275.8772103	270.0917834	273.5701498	273.545543
	0.632186651	972.1607783	275.3166667	275.6324792	274.4809735	277.0606013	272.0103336	275.3272739	275.111761
	0.632186651	1310.003886	277.5944444	277.4300264	276.8402607	278.8014298	274.7337839	277.6764989	277.3372043
(Sample J	0.6294292	1813.321168	280.3722222	279.5716385	279.3514991	280.6869834	277.4473912	279.9981435	279.625254
	0.6294292	882.5289335	273.7055556	275.0815741	273.6523485	276.474201	270.9509644	274.4625963	274.3201983
	0.6294292	951.4765065	274.2611111	275.5086784	274.2476762	276.9112902	271.6567831	275.0985851	274.8951382
	0.6294292	1020.424079	274.8166667	275.9141922	274.8013373	277.318408	272.3075055	275.6737432	275.4252713
	0.6294292	1027.318837	274.8166667	275.9536542	274.8546313	277.3576277	272.3698527	275.728352	275.4760714
	0.6294292	1172.10874	275.9277778	276.7417755	275.8981257	278.1266659	273.5803602	276.7739972	276.4627727
	0.6294292	1441.004274	277.5944444	278.0374033	277.5326763	279.3355912	275.4373251	278.3373949	277.9787892
	0.6294292	1454.793789	277.5944444	278.0990071	277.6080495	279.3914644	275.5218003	278.4076813	278.0478512
	0.6294292	2027.058644	280.3722222	280.3524556	280.2333364	281.3445432	278.4006249	280.7808677	280.4088589
	0.6294292	1992.584858	280.3722222	280.2306345	280.0975848	281.2432171	278.2547894	280.6611821	280.288837
	0.6294292	2006.374372	280.3722222	280.2795424	280.1521652	281.2839519	278.3134638	280.7093366	280.3371194
	0.6294292	2840.640005	283.15	282.8741545	282.9039076	283.34532	281.2024614	283.0871035	282.7265826
	0.6294292	3764.537482	285.3722222	285.1723005	285.132491	285.0258489	283.4428163	284.95962	284.6004855
	0.6294292	4033.433017	285.9277778	285.7640573	285.6785093	285.439108	283.9781526	285.4133256	285.0516708
	0.6294292	4026.538259	285.9277778	285.7492419	285.6649694	285.4288529	283.964942	285.4020948	285.0405192
	0.6294292	4054.117288	285.9277778	285.8083949	285.7189909	285.4697707	284.0176296	285.4468972	285.0850004
	0.6294292	4364.381367	286.4833333	286.4548379	286.3026061	285.9121954	284.5835004	285.9299583	285.5636687
	0.6294292	4674.645445	287.0388889	287.0692079	286.8461235	286.3248395	285.1050069	286.3783758	286.0063908
	0.6294292	4681.540202	287.0388889	287.0825249	286.8577876	286.3337016	285.1161407	286.3879849	286.0158599
	0.6294292	5067.64661	287.5944444	287.8068855	287.4849772	286.8106254	285.7112248	286.9038611	286.5230575
	0.6294292	5433.068747	288.15	288.456943	288.0360188	287.2303007	286.2282449	287.3558997	286.9655349
	0.6294292	5812.280398	288.7055556	289.0992725	288.5699759	287.6375503	286.7240477	287.7929771	287.3915337
	0.6294292	6984.389138	289.8166667	290.9121216	290.0238369	288.7493403	288.0481425	288.9791789	288.5379803
(Sample K	0.718621772	8384.024868	290.9277778	292.8111645	293.1164505	290.6282836	292.3476373	291.7661373	291.3617753
	0.718621772	1068.68738	274.2611111	276.186533	277.0681897	278.3243719	276.978527	277.5793923	277.3943368

	0.718621772	1220.372041	275.3722222	276.9889465	278.1022216	279.1012044	278.1122586	278.6250604	278.3888151
	0.718621772	2247.690878	280.3722222	281.098948	282.8604391	282.7039273	283.0745829	283.05982	282.7799093
	0.718621772	3164.693598	283.15	283.7340436	285.5260859	284.7425293	285.6717121	285.3863796	285.1181075
(Sample L	0.582200927	4591.908357	285.9833333	286.9082985	285.6916772	285.7713466	282.6411782	285.330121	284.9069284
	0.582200927	1261.740585	273.7055556	277.1953031	275.37442	278.1231858	271.5133096	276.4383093	276.053697
	0.582200927	1427.21476	274.8166667	277.9753765	276.3586431	278.8438688	272.6556292	277.3605318	276.9518558
	0.582200927	1420.320002	274.8166667	277.9442024	276.3199665	278.8155132	272.6110615	277.3247811	276.9167951
	0.582200927	2027.058644	277.5944444	280.3524556	279.1608672	280.9060005	275.8146824	279.8669268	279.4431162
	0.582200927	2854.429519	280.3722222	282.9121374	281.8946071	282.93243	278.7634635	282.1980855	281.7854216
	0.582200927	4047.222531	283.15	285.7936337	284.6832367	285.0146099	281.6360463	284.5066342	284.0921019
	0.582200927	7425.653605	287.7055556	291.5380972	289.5304484	288.6703988	286.3037468	288.4318314	287.920978
	0.582200927	10328.34643	289.8166667	295.1040339	292.1656745	290.6775363	288.6680071	290.5443727	289.9146725
Salufu, S., & Nwakwo, P. (2013).	1	413.6854376	274.8166667	271.2536889	274.7060118	274.6410437	274.7247618	270.9958308	273.7696144
	1	1344.477672	283.15	277.5939266	283.52628	281.5237193	283.1473649	283.249724	283.2141517
	1	3033.693209	288.7055556	283.3943761	289.6160309	286.3761003	288.0531801	289.0677212	289.0270648
	0.7	827.3708752	274.8166667	274.7223642	274.6913651	276.6871765	273.9288462	275.1197329	275.1128983
	0.7	2344.21748	283.15	281.4091053	282.8305762	282.8051297	282.7222826	283.0392059	282.743189
	0.7	4757.382532	288.7055556	287.2280938	288.3617803	287.0397587	288.0037402	287.7681427	287.4670613
	0.7	23442.1748	297.0388889	305.558963	300.8258295	296.8159826	297.8453803	298.0724699	297.0398097
	0.65	758.4233022	274.8166667	274.2484156	272.9245695	275.7730219	270.6538414	273.481536	273.5348349
	0.65	2688.955344	283.15	282.4473749	282.9033373	283.2010691	281.7262483	283.0977481	282.7570828
	0.65	14134.25245	294.2611111	298.8199783	295.9867611	293.2441539	293.5211015	293.8991247	293.1824881
	0.6	1723.689323	277.5944444	279.22453	278.2846823	280.1199433	275.4098623	279.0784796	278.6747725
	0.6	3309.483501	283.15	284.0979641	283.476333	283.9836623	280.9574811	283.5393898	283.1493622
	0.6	6756.862147	288.7055556	290.5782424	289.1569754	288.2723823	286.4807394	288.1882898	287.7226879
	0.6	18098.73789	294.2611111	301.9919093	296.9985372	294.2991482	293.1661382	294.4998031	293.566319
Chen, G.J., and Guo, T.M.:	0.631090548	841.999781	274	274.8192621	273.3186907	276.2159487	270.6005108	274.0848923	273.9901979
	0.631090548	940.9997552	274.612	275.4452369	274.1981771	276.8615075	271.6459418	275.0364764	274.8428779
	0.631090548	989.9997425	275.113	275.7377463	274.5997879	277.1567986	272.11872	275.4570341	275.2285223

	0.631090548	1113.99971	276.449	276.4343304	275.5334245	277.8444884	273.2066313	276.4062571	276.1162332
	0.631090548	1435.999626	278.174	278.0149411	277.5422327	279.3299093	275.4944138	278.3423509	277.9859524
	0.631090548	2004.999478	281.234	280.2746768	280.1830116	281.2947321	278.3919137	280.735483	280.365009
	0.631090548	2846.999259	284.349	282.8916873	282.9570164	283.373565	281.3010025	283.133324	282.7746416
	0.631090548	3761.999021	286.739	285.1665722	285.1618805	285.0368381	283.5148725	284.9865749	284.6292434
	0.631090548	4034.99895	287.461	285.7674196	285.7161373	285.4564835	284.0576906	285.4473234	285.0874383
	0.631090548	4306.99888	288.072	286.337815	286.2322578	285.8478101	284.5582094	285.8748823	285.5112987
	0.631090548	4628.998796	288.627	286.9806872	286.8026835	286.2809356	285.1058384	286.3459336	285.9766539
	0.631090548	5024.998693	289.182	287.7288563	287.45211	286.7748455	285.7222126	286.8805274	286.5025537
	0.631090548	5370.998603	289.904	288.3487768	287.9789378	287.176141	286.2166752	287.3130292	286.9261677
	0.631090548	5816.998487	290.403	289.1070729	288.6100563	287.6576164	286.8024734	287.8299408	287.4301514
	0.631090548	7029.998171	291.622	290.9781107	290.1085435	288.8040365	288.164761	289.0529675	288.6118942
	0.631090548	8365.997824	292.839	292.7882043	291.485089	289.8611909	289.3807292	290.172532	289.6795653
Jossang, A. and Stange, E.: “A	0.703130909	4758.998762	289.631	287.2311779	288.4222536	287.0674273	288.1095248	287.8240522	287.5260014
	0.703130909	30075.99218	299.688	309.2528046	302.823475	298.3999246	299.1903323	299.7398943	298.4813266
	0.703130909	59961.9844	304.483	320.9617117	308.2129958	302.7551126	302.3567239	304.2309654	302.1739016
	0.703130909	4758.998762	287.522	287.2311779	288.4222536	287.0674273	288.1095248	287.8240522	287.5260014
	0.703130909	29694.99228	296.891	309.0573892	302.7238928	298.320046	299.1268021	299.6573211	298.4112381
	0.703130909	59771.98445	301.686	320.9024125	308.1882057	302.7349353	302.3433821	304.2101973	302.157352
	0.703130909	66814.98262	303.176	323.0161226	309.0582849	303.4439205	302.8048923	304.9397856	302.7359051
Sloan, E.D. Jr.:	0.668408755	1254.999674	278.8	277.162011	277.2919023	278.8609641	276.1771573	277.9975504	277.7053542
	0.668408755	1923.999499	282.9	279.9837177	280.649487	281.3743551	279.8221813	281.1210793	280.7883419
	0.668408755	4122.998927	288.7	285.9548895	286.6388178	285.9141743	285.8157942	286.2755243	285.9536453
	0.668408755	6963.998188	292.2	290.8825194	290.7578805	289.078798	289.5596298	289.687007	289.2877182
	0.668408755	9679.997482	294.1	294.3766612	293.3456518	291.0848408	291.7540326	291.8092748	291.3013167
	0.668408755	12269.99681	295.1	297.1033633	295.2087976	292.537767	293.2586414	293.3334861	292.715124
	0.668408755	16839.99562	296.1	301.0439093	297.6967057	294.4892121	295.1694666	295.368316	294.5587137
	0.668408755	20679.99462	297.1	303.7974265	299.3108615	295.7622677	296.3490717	296.6899663	295.7290035
	0.668408755	27319.99289	298.3	307.7969951	301.4989964	297.4968015	297.8725673	298.4851875	297.2845378
	0.596668956	1599.999584	277.7	278.7236669	277.6142754	279.651113	274.5544288	278.4795318	278.0755465

	0.59666 8956	3391.99 9118	283.9	284.300 2932	283.598 4521	284.098 9347	280.982 4274	283.636 4856	283.242 735
	0.59666 8956	6963.99 8188	289.2	290.882 5194	289.327 1338	288.423 1173	286.542 6112	288.315 4487	287.838 5605
	0.59666 8956	10500.9 9727	292.1	295.292 2006	292.598 0245	290.921 5389	289.456 9818	290.948 7281	290.328 3671
	0.59666 8956	13779.9 9982	293.3	298.506 8065	294.762 1892	292.586 4895	291.281 2405	292.686 943	291.926 9687
	0.59666 8956	1923.99 9499	279.1	279.983 7177	279.082 8339	280.736 1495	276.190 5474	279.790 0774	279.381 7609
	0.59666 8956	2647.99 9311	281.8	282.329 199	281.626 4789	282.625 4781	278.934 1679	281.983 011	281.584 3807
	0.59666 8956	4819.99 8746	286.7	287.347 0317	286.396 5898	286.202 8936	283.770 778	285.938 3249	285.526 991
	0.59666 8956	8135.99 7883	290.3	292.492 1119	290.565 8703	289.366 7737	287.668 5891	289.314 2709	288.792 2907
	0.59666 8956	9480.99 7534	291.2	294.146 4352	291.784 2712	290.297 9504	288.749 6078	290.294 6679	289.717 4303
	0.59666 8956	17159.9 9554	294.3	301.289 5901	296.509 1633	293.937 4319	292.693 4106	294.090 3344	293.190 6857
	0.59666 8956	20264.9 9473	295	303.518 4585	297.833 667	294.965 8318	293.728 1001	295.155 3525	294.133 5342
	0.59666 8956	22989.9 9402	295.6	305.281 1415	298.838 4207	295.748 364	294.492 3081	295.964 1567	294.840 2599
	0.59666 8956	27499.9 9285	296.7	307.895 2044	300.264 9614	296.862 9638	295.546 6529	297.114 1729	295.831 4079
	0.64944 1297	1206.99 9686	276.8	276.921 1731	276.575 7349	278.472 308	274.899 0822	277.363 7207	277.063 561
	0.64944 1297	2185.99 9431	281.6	280.895 7002	281.258 9165	281.967 3449	280.011 406	281.672 6659	281.323 6639
	0.64944 1297	3515.99 9085	284.9	284.597 8256	285.006 2678	284.795 5426	283.817 1533	284.881 1738	284.544 4522
	0.64944 1297	5446.99 8583	288.7	288.481 0962	288.457 8562	287.425 6132	287.098 3777	287.748 72	287.379 3306
	0.64944 1297	8204.99 7866	291.2	292.581 5613	291.688 1733	289.909 0761	289.974 538	290.395 3534	289.928 4983
	0.64944 1297	11999.9 9688	293.2	296.839 5657	294.685 7584	292.232 8058	292.475 0724	292.837 9088	292.211 36
	0.64944 1297	6170.99 8395	289.2	289.679 8658	289.441 872	288.179 8614	287.994 4505	288.557 5238	288.166 0869
	0.64944 1297	9307.99 7579	292.1	293.943 4644	292.682 7126	290.677 988	290.822 1365	291.206 5257	290.694 4124
	0.64944 1297	14069.9 9634	293.9	298.763 5937	295.940 5634	293.211 053	293.473 6743	293.859 3144	293.144 7966
	0.64944 1297	18199.9 9527	295	302.066 096	297.969 9791	294.800 1233	295.028 6035	295.512 0123	294.628 1301
	0.64944 1297	26549.9 9309	296.9	307.371 5763	300.947 4197	297.147 1141	297.175 4241	297.941 8992	296.748 3233
	0.64944 1297	22549.9 9413	295.9	305.007 0278	299.659 841	296.129 8858	296.266 6708	296.890 1031	295.839 4065
	0.80260 126	626.999 8369	274.8	273.251 9461	274.554 1887	275.834 1152	275.299 9816	274.018 7385	274.576 4423
	0.80260 126	1261.99 9672	280.3	277.196 5801	279.931 9667	279.915 9248	281.079 9549	280.174 5767	280.003 2492
	0.80260 126	1805.99 953	283.2	279.543 7509	282.687 4598	282.030 731	283.828 8606	282.828 259	282.618 6008
	0.80260 126	2570.99 9331	285.9	282.103 4343	285.402 6972	284.130 27	286.396 6495	285.297 6462	285.098 481
	0.80260 126	3591.99 9066	288.7	284.776 493	287.973 6603	286.132 6541	288.699 0334	287.556 6627	287.364 6451
	0.80260 126	4295.99 8882	290.1	286.315 255	289.349 6145	287.210 1012	289.879 7124	288.745 2412	288.546 814

	0.80260126	5363.998605	291.5	288.3365223	291.0565385	288.5523559	291.2944549	290.2062705	289.9851914
	0.80260126	6301.998361	292.6	289.8858732	292.2955077	289.5305576	292.2867098	291.2599578	291.0104792
	0.80260126	8535.997779	294	293.0033354	294.6282305	291.3813176	294.075858	293.233772	292.9000585
	0.650836699	599.9998439	273.7	273.0290494	271.0963498	274.4264582	268.4532302	271.1597715	271.6887141
	0.650836699	737.999808	275.4	274.1021293	272.7282432	275.6220686	270.4404218	273.2416611	273.3362766
	0.650836699	992.9997417	277.6	275.7553156	275.067815	277.345254	273.2055073	275.8368564	275.6267943
	0.650836699	1337.999652	280.4	277.5633591	277.4185312	279.0874982	275.8842529	278.1736202	277.8492012
	0.650836699	1778.999537	282.6	279.4402057	279.6642055	280.762111	278.3501368	280.2541174	279.9036954
	0.650836699	2088.999457	283.7	280.5676661	280.9304845	281.7108095	279.700449	281.383328	281.0343821
	0.650836699	2247.999415	284.3	281.0999544	281.5087457	282.1451094	280.3074581	281.8909274	281.5443313
	0.650836699	2667.999306	285.9	282.3870697	282.8590112	283.1618275	281.7013485	283.0600463	282.7199685
	0.650836699	2860.999256	286.5	282.9301875	283.4095766	283.5774411	282.2602562	283.5311846	283.1934005
	0.693380674	723.9998117	273.7	274.0001717	273.5085845	275.8603661	272.4070266	273.7843612	273.9518264
	0.693380674	806.9997901	274.8	274.5853697	274.3577498	276.4898179	273.4012319	274.7878519	274.8033035
	0.693380674	902.9997651	275.9	275.2108015	275.2371677	277.1432088	274.4169296	275.771738	275.6734054
	0.693380674	971.9997471	276.5	275.6315227	275.8132802	277.5720864	275.074637	276.3912943	276.2371235
	0.693380674	1171.999695	277.6	276.7412089	277.277253	278.6649056	276.7185893	277.8950364	277.6479152
	0.693380674	1240.999677	278.2	277.0924571	277.7248359	278.9998731	277.2133588	278.338024	278.0731955
	0.693380674	1461.99962	279.8	278.1310328	279.0071077	279.9617458	278.610492	279.5726242	279.2764402
	0.693380674	2212.999424	283.2	280.9851522	282.250531	282.409569	282.0099633	282.5295334	282.2249227
	0.679262806	751.9998044	273.7	274.2027132	273.5036347	275.9667093	272.0803821	273.9063466	274.0013759
	0.679262806	882.9997703	274.8	275.0845703	274.7631691	276.8989412	273.5550255	275.3427307	275.2503928
	0.679262806	1088.999717	276.5	276.298525	276.407814	278.120951	275.4370029	277.0771512	276.845733
	0.679262806	1399.999636	278.7	277.8516913	278.3781288	279.592044	277.6267074	279.0106832	278.7067326
	0.679262806	1674.999564	280.4	279.0305356	279.7847397	280.6470176	279.1466335	280.3238957	280.0035674
	0.679262806	2095.999455	282.1	280.5916991	281.5433284	281.9715795	280.9961427	281.9098789	281.5896754
	0.638798761	764.999801	273.7	274.2949207	272.7378635	275.727152	270.1218916	273.3625563	273.3921191
	0.638798761	1240.999677	277.6	277.0924571	276.5600415	278.5427457	274.5978459	277.3857453	277.0665706
	0.638798761	1730.99955	280.4	279.2533165	279.1891428	280.4961362	277.5242398	279.840625	279.4783285
	0.638798761	3460.9991	285.9	284.466797	284.6629842	284.6071973	283.2184883	284.5800658	284.2322648
	0.638798761	8652.997749	292.1	293.1496227	291.9024825	290.1370197	289.9224444	290.5366568	290.0403214

	0.638798761	9390.997557	292.7	294.041177	292.5490943	290.6361244	290.4754018	291.0624856	290.5355831
	0.639836517	757.9998028	273.7	274.245411	272.6890448	275.6828802	270.0920964	273.2962715	273.3398546
	0.639836517	1233.999679	277.6	277.0574695	276.5384215	278.5187019	274.601454	277.3612134	277.0446844
	0.639836517	1722.999552	280.4	279.2218092	279.1751106	280.4779567	277.536474	279.8265202	279.4654255
	0.639836517	3467.999098	285.9	284.4835557	284.700455	284.6285137	283.2815886	284.6127638	284.26605
	0.639836517	5032.998691	288.7	287.7435292	287.6422942	286.8633789	286.1165234	287.0559694	286.6871814
	0.639836517	7728.997989	291.5	291.9531488	291.0306175	289.459184	289.1889086	289.8299943	289.3717783
	0.691360127	757.9998028	274.2	274.245411	273.8248492	276.1102337	272.7344742	274.1824562	274.277837
	0.691360127	944.9997542	275.4	275.469518	275.5506698	277.3917358	274.7321383	276.1226828	275.9864069
	0.691360127	1254.999674	277.6	277.162011	277.7711782	279.0493199	277.2221816	278.3901398	278.1203655
	0.691360127	1757.999543	280.4	279.358891	280.4091312	281.0313997	280.0629985	280.8778239	280.5679277
	0.691360127	2130.999446	282.1	280.7110105	281.9151207	282.1692622	281.6276638	282.2332133	281.9253697
	0.718621772	1068.999722	274.3	276.1882666	277.0704663	278.3260799	276.9810448	277.5817412	277.3965432
	0.718621772	1219.999683	275.4	276.9870665	278.0998441	279.0994158	278.1096746	278.6227013	278.3865459
	0.718621772	1606.999582	277.6	278.7527378	280.2463536	280.718933	280.4001566	280.6845217	280.4038994
	0.718621772	2247.999415	280.4	281.0999544	282.8615084	282.7047421	283.0756511	283.0607695	282.780864
	0.718621772	3164.999177	283.2	283.734824	285.5268381	284.7431066	285.6724265	285.3870265	285.1187558
	0.718621772	4591.998805	286	286.9084755	288.4262854	286.9772109	288.3482057	287.8521543	287.5724142
	0.582200927	1261.999672	273.7	277.1965801	275.3760599	278.1243849	271.515227	276.4398688	276.0552039
	0.582200927	2026.999473	277.6	280.3522477	279.160634	280.9058283	275.8144253	279.8667241	279.4429128
	0.582200927	2854.999257	280.4	282.9137039	281.896201	282.9336158	278.7651445	282.1994217	281.7867633
	0.582200927	4046.998947	283.2	285.7931547	284.6827955	285.0142792	281.6356026	284.5062729	284.0917432
	0.582200927	7424.998068	287.7	291.5371873	289.5297433	288.6698636	286.3030979	288.4312649	287.9204366
	0.703124418	1764.999541	281.6	279.3860727	280.6744115	281.149714	280.5704392	281.1044031	280.8057421
	0.703124418	2516.999345	283.9	281.9422052	283.4467021	283.2530238	283.3947942	283.5792106	283.2890705
	0.703124418	3846.998999	287.7	285.3568997	286.7603709	285.7877262	286.5853113	286.4248415	286.1404315
	0.703124418	4460.99884	288.9	286.6494133	287.9170326	286.6778138	287.6514548	287.4001196	287.1077808
	0.703124418	5832.998483	290.9	289.133492	290.0116441	288.2967448	289.5195437	289.1511372	288.8249555
	0.673682203	2185.999431	283.3	280.8957002	281.7602254	282.1740804	281.0999999	282.104464	281.780039
	0.673682203	2929.999238	285.7	283.1179954	284.0599819	283.9152269	283.4284002	284.100701	283.7868991
	0.673682203	3577.999069	287.2	284.743785	285.6286039	285.1089904	284.9613436	285.4337957	285.1217756

	0.673682203	4612.9988	289.4	286.9495114	287.6233167	286.6342728	286.8460086	287.1060537	286.7816258
	0.673682203	5660.998527	291	288.846723	289.2305698	287.8692136	288.3119105	288.4402715	288.0898479
	0.617718353	13549.99648	293.6	298.3003807	295.0435642	292.685966	292.0519928	293.0036083	292.2769042
	0.617718353	27679.9928	297.5	307.9929552	300.7092953	297.1095842	296.3655717	297.5870553	296.3213105
	0.617718353	41339.98925	300	314.3658555	303.8908233	299.6228658	298.5368685	300.1752894	298.4929946
	0.617718353	52159.98643	301.7	318.407079	305.7348049	301.0892591	299.7127129	301.6822244	299.721456
	0.617718353	62849.98365	303.1	321.8469496	307.2135335	302.2703749	300.6118438	302.8947381	300.6912874
	0.617718353	20239.99473	295.8	303.5015232	298.2263127	295.1627815	294.5456188	295.5754848	294.5779817
	0.617718353	33749.99122	298.6	311.0520118	302.2818965	298.3492312	297.4613819	298.8646774	297.4032143
	0.6294292	882.9997703	273.7	275.0845703	273.6565696	276.4772978	270.9559913	274.4671758	274.324293
	0.6294292	951.9997523	274.3	275.5118338	274.2520272	276.9144873	271.6619183	275.1031634	274.8993214
	0.6294292	1171.999695	275.9	276.7412089	275.8973894	278.1261225	273.5795129	276.773274	276.4620817
	0.6294292	2840.999261	283.2	282.8751457	282.9049085	283.3460725	281.2034874	283.0879533	282.7274361
	0.6294292	3764.999021	285.4	285.1733417	285.1334613	285.0265827	283.4437723	284.9604278	284.6012899
	0.6294292	4363.998865	286.5	286.4540615	286.3019124	285.9116691	284.5828315	285.9293852	285.5631018
	0.6294292	5067.998682	287.6	287.8075277	287.485527	286.8110438	285.7117433	286.9043127	286.5235005
	0.6294292	5432.998587	288.2	288.4568212	288.0359166	287.2302228	286.2281496	287.355816	286.9654531
	0.6294292	5811.998488	288.7	289.0988063	288.569592	287.6372573	286.7236931	287.7926632	287.3912284
	0.6294292	6984.998183	289.8	290.9130048	290.024527	288.7498691	288.048762	288.9797408	288.5385199
	0.6294292	8383.997819	290.9	292.8111301	291.469331	289.8589923	289.3270881	290.1543721	289.6588749
Nasrifar, K. and Moshfeghian, M.:	0.574755795	908.1997637	273.476	275.2432937	272.561942	276.1384242	267.9006858	273.665882	273.4387154
	0.574755795	1111.799711	274.987	276.4224675	274.1798438	277.3138695	269.8513223	275.3124958	274.9619
	0.574755795	1336.899652	276.593	277.558158	275.6545866	278.3896649	271.589376	276.7257393	276.3196093
	0.574755795	1476.299616	277.695	278.1942551	276.4479398	278.9701255	272.5086057	277.4598287	277.0383843
	0.574755795	1594.099585	278.766	278.6990936	277.0620016	279.4202376	273.2125208	278.0176815	277.5893077
	0.574755795	1851.699518	279.71	279.7165164	278.2601631	280.3005913	274.5669699	279.0841904	278.6510282
	0.574755795	2205.999426	280.938	280.9620362	279.6605471	281.3330448	276.1181188	280.300537	279.8704531
	0.574755795	2635.699314	281.914	282.2934531	281.0840559	282.3864452	277.659643	281.510952	281.0872022

REFERENCE

- Andersson, V., & Gudmundsson, J. S. (2006). Flow Properties of Hydrate-in-Water Slurries. *Annals of the New York Academy of Sciences, 912*(1), 322–329. https://doi.org/10.1111/j.1749-6632.2000.tb06786.x
- Ameripour, S., & Barrufet, M. (2009). Improved Correlations Predict Hydrate Formation Pressures or Temperatures for Systems with or Without Inhibitors. *Journal of Canadian Petroleum Technology - J CAN PETROL TECHNOL*, *48*, 45–50. https://doi.org/10.2118/09-05-45
- Bahadori, A., & Vuthaluru, Hari. B. (2009). A novel correlation for estimation of hydrate forming condition of natural gases. *Journal of Natural Gas Chemistry*, *18*(4), 453–457. https://doi.org/10.1016/S1003-9953(08)60143-7
- Bellarby, J. (2009). Well, completion design. *(Amsterdam, Netherlands; Boston, Mass: Elsevier)*, 410-419.
- Berge, B. K. (1986, January 1). *Hydrate Predictions on a Microcomputer*. Petroleum Industry Application of Microcomputers. https://doi.org/10.2118/15306-MS
- Bishnoi, P. R., & Dholabhai, P. D. (1999). Equilibrium conditions for hydrate formation for a ternary mixture of methane, propane, and carbon dioxide, and a natural gas mixture in the presence of electrolytes and methanol. *Fluid Phase Equilibria, 158–160*, 821–827. https://doi.org/10.1016/S0378-3812(99)00103-X
- Brustad, S., Løken, K. P., & Waalmann, J. G. (2005). Hydrate Prevention using

- MEG instead of MeOH: Impact of experience from major Norwegian developments on technology selection for injection and recovery of MEG. *Offshore Technology Conference*. Presented at the Offshore Technology Conference, Houston, Texas. https://doi.org/10.4043/17355-MS
- Chavoshi, S., Safamirzaei, M., & Pajoum Shariati, F. (2018). Evaluation of Empirical Correlations for Predicting Gas Hydrate Formation Temperature. *Gas Processing, 6*(2). https://doi.org/10.22108/gpj.2018.112052.1036
- Chaudhari, P., Zerpa, L. E., & Sum, A. K. (2018). A correlation to quantify hydrate plugging risk in oil and gas production pipelines based on hydrate transportability parameters. *Journal of Natural Gas Science and Engineering*, *58*, 152–161. https://doi.org/10.1016/j.jngse.2018.08.008
- Chen, G.J. and Guo, T.M.: "Thermodynamic Modeling of Hydrate Formation Based on New Concepts," *Fluid Phase Equilibria* (1996) **122**, 43–65. https://doi.org/10.1016/0378-3812(96)03032-4
- Chein, R., & Liao, W. (2005). Analysis of particle-wall interactions during particle-free fall. *Journal of Colloid and Interface Science*, *288*, 104–113. https://doi.org/10.1016/j.jcis.2005.02.071
- Clennell, M. B., Hovland, M., Booth, J. S., Henry, P., & Winters, W. J. (1999). Formation of natural gas hydrates in marine sediments: 1. Conceptual model of gas hydrate growth conditioned by host sediment properties. *Journal of Geophysical Research: Solid Earth*, *104*(B10), 22985–23003. https://doi.org/10.1029/1999JB900175

- Davarnejad, R. (2014). Prediction of Gas Hydrate Formation using HYSYS Software. *International Journal of Engineering*, *27*(9 (C)). https://doi.org/10.5829/idosi.ije.2014.27.09c.01
- Deaton, W. M., & Frost, E. M. (n.d.). *Gas Hydrates and Their Relation to the Operation of Natural-gas Pipe Lines*. 126.
- Dorstewitz F. (1995). Hydrate Formation in Pipelines: Proceedings of the Fifth International Offshore and Polar Engineering Conference. *The International Society of Offshore and Polar Engineers,* (1), 244-249.
- Dorstewitz, F., & Mewes, D. (1994). The influence of heat transfer on the formation of hydrate layers in pipes. *International Journal of Heat and Mass Transfer*, *37*(14), 2131–2137. https://doi.org/10.1016/0017-9310(94)90314-X
- Du, Y., & Guo, T.-M. (1990). Prediction of hydrate formation for systems containing methanol. *Chemical Engineering Science*, *45*(4), 893–900. https://doi.org/10.1016/0009-2509(90)85011-2
- Eenews.net, 2013. Assessing the Emissions from the Oil and Gas Development in the Bakken Formation and Their Impact on Air Quality in National Parks, Retrieved November 8, 2019, from https://www.eenews.net/assets/2013/11/06/document_gw_01.pdf
- Elgibaly, A. A., & Elkamel, A. M. (1998). A new correlation for predicting hydrate formation conditions for various gas mixtures and inhibitors. *Fluid Phase Equilibria*, *152*(1), 23–42. https://doi.org/10.1016/S0378-3812(98)00368-9
- Elhady, A. (2005, January 1). *Operating Experiences of DEG and MEG for Hydrate and Dew Point Control in Gas Production Offshore Mediterranean*. https://doi.org/10.2523/IPTC-10103-MS

- Englezos, P., & Bishnoi, P. R. (1988). Prediction of gas hydrate formation conditions in aqueous electrolyte solutions. *AIChE Journal*, *34*(10), 1718–1721. https://doi.org/10.1002/aic.690341017
- Eslamimanesh, A., Mohammadi, A. H., Richon, D., Naidoo, P., & Ramjugernath, D. (2012). Application of gas hydrate formation in separation processes: A review of experimental studies. *The Journal of Chemical Thermodynamics*, *46*, 62–71. https://doi.org/10.1016/j.jct.2011.10.006
- Eucken, A. (1925). Fundamentals of Physical Chemistry. *McGraw-Hill Book Co.*, 371. http://archive.org/details/in.ernet.dli.2015.84084
- Michael Riedel, Eleanor C. Willoughby, and Satind (2010), *Geophysical Characterization of Gas Hydrates Geophysical Developm edition by Edited, Hardcover* (Geophysical Developm edition). (1600). Society of Exploration Geophysicists.
- Gas Hydrates Student Energy. (2013). Accessed: September 14, 2019, from https://www.studentenergy.org/topics/hydrates
- Giavarini, C., & Hester, K. (2011). *Gas Hydrates: Immense Energy Potential and Environmental Challenges*. Springer Science & Business Media. 75-92
- Ghayyem, M. Ali, Izadmehr, M., & Tavakoli, R. (2014). Developing a simple and accurate correlation for initial estimation of hydrate formation temperature of sweet natural gases using an eclectic approach. *Journal of Natural Gas Science and Engineering*, *21*, 184–192. https://doi.org/10.1016/j.jngse.2014.08.003
- Gorbunov, B., Hamilton, R., Clegg, N., & Toumi, R. (1998). Water nucleation on aerosol particles containing both organic and soluble inorganic substances. *Atmospheric Research*, 271–283. https://doi.org/10.1016/S0169-8095(98)00035-0

- Gu, R., Ding, J., Wang, Y., Yuan, Q., Wang, W., & Lu, J. (2019). Heat transfer and storage performance of steam methane reforming in a tubular reactor with a focused solar simulator. *Applied Energy*, 789–801. https://doi.org/10.1016/j.apenergy.2018.10.072
- Hammerschmidt, E. G. (1934). Formation of Gas Hydrates in Natural Gas Transmission Lines. *Industrial & Engineering Chemistry*, *26*(8), 851–855. https://doi.org/10.1021/ie50296a010
- Harju, J., Wocken, C., Stevens, B., Almlie, J., & Schlasner, S. (n.d.). *End-Use Technology Study – An Assessment of Alternative Uses for Associated Gas*. 21. https://ndpipelines.files.wordpress.com/2012/11/eerc-slides-nov-5-2012.pdf
- Jossang, A. and Stange, E.: "A New Predictive Activity Model for Aqueous Salt Solutions," *Fluid Phase Equilibria* (2001) **181**, 33.
- Jujuly, M. M., Rahman, M. A., Maynard, A., & Addy, M. (2017). Hydrate Induced Vibration in an Offshore Pipeline. *SPE Annual Technical Conference and Exhibition*. Presented at the SPE Annual Technical Conference and Exhibition, San Antonio, Texas, USA. https://doi.org/10.2118/187378-MS
- Khamehchi, E., Shamohammadi, E., & Yousefi, S. (2013). Predicting the Hydrate Formation Temperature by a New Correlation and Neural Network. *Gas Processing*, *1*, 4150.
- Koh, C. A., Westacott, R. E., Zhang, W., Hirachand, K., Creek, J. L., & Soper, A. K. (2002). Mechanisms of gas hydrate formation and inhibition. *Fluid Phase Equilibria*, *194–197*, 143–151. https://doi.org/10.1016/S0378-3812(01)00660-4
- Kvenvolden, K. A., & Lorenson, T. D. (2001). The Global Occurrence of Natural Gas Hydrate. In *Natural Gas Hydrates: Occurrence, Distribution, and Detection*

(pp. 3–18). American Geophysical Union (AGU). https://doi.org/10.1029/GM124p0003

- Lingelem, M. N., Majeed, A. I., & Stange, E. (1994). Industrial Experience in Evaluation of Hydrate Formation, Inhibition, and Dissociation in Pipeline Design and Operation. *Annals of the New York Academy of Sciences*, *715*(1), 75–93. https://doi.org/10.1111/j.1749-6632.1994.tb38825.x
- Liu, W., Li, X., Hu, J., Wu, K., Sun, F., Sun, Z., … Qi, X. (2019). Research on flow assurance of deepwater submarine natural gas pipelines: Hydrate prediction and prevention. *Journal of Loss Prevention in the Process Industries*, *61*, 130–146. https://doi.org/10.1016/j.jlp.2019.06.007
- Liu, Z., Li, H., Chen, L., & Sun, B. (2018). A New Model of and Insight into Hydrate Film Lateral Growth along the Gas-Liquid Interface Considering Natural Convection Heat Transfer. *Energy & Fuels*, *32*(2), 2053–2063. https://doi.org/10.1021/acs.energyfuels.7b03530
- Makogon, Y. F., & Makogon, T. Y. (2016). Natural Gas Hydrates. In M. Riazi (Ed.), *Exploration and Production of Petroleum and Natural Gas* (pp. 429–459). ASTM International. https://doi.org/10.1520/MNL7320140017
- Milkov, A. V., & Sassen, R. (2002). Economic geology of offshore gas hydrate accumulations and provinces. *Marine and* Petroleum *Geology*, *19*(1), 1–11. https://doi.org/10.1016/S0264-8172(01)00047-2
- Nasrifar, K. and Moshfeghian, M A Model for Prediction of Gas Hydrate Formation Conditions in Aqueous Solutions Containing Electrolytes and/or Alcohol," J. Chem. Thermodynamics (2001) 33, 999"

- Nicholas, J. W., Koh, C. A., & Sloan, E. D. (2008). A preliminary approach to modeling gas hydrate/ice deposition from dissolved water in a liquid condensate system. *AIChE Journal*, *55*(7), 1889–1897. https://doi.org/10.1002/aic.11921
- Pakulski, M., & Services, B. C. (2007). *Accelerating Effect of Surfactants on Gas Hydrates Formation*. SPE 106166. 5.
- Peytavy, J. L., Monfort, J. P., & Gaillard, C. (1999). Investigation of Methane Hydrate Formation in a Recirculating Flow Loop: Modeling of the Kinetics and Tests of Efficiency of Chemical Additives on Hydrate Inhibition. *Oil & Gas Science and Technology*, *54*(3), 365–374. https://doi.org/10.2516/ogst:1999033
- PIC chemicals, Mechanical Pig Aides. (2014). Accessed: August 22, 2019, from Production Improvement Consultants, LLC website: http://picchemicals.com/maintenance.html
- Poberezhny, L., Hrysanchuk, A., & Grytsuliak, H. (2019). Influence of the gas hydrates on the corrosion rate of gas gathering pipelines. *Procedia Structural Integrity*, *16*, 141–147. https://doi.org/10.1016/j.prostr.2019.07.033
- PolarTREC (2010). Piston Coring. Accesses October 12, 2019, from https://www.polartrec.com/expeditions/international-continental-shelf-survey/journals/2010-08-13
- Rao, I., Koh, C. A., Sloan, E. D., & Sum, A. K. (2013). Gas Hydrate Deposition on a Cold Surface in Water-Saturated Gas Systems. *Industrial & Engineering Chemistry Research*, *52*(18), 6262–6269. https://doi.org/10.1021/ie400493a
- Rich, S. R., & Pantazelos, T. G. (1974). Flux Force Condensation Aspirative Wet Scrubbing of Submicron Particles. *Journal of the Air Pollution Control Association*, *24*(10), 952–954. https://doi.org/10.1080/00022470.1974.10469995

- Safamirzaei, M. (2015). Predict gas hydrate formation temperature with a simple correlation. *Gas, 51*. http://www.gasprocessingnews.com/features/201508/predict-gas-hydrate-formation-temperature-with-a-simple-correlation.aspx
- Saleh, J. M. (2002). Fluid Flow Handbook: Flow Assurance, *McGraw-Hill Education*, Ch. 29. https://www.accessengineeringlibrary.com/content/book/9780071363723/chapter/chapter20
- Salufu, S., & Nwakwo, P. (2013). *New Empirical Correlation for Predicting Hydrate Formation Conditions*. https://doi.org/10.2118/167571-MS
- Sami, N. A., Sangwai, J. S., & Balasubramanian, N. (2013). Gas Hydrate Applications and Problems in Oil and Gas Industry. *Research gate. 4*(8), 6.
- Sloan, E.D. Jr.: *Clathrate Hydrates of Natural Gases*, Marcel Dekker, New York (1990).
- Sloan E. D. (1998). *Clathrate hydrates of natural gas 2nd Edition.* New York: Marcel Dekker. 24, 110 https://doi.org/10.1021/ef000056e
- Sloan, E. D., Koh, C. A., & Koh, C. (2008). *Clathrate Hydrates of Natural Gases 3rd Edition*. New York: CRC Press.
- Sorheim, R. (2005). Transportation of petroleum in subsea pipelines: A Competitive Analysis. *University of Science and Technology Norway (NTNU)*. 2005.
- Sun, C.-Y., Chen, G.-J., Lin, W., & Guo, T.-M. (2003). Hydrate Formation Conditions of Sour Natural Gases. *Journal of Chemical & Engineering Data, 48*(3), 600–602. https://doi.org/10.1021/je020155h

- Tang, C., Dai, X., Du, J., Li, D., Zang, X., Yang, X., & Liang, D. (2010). Kinetic studies of gas hydrate formation with low-dosage hydrate inhibitors. *Science China Chemistry*, *53*(12), 2622–2627. https://doi.org/10.1007/s11426-010-4145-2
- Towler, B., & Mokhatab, S. (2005). Quickly estimate hydrate formation conditions in natural gases. *Hydrocarbon Processing*, *84*, 61–62.
- USGS. (2017). EarthWord – Gas Hydrate. Accessed: September 12, 2019, from https://www.usgs.gov/news/earthword-gas-hydrate
- Vysniauskas, A., & Bishnoi, P. R. (1983). A kinetic study of methane hydrate formation. Chemical Engineering Science, 38, 1061}1972.
- Wang, Z., Zhang, J., Chen, L., Zhao, Y., Fu, W., Yu, J., & Sun, B. (2018a). Modeling of hydrate layer growth in horizontal gas-dominated pipelines with free water. *Journal of Natural Gas Science and Engineering*, *50*, 364–373. https://doi.org/10.1016/j.jngse.2017.11.023
- Wilcox, W. I., Carson, D. B., & Katz, D. L. (1941). *Natural Gas Hydrates*. *33*(5), 4.
- Xiaolan, L., Zuohui, L., Yong, Z., & Rongqiang, L. (2011). Gas Hydrate Inhibition of Drilling Fluid Additives. *Proceedings of the 7th International Conference on Gas Hydrates*, 7.
- Zahedi, G., Karami, Z., & Yaghoobi, H. (2009). Prediction of hydrate formation temperature by both statistical models and artificial neural network approaches. *Energy Conversion and Management*, *50*(8), 2052–2059. https://doi.org/10.1016/j.enconman.2009.04.005
- Zhang, J., Wang, Z., Liu, S., Zhang, W., Yu, J., & Sun, B. (2019). Prediction of hydrate deposition in pipelines to improve gas transportation efficiency and

safety. *Applied Energy*, *253*, 113521.

https://doi.org/10.1016/j.apenergy.2019.113521

- Zhong, Y., & Rogers, R. E. (2000). Surfactant effects on gas hydrate formation. *Chemical Engineering Science*, 13.